Robust Control Volume Methods for Reservoir Simulation on Challenging Grids

PhD Thesis

Eirik Keilegavlen

Department of Mathematics
University of Bergen

November 2009

Preface and Acknowledgements

Preface

This dissertation is submitted as a partial fulfilment of the requirements for the degree Doctor of Philosophy (PhD) at the University of Bergen. The research has been conducted at the Centre for Integrated Petroleum Research at the University of Bergen.

Outline

The dissertation consists of three parts. The first part is devoted to background theory, and is structured as follows. Chapter 1 gives a high-level overview over important concepts and challenges in reservoir simulation. In Chapter 2, mathematical models for flow in porous media are presented. The next three chapters are devoted to numerical techniques for solving the equations. In Chapter 3, we consider various aspects of reservoir simulation. Discretisation techniques for elliptic and hyperbolic equations are discussed in Chapter 4 and 5, respectively. Summary of papers produced are given in Chapter 6, while in the last chapter, conclusions are drawn, and future research directions are pointed out.

The second part consists of in total five papers and manuscripts that have been produced during the work with the thesis. Three of these are published in journals or accepted for journal publication, one is submitted, and one is still in a draft stage.

The third part contains a conference proceedings paper that is not considered part of the thesis, however, some of the results therein is useful for the understanding of the rest of the work.

Acknowledgements

The completion of this dissertation marks the end of three years of happiness and enthusiasm, as well as frustrations. First and foremost, it has been a period of acquiring experience and knowledge.

My principle supervisor has been Ivar Aavatsmark. He has been a source of inspiration for me, and he has always been willing to share his knowledge. For this I am deeply grateful. Magne Espedal and Edel Reiso have been my co-supervisors.

Their help and guidance have been of great importance. I will especially thank Magne for always taking time to listen and give advice whenever needed.

Funding provided by the Centre for Integrated Petroleum Research at the University of Bergen is gratefully appreciated.

During the work with this dissertation, I have greatly benefited from interaction with many colleagues. Above all, I will thank Sissel Mundal for professional cooperation, as well as for being a great friend. Randi Holm has read the dissertation, and given valuable feedback. I will further apologise to both Sissel and Randi for all the convenient (perhaps less convenient for them) invasions of their office whenever I did not feel like working. To the rest of the PhD students and employees at CIPR and the Department of Mathematics, thanks for providing a good research and social environment.

While working with this thesis, I had the pleasure to visit Stanford University for a couple of months. This was an instructive and exciting time for me, both professional and socially, and I will thank Hamdi Tchelepi for giving me the opportunity to visit Palo Alto. My main collaborators there were Jeremy Kozdon at Stanford, and Brad Mallison at Chevron. I highly appreciate their hospitality and their willingness to discuss whatever I was wondering about.

I am lucky to have great friends to remind me there is a world outside the concrete walls of the science building. Their support and encouragement has been of great importance to me. Furthermore, I will thank my family for always being there whenever I need them.

And finally, I will thank Lena for making the final year of the dissertation a joy. Your love, patience, and understanding have been an invaluable support to me.

Eirik Keilegavlen
Bergen, November 2009

Contents

Part I

Background

Chapter 1

Introduction

Understanding of flow in subsurface porous media is of importance for several reasons. Recovery of petroleum stored in the underground has been a vital source of energy for the last 100 years or so, and it likely to be so for several decades to come. Also, the subsurface stores vast amounts of geothermal energy that can be exploited. Further, ground water is the main water supply in large parts of the world, and thus contamination of water resources by industrial pollution or nuclear waste is a major concern. Geological storage of CO_2 is one of the proposed solutions to reduce global warming, which is related to an increase in the concentration of CO_2 in the atmosphere. These are some of the motivating factors for getting better knowledge of processes that takes place in porous media. The main focus in this work is recovery of hydrocarbons, however, many of the results can be relevant for other applications as well.

In this introductory chapter, we provide a brief overview of important concepts in reservoir technology that serve as a motivating background for the thesis. Some of the concepts will be studied in more depth in the following chapters, for further information, see, e.g., [65, 97, 98, 180, 208, 235]. At the end of the chapter, the main directions of the thesis are outlined.

1.1 Reservoir Characteristics

1.1.1 Reservoir Geology

A petroleum reservoir consists of rock perforated by small channels, or pores, that are filled with hydrocarbons. To act as a reservoir, the pores must be connected, so that the fluids can flow. The rock in a reservoir has originated from sedimentary deposition processes that took place millions of years ago. It therefore has a layered structure, where each layer consists of a different type of rock, as seen in

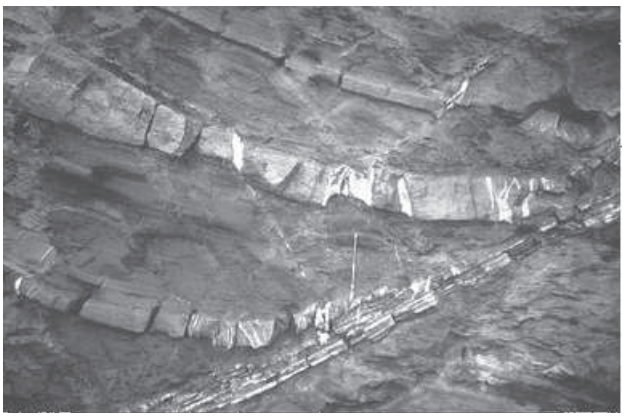

Figure 1.1: An picture of a meter-scale outcrop. Note the layering, and the irregularities in the geology.

Figure 1.1. Geological activity can later have modified the structure. The reservoir may contain fractures, that is cracks in the rock. Further, the layers may have been displaced along a fracture, creating a fault. These are some examples of the highly heterogeneous nature of a porous medium; it contains characteristic features on a continuum of length scales.

To create a viable model of the reservoir is a difficult task. Hard data is only available from core samples obtained from wells. Due to rock heterogeneities, information from the core samples is only locally representative. To obtain more knowledge of the reservoir, we must resort to indirect methods. A much used source of information is seismic data. In seismic surveys, sound waves are sent from the surface towards the rock. When the waves propagate through the rock, the signal is altered. Indeed, different types of rock have different impact on the waves. Hence, a careful interpretation of the reflected signal can expose features of the rock. Seismic surveys are thus based on the elastic properties of the rock. In electromagnetic surveys, one instead utilise the rock's electric conductivity, by sending electromagnetic waves through the rock, and analyse the reflected signal. Further, dynamic data from wells, such as pressure and flow rate can also inform on the structure of the reservoir. We emphasis that all these data sources can inform on the distribution of fluids in the reservoir as well as on the geology.

Based on these various sources of information, a geological model of the reservoir is build. Due to the lack of hard data, the geo-model relies heavily upon statistical methods. The sparsity of information on the rock means it is impossible to model each individual pore. Moreover, if such a description of the pore system was available, numerical simulations of flow based on this model would require computational resources far beyond what is available. Therefore, the rock parameters in the geological model describe average properties. Despite the introduction

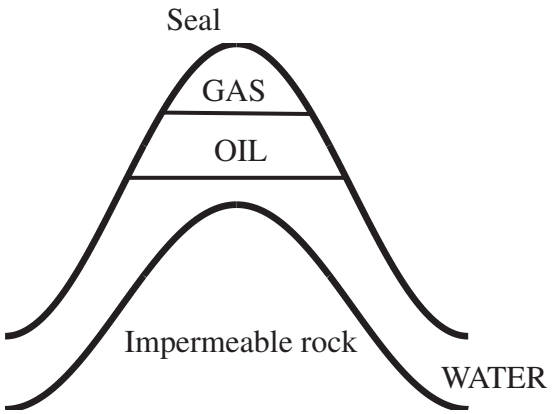

Figure 1.2: Schematic overview of a petroleum reservoir. The hydrocarbons are trapped by a sealing rock. The fluids are in hydrostatic equilibrium.

of average parameters, the geo-model can consist of up to $10^7 - 10^8$ grid cells. This is at least one to two orders of magnitude more than what is possible for a traditional reservoir simulator to handle. Therefore, a coarser grid is constructed, and the rock properties are represented on the new cells. The coarsening process is known as *upscaling*. Ideally, the upscaling should not be detrimental to the quality of the reservoir model. It is therefore crucial to construct the coarser grid so that the rock parameters can be represented accurately in each cell.

1.1.2 Fluid Characterisation

Together with the sediments that later became the reservoir rock, organic material was also deposited. This material has since evolved into oils and gasses by chemical reactions. It is commonly believed that the hydrocarbons are not formed in the reservoir, but in some source rock. Later, the hydrocarbons migrate through the reservoir. The main driving forces of the migration are buoyancy effects, but also capillary forces can affect the movement. Eventually, the hydrocarbons may reach a low conductivity rock formation, a seal, which prevents them from propagating any further. When trapped, the fluids are in hydrostatic balance, as illustrated in Figure 1.2.

The petroleum in a reservoir can consist of hundreds of different chemical components. In general, they are either liquids or vapour, commonly referred to as oil and gas, respectively. The vapour phase has lower density than the liquid phase. Moreover, all the hydrocarbons are in general lighter than water. The gas components can be highly mobile due to low viscosities, whereas the heavy oils can have much larger viscosity than water. During a recovery process, the hy-

drocarbons experience a wide range of pressure and temperature regimes. Both viscosity and density can be highly dependent on pressure and temperature. Further, the hydrocarbons can undergo phase transitions during production. A proper description of flow in the reservoir requires knowledge of these PVT-properties of the fluids. The properties can be quantified by laboratory analysis of the produced hydrocarbons. However, due to the complex chemical composition of the fluids, this is a highly challenging task.

When more than one phase is present, there are forces acting on the interface between the phases. The fluids feel the action of these capillary forces in the form of reduced rock conductivity. To accurately measure these petrophysical properties is difficult at best.

1.2 Production Processes

The reservoir is initially at rest. This balance is disturbed when a well is opened, and the fluids start to flow. The initial reservoir pressure is often high enough to bring the fluids all the way to the surface without external supply of energy. This period is called *primary production*. There are a few physical processes that can provide the energy necessary to recover the hydrocarbons. They are all initiated by the pressure drop, and tend to counteract the decline in pressure. The reservoir rock can experience a deformation and a decrease in pore volume, causing a compaction drive. Water located beneath the hydrocarbons can flow upwards and maintain the pressure. This is called (natural) water drive. A decline in pressure also cause the highly compressible gas to expand, and cause a gas expansion drive. Moreover, at high pressures, gas can be dissolved into the liquid phase. As the pressure decreases, the gas is released again, sustaining the pressure.

The primary production is rather ineffective, and can at best lead to a recovery rate of about 20%. Sometimes the rate is much lower. To produce more hydrocarbons, energy must be supplied to the reservoir. An easy and cheap way to do this is to maintain the pressure by injecting water. This water flooding stage is called *secondary production*. The injection is most often done in the water layer beneath the hydrocarbons.

The injection of water can be effective, and yield recovery rates of up to 40-50 %. However, the reservoir is heterogeneous, and water often find a highly conductive path between the injection well and a producer. After water breakthrough, water flooding have limited effect, and large amounts of hydrocarbons are left in less conductive parts of the reservoir. The effect of water flooding is also limited by the high viscosity of heavy oil relative to water, and by capillary trapping of oil. To recover even more petroleum *enhanced oil recovery* (EOR) techniques are employed. This is called the *tertiary production* period. There are many EOR-

methods, we will mention some of those most commonly applied. The adverse viscosity ratio between heavy oil and water can essentially be improved in two ways. The water viscosity can be increased, for instance by adding polymers to the injected water. The oil viscosity is reduced with an increase in temperature, which can be achieved by injection of hot water or steam. Also, if the supply of oxygen is carefully controlled, one can start in situ combustion of some of the viscous oil, and thereby heat the surrounding hydrocarbons. Other EOR-techniques aim at reduced interfacial tensions between the phases. If a mixture of gasses, notably containing CO_2, is injected, these can mix with the oil, and initiate a miscible displacement, where the gas and oil components act as a single phase with higher mobility. Gas injection is often employed in combination with injection of water. The interface tension can also be reduced by injection of surfactants, or by a careful accommodation for growth of micro-organisms, that can help change the flow pattern.

1.3 Numerical Simulations

Numerical simulations of flow in the reservoir have been employed in the industry for several decades. To optimise the recovery rate, a long term field development plan is made, that involves drilling of wells, application of EOR-techniques, etc. The planning is supported by numerical predictions of the impact of different production scenarios. Also, numerical simulations can help day to day decisions on closing and opening wells etc.

Reservoir models have an inherently high level of uncertainty, due to for instance the sparsity of geological information. To quantify the uncertainty, one can apply Monte Carlo simulations, where several realisations of possible geological models are employed in simulations, and statistics are computed from the results. Uncertainty estimation and prediction of worst case scenarios will also play a major role for large scale geological storage of greenhouse gasses.

We emphasis that modelling and simulation of porous media flow are challenging mathematical and numerical problems. The geology is highly heterogeneous, and the fluid behaviour can be complex with frequent phase transitions. The time scale of the processes of interest spans from day-to-day production management, to the fate of CO_2 hundreds of years after it is injected in the porous medium. A typical well has a diameter on the scale of centimetres, whereas the size of the reservoir can be several kilometres, yielding a vast difference in spatial scale. To give a proper mathematical description of the flow is therefore non-trivial. Further, the model is discretised using advanced numerical techniques. The discretisation often leads to a large system of ill-conditioned equations. The choice of a mathematical model and numerical schemes is a trade-off between ac-

curacy and computational cost. Due to the large span in processes and simulations of interest, there is a need for diverse numerical methods with different forte.

1.4 Scope of the Thesis

Even though numerical simulations successfully have been applied in the industry for decades, there is a constant need for further improvements of the methods. The work can be aimed at developing new techniques, or to extend already existing methods to new areas of applications. Also, it is important to achieve a better understanding of properties and limitations of already existing approaches.

The focus in this work has been development and analysis of a class of numerical schemes known as *control volume methods*, which are prevailing in commercial reservoir simulators. In the present work, we have investigated a broad range of subjects related to control volume methods.

The main computational overhead in reservoir simulations come from solution of linear systems of equations. So far, most simulation grids have been structured, partly due to a lack of efficient linear solvers that allows for more general grid structures. However, usage of such general solvers seems to become more widespread, and thus flexible grids can be used to a larger extent. This will render possible a better representation of complex geological structures. In this work, we analyse the robustness of control volume methods on realistic and flexible grids. Moreover, we study applications of transport schemes designed for simulating EOR-scenarios with adverse mobility ratios on unstructured grids.

All the recovered hydrocarbons are transported through wells. A proper description of flow in near-well regions is therefore a key issue. In the vicinity of a well, the flow rates are high, and the flow pattern radial like. Moreover, to optimise the recovery rate, skew and horisontal wells are drilled, yielding highly heterogeneous near-well regions. The numerical schemes must be adapted to these challenges. In this work, we perform systematic tests of different grids and discretisation techniques in the vicinity of wells.

Chapter 2

Mathematical Modelling

The goal of this chapter is to provide insight in some physical effects that are important for flow in porous media. Since this work mainly has been devoted to development and analysis of numerical methods, we will put emphasis on mathematical modeling. We start by describing some important physical parameters. Further, we discuss several sets of governing equations that model increasingly complex physical processes. During the presentation, we will highlight properties that are important for a numerical solution procedure.

2.1 Physical Parameters

The physical properties used to describe the flow in a reservoir can be divided into three groups, describing the rock, the fluid, and the interaction between rock and fluid. To characterise any of these properties is a research area in itself, thus we will only give a high-level presentation.

2.1.1 Rock Properties

A reservoir consists of rock perforated by channels, or pores, filled with fluids. It is impossible to obtain an accurate description of the channel system for a full-scale reservoir, and the computational cost of simulations on such a model will be far too high. Therefore, we must base the modelling on a macroscopic description of the reservoir.

To bridge the gap between the microscopic pores and the spatial resolution feasible for simulations, we introduce the concept of *representative elementary volumes* (REV). The size of an REV must be much larger than the size of an individual pore. On the other hand, we define parameters describing the properties of the REV based on averaging. Hence, the size of the volume must be smaller than

the length scale on which the rock properties vary considerably. It is important to keep in mind that all parameters, equations and so on are defined for REVs, and are not valid for smaller scales. See e.g. [32] for a further discussion. For simplicity, we treat the rock properties as constant in time, i.e. we ignore compaction. See however Section 2.5.

Porosity

To describe the flow through the pores, we need a measure of pore volume. Denote by V_{pore} the pore volume in an REV. The porosity, ϕ, is defined as the volume fraction occupied by pores to the total volume,

$$\phi = \frac{V_{pore}}{V_{tot}}, \tag{2.1}$$

where V_{tot} is the total volume of the rock. Note that V_{pore} only consists of the volume of interconnected pores, that is, we have neglected solitary caves.

Absolute Permeability

The flow in the reservoir is driven by differences in the pressure. The flow rate generated by a pressure gradient depends on the distribution of pores. In reservoir-scale modelling, the flow conductivity of the rock is described by the permeability, denoted by $\mathbf{K}$. The permeability is a tensor, and according to Onsager's principle, it is symmetric and positive definite. A realistic permeability field is highly heterogeneous. Further, the permeability might be anisotropic, that is, the conductivity is different in different directions.

2.1.2 Fluid Properties

The fluid in the reservoir can exist in several phases. In this work, we allow for three different phases; aqueous, liquid, and vapour, denoted by a, l, and v, respectively. For our modelling, we need expressions for viscosity and density for each of the phases. The process of quantifying these properties is known as PVT-analysis.

The aqueous phase most often consist of water only, although some models, notably those related to CO_2-sequestration, can allow for other species in the aqueous phase. Since the chemical composition of the aqueous phase is fairly homogeneous, the PVT-characteristics are not very complex. On the contrary, the hydrocarbons in a reservoir can consist of hundreds of different chemical components. Since the PVT-properties are dependent on the chemical composition of the phase, as well as on temperature and pressure, state of the art experimental

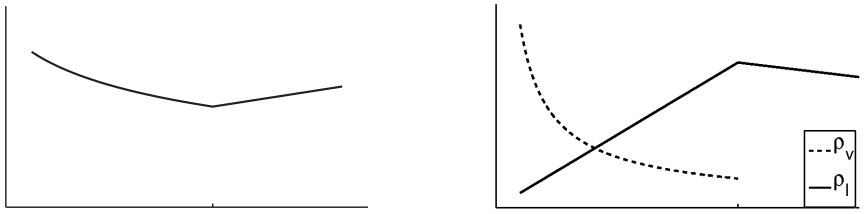

(a) Vapour viscosity (b) Density

Figure 2.1: Qualitative behaviour of viscosity and density for a black oil model (Section 2.4.1). For high pressures, all of the hydrocarbons are in the vapour phase. When pressure drops below the bubble point pressure p_b, the components with small molecules evaporate. The bubble point pressure is dependent on temperature and chemical composition of the hydrocarbons. The y-axes are not to a specific scale.

analysis is needed for quantification. As a rule of thumb, the fluid properties can be characterised by the molecular weight of the components. Components that consist of large molecules, usually exhibit fairly stable behaviour under changes in pressure and temperature. If the molecular weight of a component is small, its PVT-characteristics is often highly sensitive to pressure and temperature changes. In general, a hydrocarbon component is found in both the liquid and vapour phase simultaneously. The larger the molecular weight, the larger portion of the component can be expected to be found in the liquid phase.

We remark that in the literature, the phases are called water, oil, and gas. Further, the hydrocarbon components are often called to as oil and gas components referring to their state under some standard conditions. The present terminology is chosen to avoid confusion between phases and components.

Throughout the thesis, α denotes a generic phase.

Viscosity

The viscosity, μ_α, represents the internal friction in the fluids. For the aqueous phase, μ_a is usually only weakly pressure dependent, it is often considered constant. The viscosity of the liquid phase depends upon both the pressure, and the molar composition of the phase. A possible viscosity behaviour is illustrated in Figure 2.1(a). For the vapour phase, the viscosity is generally increasing with pressure. We remark that viscosity is highly dependent on temperature, this must be taken into account for non-isothermal flow.

Compressibility and Density

The compressibility c, of a fluid is defined by

$$c = \frac{1}{\rho}\frac{\partial \rho}{\partial p}\,, \tag{2.2}$$

where ρ is the density of the fluid. For ideal fluids the compressibility is constant, and Equation (2.2) can be integrated to yield

$$\rho = \rho_0 e^{(c(p-p_0))}\,, \tag{2.3}$$

where ρ_0 is a reference density, measured at a reference pressure p_0.

Water can usually be considered an ideal fluid in reservoir simulation, moreover, the water compressibility is small. So can the liquid phase, if it is composed by large hydrocarbons. However, hydrocarbons with small molecular weight, which are likely to be found in the vapour phase are generally not ideal fluids. In that case, the relation is given by more advanced equations of state, see e.g. [191]. See also Figure 2.1(b) for density behaviour of black oil fluids.

For simplicity, we often make an assumption of an incompressible fluid by setting $c = 0$. Although not physically valid, this assumption eases both implementation and analysis of the problems. The impact of compressibility varies from one problem to another. Sometimes it can be seen as the limiting case when compressibility goes to zero, see for instance the remark at the end of Section 4.5. Under other circumstances, incompressibility is not a limiting case, but a singularity, and the properties of the model change significantly when incompressibility is assumed. For instance, we will see that the pressure variable no longer needs initial values if the fluids are assumed incompressible. Throughout the thesis, we often make this assumption. It is important to keep in mind that extensions to physically valid conditions may add significant challenges.

2.1.3 Petrophysics

When more than one phase is present in the pore system, there is a surface tension on the interface between the fluids. This generates a capillary pressure on the interface. The interactions are determined by the geometry and the topology of the pore system, as well as on the fluids. For a two-phase system, the *wetting* phase tends to stick to the pore walls, whereas the *non-wetting* phase is found in the middle of the pores. We can also have *mixed-wet* conditions, where which phase is wetting depends on the pore size. The wettability depends on the rock, as well as on the fluids, see e.g. [113, 214]. For three-phase systems, the wettability of a phase is defined relative to each of the other phases.

To find functions for the relative permeabilities and the capillary pressure (defined below) is a non-trivial task. Since they both are caused by interface tension, they must be defined consistently. For two-phase flow, there are several models,see [110, 113] and the references therein. These models contain tuning parameters that must be determined from laboratory experiments. To measure the flow functions for three-phase flow is nearly impossible. Instead, one must resort to interpolation of data from two-phase experiments.

Saturations

The forces between the phases depend on how large portion of the pore space is occupied by each phase. The saturation of a phase α, S_α, is defined by

$$S_\alpha = \frac{\text{Volume occupied by phase } \alpha}{\text{Total pore volume}} . \tag{2.4}$$

By definition, $0 \leq S_\alpha \leq 1$. In general, some fluid will be immobile due to capillary forces. The saturation of this immobile fluid is called residual saturation, $S_{\alpha,r}$. We define the effective saturation as

$$S_{\alpha,e} = \frac{S_\alpha - S_{\alpha,r}}{1 - \sum_\alpha S_{\alpha,r}} . \tag{2.5}$$

An assumption that the fluids together fill the entire pore space yields the constitutive relation

$$\sum_\alpha S_\alpha = 1 . \tag{2.6}$$

Capillary Pressure

On the interface between two phases, the pressure is discontinuous due to the surface tension. We define the capillary pressure as

$$p_{cla} = p_l - p_a , \qquad p_{cvl} = p_v - p_l , \tag{2.7}$$

where $p_\alpha, \alpha = a, v, l$ is the phase pressures. The capillary pressures are considered functions of phase saturations.

Capillary forces are of great importance for small scale processes, but the influence diminishes for larger length scales. Therefore, the capillary pressure is often neglected in simulations. Nevertheless, capillary forces have been shown to be important for simulation of certain EOR-processes [66].

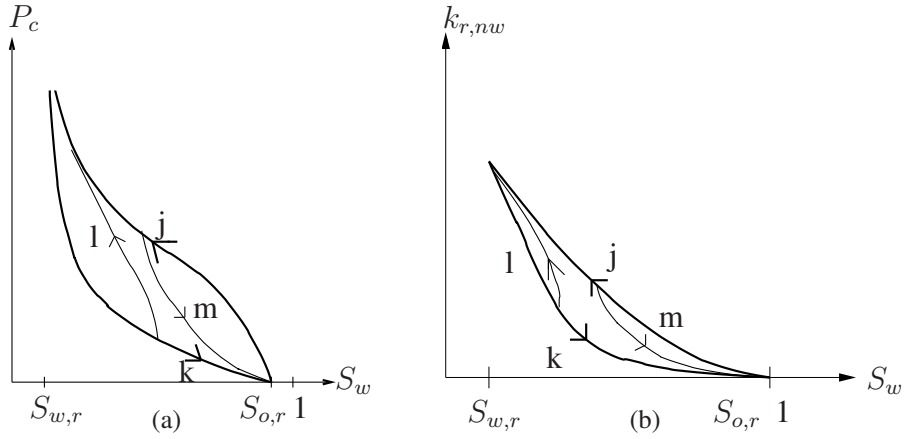

Figure 2.2: Curves for capillary pressure (left) and relative permeability (right) with hysteresis in a water-wet system. The figure shows the bounding curves for drainage (j) and imbibition (k), and two examples of scanning curves for drainage (l) and imbibition (m). Note that both the capillary pressure and the relative permeability is considered functions of water saturation.

Relative Permeability

The absolute permeability represents the conductivity when the pores are occupied by a single phase. When more than one phase is present, the phases will interact, and thereby reduce the flow. To describe this reduced conductivity, we introduce the relative permeability, $k_{r,\alpha}$, for each phase. The relative permeability for a phase is zero for saturation values below $S_{\alpha,r}$. If $S > S_{\alpha,r}$, $k_{r,\alpha}$ increases, but it never exceeds unity. The effective permeability, $\boldsymbol{K}_\alpha$, is then defined by

$$\mathbf{K}_\alpha = k_{r,\alpha} \cdot \mathbf{K} \,. \tag{2.8}$$

The relative permeabilities are strongly non-linear functions of the phase saturations. Moreover, the fluid interactions also reduce the total flow, that is, $\sum_\alpha k_\alpha < 1$. We now define the *mobility* of a phase, λ_α as relative permeability divided by viscosity,

$$\lambda_\alpha = \frac{k_{r,\alpha}}{\mu_\alpha} \,. \tag{2.9}$$

Hysteresis

The flow functions depend not only on the saturations, but also on the saturation history. This is known as *hysteresis*. Figure 2.2(a) shows how the capillary pressure is different during drainage (S_w decreases) and imbibition (S_w increases). If

the saturation change is reversed before it reaches the endpoint ($S_{w,r}$ or $1 - S_{o,r}$), the capillary pressure will follow a *scanning curve* instead of the bounding curve. The relative permeabilities can also experience hysteresis, mainly for the non-wetting phase, see Figure 2.2(b), albeit the effect is not that important.

2.2 Single Phase Flow

A model for single phase flow is of limited importance in practical simulations, although it can be representative for the dynamics in the primary stages of production. However, the equations governing this flow will serve as model problems in later chapters.

When only one phase is present, the flux, $\mathbf{q}$, is computed from the gradient of the pressure by Darcy's law, which reads

$$\mathbf{q} = -\frac{1}{\mu}\mathbf{K}\nabla(p - \rho g z)\,, \tag{2.10}$$

where g is the acceleration of gravity, and z is the vertical coordinate. Darcy's law was originally found experimentally, however, it can be derived as a first-order approximation of a volume averaged Navier-Stokes equation, see e.g. [227]. The Darcy model is only accurate for laminar flow; in high flow-regimes, this assumption breaks down. Such non-Darcy effects can be modelled by Forchheimer's law, see e.g. [26].

Consider an arbitrary volume Ω. For conservation of mass within the volume, the total flux out of Ω must equal the accumulation in the volume. Thus we get the conservation equation

$$\phi \int_\Omega \frac{\partial \rho}{\partial t}\, dV + \int_{\partial\Omega} \mathbf{n} \cdot (\mathbf{q}\rho)\, dS = \int_\Omega q\, dV\,, \tag{2.11}$$

where $\mathbf{n}$ is the outer normal vector of the boundary $\partial\Omega$, and we have taken possible source or sink terms, q, into account. By using the divergence theorem and Darcy's law, we get the equation for single phase flow

$$\phi\frac{\partial \rho}{\partial t} - \nabla \cdot \Big(\frac{\rho}{\mu}\mathbf{K}\nabla(p - \rho g z)\Big) = q\,. \tag{2.12}$$

Since density is a function of pressure, Equation (2.12) is non-linear. For weakly compressible fluids, i.e. water or hydrocarbons with large molecular weight, Equation (2.11) can be approximated by a linear parabolic equation

$$c\phi\frac{\partial p}{\partial t} - \nabla \cdot \Big(\frac{1}{\mu}\mathbf{K}\nabla(p - \rho g z)\Big) = \frac{q}{\rho}\,, \tag{2.13}$$

where we have neglected terms of order $(\nabla p)^2$. In the limit of incompressible fluids, we get the elliptic equation

$$-\nabla \cdot \Big(\frac{1}{\mu}\mathbf{K}\nabla(p - \rho g z)\Big) = \frac{q}{\rho}\,. \tag{2.14}$$

2.3 Immiscible Two-Phase Flow

In some cases, the hydrocarbons are solely in the liquid phase, and the liquid and aqueous phase make up a two-phase system. Especially during secondary production, the fluids are separated into two phases, provided the pressure is above the bubble point pressure. Moreover, many of the mathematical properties of the equations governing flow in porous media can be illustrated by the flow of two immiscible fluids. It is therefore of interest for us to study two-phase flow before we continue to more complex models.

Let the two phases present be aqueous (a) and liquid (l). For each phase α, the flux is modeled by a generalised Darcy law

$$\mathbf{q}_\alpha = -\lambda_\alpha \mathbf{K}\nabla(p_\alpha - \rho_\alpha g z)\,. \tag{2.15}$$

For a discussion of the validity of this generalisation, we refer to [128] and the references therein. The conservation of mass for each phase can be stated on integral form as

$$\int_\Omega \phi \frac{\partial(\rho_\alpha S_\alpha)}{\partial t}\,dV + \int_{\partial\Omega} \mathbf{n}\cdot(\mathbf{q}_\alpha\rho_\alpha)\,dS = \int_\Omega q_\alpha\,dV\,. \tag{2.16}$$

Now, the divergence theorem gives us

$$\phi\frac{\partial(\rho_\alpha S_\alpha)}{\partial t} + \nabla\cdot(\mathbf{q}_\alpha\rho_\alpha) = q_\alpha\,. \tag{2.17}$$

The Equations (2.15) and (2.17) for both phases, together with two-phase versions of (2.6) and (2.7) constitute a closed set of equations for the phase pressures and saturations.

To the end of this section, we assume incompressibility of the fluids. After dividing by ρ_α, summing Equation (2.17) over the phases, and using Equation (2.6), we get the pressure equation

$$\nabla\cdot\mathbf{q}_T = \sum_{\alpha=a,l}\frac{q_\alpha}{\rho_\alpha}\,, \tag{2.18}$$

where the total velocity, $\mathbf{q}_T = \mathbf{q}_a + \mathbf{q}_l$, is given by

$$\mathbf{q}_T = -(\mathbf{K}(\lambda_T\nabla p_l - \lambda_w\nabla p_{cla} - (\lambda_a\rho_a + \lambda_l\rho_l)g\nabla z))\,. \tag{2.19}$$

Here $\lambda_T = \lambda_a + \lambda_l$ is the total mobility. This is an elliptic equation, which can be solved for the pressure.

To get an equation for the saturation, we combine (2.15) with (2.19), and insert the result in Equation (2.17) for water to get

$$\phi \frac{\partial S_w}{\partial t} + \nabla \cdot \Big(\mathbf{K} \frac{\lambda_a \lambda_l}{\lambda_T} \nabla (p_{cla} + (\rho_l - \rho_a) g \nabla z) + \mathbf{q}_T \frac{\lambda_w}{\lambda_T} \Big) = \frac{q_a}{\rho_a} \,. \tag{2.20}$$

This is a parabolic equation describing conservation of the aqueous phase. However, the capillary term is often dominated by the advection term, thus the saturation is governed by an almost hyperbolic equation.

We point out that the governing equations can be modified to apply other primary variables, notably by introducing a global pressure [52]. The change of variables can both ease analysis of the equations, and make the problem better posed for numerical methods [57]. We will, however, not pursue this any further.

2.4 Three-Phase Flow

In general, there will be hundreds of different chemical species present in the reservoir. To describe the motion of each individual component is far beyond the power of the computer resources available. It is therefore common to define *pseudo-components*, each representing several chemical species. Denote by n_c the number of (pseudo-) components present. For notational simplicity, we assume the water to be separated from the hydrocarbons, i.e., the water component is only found in the aqueous phase, and the aqueous phase contains only water. Throughout this section, the subscript c denotes a generic component.

Denote by $\xi_{c,\alpha}$ the molar density of component c in phase α. The molar density of phase α is found by

$$\xi_\alpha = \sum_{i=1}^{n_c} \xi_{i,\alpha}, \qquad \alpha = l, v \,. \tag{2.21}$$

Then the mole fraction of component c in phase α is defined as

$$C_{c,\alpha} = \frac{\xi_{c,\alpha}}{\xi_\alpha} \,. \tag{2.22}$$

We can now write the conservation equation for component c as

$$\frac{\partial}{\partial t} \Big(\phi \sum_{\alpha=l,v} C_{c,\alpha} \xi_\alpha S_\alpha \Big) + \nabla \cdot \Big(\sum_{\alpha=l,v} C_{c,\alpha} \xi_\alpha \mathbf{q}_\alpha \Big) = \sum_{\alpha=l,v} \rho_{c,\alpha} q_\alpha \,, \tag{2.23}$$

where $\mathbf{q}_\alpha$ are the phase velocities found by the generalised Darcy law. The liquid and vapour phase are assumed to be in equilibrium,

$$f_{c,l} = f_{c,v} \qquad c = 1, \ldots, n_c \,, \tag{2.24}$$

where $f_{c,\alpha}$ are fugacity coefficients. Additional constraints that must be fulfilled are the capillary pressure relations (2.7), and further (2.6). Moreover, the sum of the mole fractions for each phase must be 1, that is

$$\sum_{i=1}^{n_c} C_{i,\alpha} = 1 \,, \qquad \alpha = a, l, v \,. \tag{2.25}$$

In total, this gives us $2 \cdot n_c + 6$ equations. The variables are n_c mole fractions for both the liquid and the vapour phase, three saturations, and three phase pressures, in total $2 \cdot n_c + 6$. However, the flow is assumed to be iso-thermal, thus there is one less degree of freedom. If we further apply Gibb's phase rule, we find that the state of the system is determined by n_c variables, see e.g. [48, 107]. We will refer to these variables as primary variables, denoted by $\mathbf{x}_p$. The remaining, secondary variables, $\mathbf{x}_s$, can be found from the primary variables. We indicate this by writing $\mathbf{x}_s = \mathbf{x}_s(\mathbf{x}_p)$, perhaps unintentionally implying a simple functional relation. In reality to compute the secondary variables most often requires solving the equilibrium relation (2.24), which can take a considerable part of the total computation time. However, our main concern is not equilibrium calculations, thus we will not go into details.

Regarding choice of primary equations and variables, there are several options available. These issues should also be seen in connection with the selection of a time stepping scheme (see next chapter). To give a presentation of the options available is beyond the scope of this work, see instead [48] and the references therein.

A large effort has been put into investigations of the mathematical structure of the equations for compositional flow. It is shown in [217] that the pressure is governed by a parabolic equation. If the compressibility is small, the pressure field will rapidly reach a steady state, thus the equation is almost elliptic. The component transport equations are hyperbolic or close to being hyperbolic, depending on the relative permeability functions, we refer to [33, 100, 101, 219].

Miscible Displacement and Dispersion

In the compositional model presented above, the hydrocarbons can exist in two phases. Under some circumstances, the liquid and vapour phase can mix, and act as a single phase. This is called miscible displacement. Since there is no surface tension between the hydrocarbons under miscible displacement, the flow

increases, and so can the recovery rate do. Therefore, initiation of miscible displacement is a popular EOR technique.

The mathematical model for miscible displacement is similar to the above compositional model. However, a process called *mechanical dispersion* that can make a considerable contribution to the overall flow pattern, is not included in Equation (2.23). The irregular pore network will naturally disperse mass at the micro scale. Frictional forces along the walls in the pores also contribute to the dispersion. To include dispersion effects, we augment the transport term $\nabla \cdot (\sum_\alpha C_{c,\alpha}\xi_\alpha \mathbf{q}_\alpha)$ in Equation (2.23) to read

$$\nabla \cdot \Big(\sum_{\alpha=l,v} C_{c,\alpha}\xi_\alpha \mathbf{q}_\alpha - \xi_\alpha S_\alpha D_c \nabla C_{c,\alpha} \Big), \tag{2.26}$$

where D_c is a dispersion tensor, see [108, 201]. For more information on dispersion, see e.g. [32].

When dispersion effects are included, the transport equations become advection-diffusion equations, where the advection dominates. We will consider numerical methods for transport problems in Chapter 5. The schemes primarily studied in this work add an artificial numerical diffusion to the problem which often is of much larger magnitude than the mechanical dispersion. Therefore, we will hardly consider transport equations with second order terms, see however Section 5.4.3.

2.4.1 The Black Oil Formulation

The computational burden of solving the compositional model can be quite heavy. By making some assumptions, a model known as the *black oil* formulation can be derived from the compositional model. The black oil formulation is computationally cheaper to solve than a compositional model. Especially during secondary production, if the liquid pressure drops below the bubble point, black oil models are appropriate. The black oil model has two hydrocarbon pseudo-components, referred to as heavy and light, in addition to water. To go from a compositional to a black oil model, we assume the following:

- Water can only exist in the aqueous phase, and the aqueous phase contains only water.
- The heavy component can only be in the liquid phase.
- The light component can be found both in the liquid and in the vapour phase.

With these assumptions, the conservation equations read

$$\phi \frac{\partial}{\partial t}\Big(b_\alpha S_\alpha\Big) + \nabla \cdot (\rho_\alpha \mathbf{q}_\alpha) \quad = q_\alpha \,, \quad \alpha = a, l \,, \tag{2.27}$$

$$\phi \frac{\partial}{\partial t}\Big(b_v S_v + R_s b_l S_l\Big) + \nabla \cdot (b_v \mathbf{q}_v + R_s b_l \mathbf{q}_l) \quad = q_v \,. \tag{2.28}$$

Here, we have replaced the densities by the inverse volume factors $b_\alpha = \frac{V_{REF}}{V_{RC}}$, where V_{RC} and V_{REF} are the volumes occupied by a unit mass under reservoir and reference conditions, respectively. The amount of the liquid phase consisting of light component is described by the dissolved gas-oil rate R_s. The water and vapour flux are given by a three-phase version of the generalised Darcy's law (2.15), with the density replaced by the inverse volume factor b_α. For the liquid phase, Darcy's law reads, in terms of the variables used in the black oil formulation,

$$\mathbf{q}_l = -\lambda_l \mathbf{K}(\nabla p_l + b_l(\rho_l + R_s \rho_v) g \nabla z) \,. \tag{2.29}$$

The conservation equations for each of the components, together with the constraints (2.6) and (2.7) form a closed set of equations. The primary variables are liquid pressure, and two phase saturations, commonly aqueous and vapour. If the pressure is sufficiently high, all of the light component will be in the liquid phase. In such cases, the vapour saturation is replaced by R_s, or equivalently by the bubble point pressure p_b, as primary variable. As for the above models, the pressure variable exhibits elliptic behaviour, whereas the saturations are governed by hyperbolic equations in the limit of zero capillary pressure [185, 218].

The black oil model can be extended to allow for vaporised heavy hydrocarbons. This is known as the extended, or volatile, black oil model [185]. We will not pursue this further.

2.5 Further Extensions

The models considered in the previous section cannot capture all of physical processes taking place in a porous medium during production. We here briefly mention two possible extensions.

Thermal Flow

So far, all processes have been considered iso-thermal. In many cases this assumption can be justified by the large heat capacity of the rock. However, if EOR-techniques such as steam injection or in situ combustion are applied, thermal effects must be accounted for by introducing a conservation equation for energy. For

an introduction to modelling of thermal processes, and associated computational challenges, see for instance [59, 107, 108].

Rock Compaction

All of the above models consider the pore volume to be constant. In reality, the pressure drop during production will change the geometry and topology of the pore system. Thus in general, the rock properties described in Section 2.1.1 will change. If these changes have significant impact on the flow pattern, both the porosity and the permeability should be considered functions of time. Moreover, rock compaction contributes significantly to sustain pressure during production. Proper handling of these issues requires a coupling between geo-mechanical and reservoir models, which will further complicate the simulations. Confer [193] and the references therein for more information.

Chapter 3

Reservoir Simulation

So far, we have given governing equations for flow in a porous medium. Even though the physical properties included in the modelling are simplified, we have to solve a set of highly non-linear equations for each time step. The number of grid blocks in the reservoir model can be of order 10^6. As we saw in the previous chapter, there may be several unknowns in each grid block, depending on which equations are employed to model the flow.

In this chapter, we will describe some aspects of reservoir simulations that will serve as background for the next two chapters. We focus on solution of equations (both non-linear and linear), gridding, and on time stepping methods. The presentation will be rather brief, and the interested reader should consult the references for more information.

Treatment of two topics that naturally belong to this chapter is postponed to Chapter 4: Gridding in near-well regions will be considered in Section 4.6. The multiscale methods introduced during the last decade are closely related to linear solvers. These methods are treated in Section 4.7.

3.1 Solution of non-Linear Systems

Except from some very simplified cases, all the models presented in Chapter 2 contain equations that are non-linear. Thus we need to solve equations of the form

$$\mathbf{F}(\mathbf{x}_p^{n+1}\mathbf{x}_s(\mathbf{x}_p^{n+1})) = \mathbf{0}\,, \tag{3.1}$$

where $\mathbf{F}$ is a discretisation of the governing equations written in residual form ($\mathbf{F} = \mathbf{0}$). The primary and secondary variables are represented by the vectors $\mathbf{x}_p$ and $\mathbf{x}_s$, respectively. Superscripts refer to time steps.

In reservoir simulation, non-linear equations are usually solved by the iterative Newton-Raphson method, or Newton's method for short. Let $\mathbf{x}_p^{n,l}$ be a member of the sequence of approximate solutions at time $n+1$, with $\mathbf{x}_p^{n,0} = \mathbf{x}_p^n$. A Taylor expansion of $\mathbf{F}$ around $\mathbf{x}_{p,i}^{n,l}$ with respect to the primary variables gives us

$$\mathbf{F}(\mathbf{x}_p^{n,l+1}, \mathbf{x}_s(\mathbf{x}_p^{n,l+1})) \approx \mathbf{F}(\mathbf{x}_p^{n,l}, \mathbf{x}_s(\mathbf{x}_p^{n,l})) + \frac{\partial \mathbf{F}(\mathbf{x}_p^{n,l}, \mathbf{x}_s(\mathbf{x}_p^{n,l}))}{\partial \mathbf{x_p}} \Delta \boldsymbol{x}_{p,i}\,, \quad (3.2)$$

where $\Delta x_p = \boldsymbol{x}_p^{n,l+1} - \boldsymbol{x}_p^{n,l}$. The differentiation is carried out with respect to the primary variables at iteration l. If the solution obtained from the next iteration is exact, the residual is zero, and thus

$$\frac{\partial \mathbf{F}(\mathbf{x}_p^{n,l}, \mathbf{x}_s(\mathbf{x}_p^{n,l}))}{\partial \mathbf{x_p}} \Delta \mathbf{x}_p = -\mathbf{F}(\mathbf{x}_p^{n,l}, \mathbf{x}_s(\mathbf{x}_p^{n,l}))\,. \quad (3.3)$$

This is a linear system to be solved for the update $\Delta \mathbf{x}_p$. If $\|\boldsymbol{F}(\boldsymbol{x}_p^{n,l+1}, \boldsymbol{x}_s(\boldsymbol{x}_p^{n,l+1}))\|$ is smaller than some tolerance, we set $\mathbf{x}_p^{n+1} = \mathbf{x}_p^{n,l+1}$. If not, we recompute the Jacobian matrix, and obtain a new linear system. We also remark that columns corresponding to explicit variables are non-zero on the diagonal only, and thus these variables can be eliminated, yielding a smaller linear system.

The algorithm presented above is a straightforward application of the Newton scheme. Provided with a good initial guess, the iterations will eventually experience second order convergence. However, in practical simulations, the equations are badly conditioned, and the iterations may not converge. The classical way to overcome convergence problems is to disregard the non-convergent iterations, reduce the time step size and start computing a new sequence of approximations.

By taking into account the physical properties described by the equations, it is possible to design algorithms that are more robust and more efficient. Since the transport equations have a hyperbolic nature, the approximation obtained by the Newton iteration might be improved by an update using local information. This approach is investigated in [20, 145], where the pressure field obtained from an iteration is used to reorder the unknowns. This allows for a local update of variables governed by hyperbolic equations. Another possibility is to rewrite the Newton-Raphson scheme to a form where it is not necessary to disregard non-convergent iterations, see [233].

3.1.1 Linear Solvers

In the Newton algorithm, a linear system of equations must be solved in each iteration. The size of the system can be several times the number of cells in the simulation grid. Thus, to solve linear systems is often a bottleneck, and the

availability of efficient linear solvers plays an important role when the simulation strategy is decided.

The large number of unknowns makes direct methods like LU-decomposition inappropriate. Instead, iterative schemes are applied, mainly methods that seek solutions in Krylov subspaces. An overview of such methods can be found in e.g. [31, 220]. For Krylov methods to be effective, they should be accompanied by a suitable *preconditioner*. A survey of preconditioning techniques can be found in, for example [35]. For the elliptic part of the problem (the pressure unknowns), the global domain of dependence makes multigrid methods with domain decomposition appropriate. The multigrid method could be geometric or algebraic, depending on the whether the grid is structured or unstructured (see next section). More information on multigrid methods can be found in e.g. [221], applications to reservoir simulation are considered in [49, 210]. We point out that the classical algebraic multigrid approaches require the system matrix (for the restricted pressure problem) to be an M-matrix. For transport equations, local methods like incomplete LU-factorisation can be expected to perform well. Different strategies for decoupling the system into pressure and transport parts are considered in [49, 148, 210, 225]

3.2 Grids

Traditionally, reservoir simulations have employed quadrilateral grids in 2D, and hexahedrals in 3D, see Figure 3.1(a) for an example. The logical ordering of the cells eases the implementation. Moreover, the natural ordering of the unknowns in the linear system makes the solution procedure faster. If higher resolution is needed in some areas, this can be achieved by using local grid refinement, see Figure 3.1(b). Note that this will introduce hanging nodes, which can cause difficulties for some numerical methods.

To fit a hexahedral grid to a complex reservoir with multiple geological layers, faults, and fractures is a non-trivial task. This is illustrated by Figure 3.2, which shows part of a simulation grid from a real North Sea field. It may be less complicated to grid the reservoir with other polyhedra. For a three dimensional domain, tetrahedra are very well suited to grid a complex domain. Another option is to construct a two-dimensional triangular grid, and extend it prismatically to three dimensions. Such a grid will have a large degree of flexibility. In a reservoir, the geological layering define a natural division into horisontal layers, which can be used for prismatic extensions of 2D-grids. However, geometrical constraints such as faults and skew and horisontal wells pose a challenge for construction of such 2-1/2-D grids.

Another class of grids is the Voronoi-grids, which are duals of a primary grid.

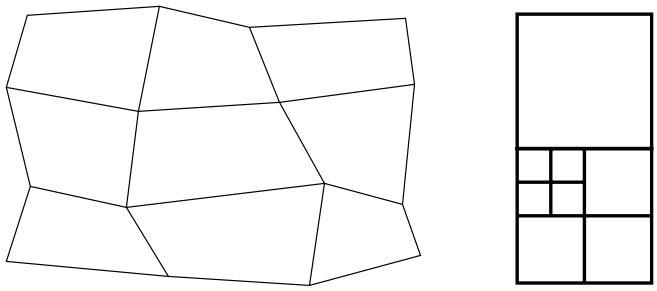

Figure 3.1: To the left, a quadrilateral grid. To the right, an example of local grid refinement.

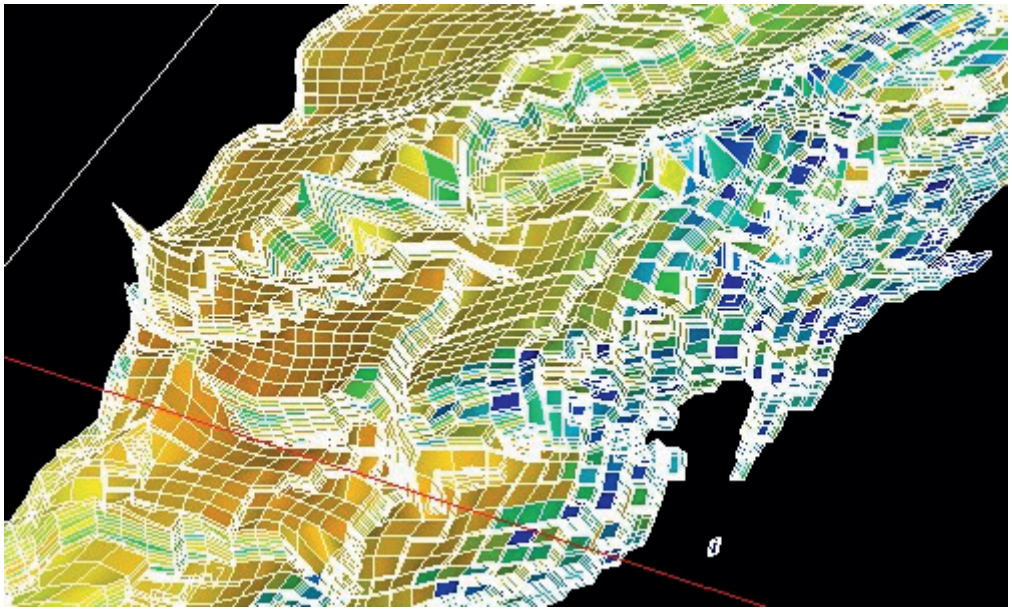

Figure 3.2: Part of a hexahedral simulation grid from a real North Sea field. Note the complex geometry.

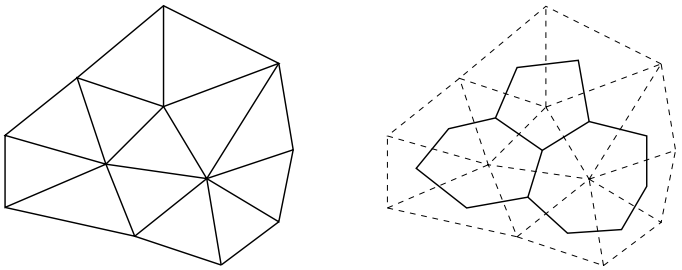

(a) A triangular grid (b) The dual

Figure 3.3: A triangular grid, and its dual. Note how cell centres and vertices change roles.

The vertices and cell centres switch roles when going from a primary to a dual grid, see Figure 3.3(a) and 3.3(b). A Voronoi-tessellation can be constructed for any grid, however, they are mostly used for unstructured (triangular or tetrahedral) grids. The Voronoi-grids are well suited for discretising the flow equations, see Chapter 4. However, to adjust a Voronoi-grid to discontinuities in the medium can be non-trivial.

Unstructured grids are appealing because of their flexibility, and there is a literature on generation of such grids in difficult domains, see e.g. [96, 146, 147]. However, the number of unknowns in the linear system is high, and the system matrix will in general not be banded. In three dimensions, tetrahedral grids suffer more from a high number of unknowns than a prismatic extension of 2D triangular grids. The dual of a tetrahedral grid in 3D can have a large number of neighbours, which can lead to computationally very demanding simulations.

The structure and bandwidth of the system matrix are determined by grid topology and geometry. Hence, properties of the numerical methods should ideally be used as constraints in the gridding process. We end this section by pointing to Figure 3.4, which shows an example taken from [114] on how a domain with constraints (fractures) can be gridded using triangles. Note that away from the fractures, the triangles are close to uniform. In these areas, other cells, such as quadrilaterals or Voronoi cells, could equally well have been fitted to the geometry. Further considerations can be found in [25, 183, 223]. We also remark that this approach can be taken one step further by introducing adaptive grid refinement based on a posteriori error estimates.

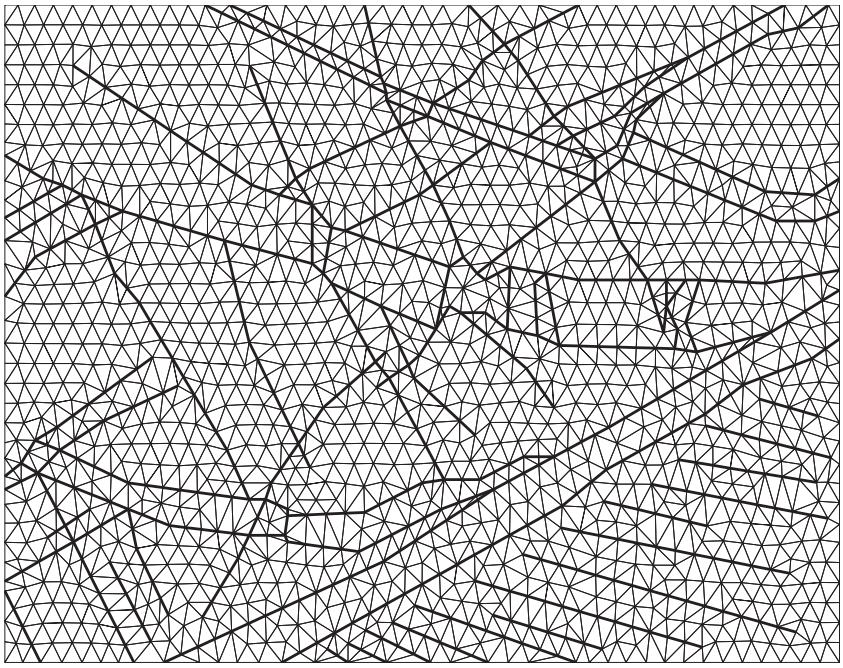

Figure 3.4: A triangular grid fitted to multiple fractures (bold lines). Note that the fractures resemble the outcrop shown in Figure 1.1.

3.3 Time Stepping Methods

There are several commonly used time stepping methods in reservoir simulations. They differ in the choice of implicit in time variables. Due to its elliptic behaviour, the pressure is always treated implicitly. For the advection dominated mass variables, there are several options. In the following we briefly describe some common time stepping strategies. For more a more detailed description and analysis of the methods, we refer to [26, 59].

As in the previous chapter, we let n_c be the number of components, which will be equal to the number of primary variables, also for two-phase and black oil models. Further, let n_e be the number of cells in the grid.

Fully Implicit

In the fully implicit method (FIM), or simultaneous simulation, all the primary variables are treated implicitly. FIM is unconditionally stable with respect to time step size, however, in practice the time steps must be small enough for the Newton iterations to converge. The robustness of the fully implicit method makes it popular for industrial simulations with relatively few variables, i.e. black oil

simulations. For problems with more unknowns, the computational cost of the simulations becomes severely high.

IMPES

As previously mentioned, it is only the pressure variable that definitely needs to be discretised implicitly in time. If we treat all other variables explicitly, we arrive at the implicit pressure explicit saturation (IMPES) or implicit pressure explicit molar mass (impem) formulation. The two models differ in which variables are used to represent masses. Common choices of primary variables lead to the use of IMPES for two-phase or black-oil simulations, whereas impem is used in compositional simulations.

In each Newton iteration with IMPES/impem, there will only be n_e linear equations to solve. Thus one time step with the method is computationally cheap, and the method is especially attractive for compositional simulations. However, the time step sizes will be limited due to a stability criterion (CFL criterion), which is typically determined by cells in high-flow regions. The restrictions on the time step size can in many situations be severe. One possible remedy is to apply Asynchronous time stepping [167], where a local time step is applied for each cell.

IMPSAT

To choose the number of implicit variables is a trade off between robustness and computational cost. FIM and IMPES can be seen as the two extrema in that sense. An alternative is to treat pressures and saturations implicitly, and the rest of the primary variables explicitly. This method is known as Implicit pressure and saturations (IMPSAT). For IMPSAT to be different from FIM, we of course need n_c to be larger than 3. The IMPSAT method can be considerably cheaper than FIM, and allows for much larger time steps than IMPES, see [48]. For more information on IMPSAT and some models employing this strategy, we refer to [107].

The Adaptive Implicit Method

So far, we have considered three time stepping methods that treat a various number of variables implicitly. However, the degree of implicitness has been static, in the sense that the choice of implicit variables is the same for every grid cell. Moreover, it is customary to maintain the same degree of implicitness during the entire simulation. With an explicit method, the time step size is dictated by the cell with the highest CFL-number, which is typically found in high flow regions, e.g. near fractures or wells. In such regions, an implicit time discretisation is

appropriate. In the Adaptive implicit method, different time stepping strategies are employed in different cells. Thus the discretisation scheme can be tuned to increase robustness and time step size.

The adaptive implicit method was introduced to the reservoir community in [213]. Criteria for switching between implicit and explicit treatment are analysed in i.e. [199]. Compositional flow was studied in [48], where FIM, IMPSAT, and IMPES all were employed in the same simulations. In [68, 69], AIM is proven to be inconsistent on the boundary between explicit and implicit cells. A remedy is also proposed, together with higher order schemes in time and space.

Chapter 4

Elliptic Discretisation Principles

As shown in Chapter 2, the pressure variable exhibits parabolic behaviour. After discretising the time derivatives, we are left with solving an elliptic equation for the pressure. This chapter is devoted to numerical methods for elliptic equations, with emphasis on control volume methods. These methods make it feasible both to solve the entire system of governing equations fully implicit (FIM), and to use some sort of operator splitting (IMPES,IMPSAT, etc.). Other methods for elliptic equations that are applied in the reservoir simulation community are mentioned in the last section.

4.1 Preliminaries

Consider the equation for an incompressible single phase, (2.14). We introduce a flow potential $u = p - \rho g z$, set the viscosity to 1, and get

$$-\nabla \cdot (\mathbf{K} \nabla u) = q \,, \tag{4.1}$$

where q represents sink/source terms. The solution u behaves similarly to the pressure variable for the more complex physical processes presented in Chapter 2, and we therefore employ Equation (4.1) as a model equation for elliptic problems. Before introducing discretisation schemes, we will briefly state some results from the theory of elliptic equations:

- Regularity: For Equation (4.1) to be well posed, q must be continuous, and $\mathbf{K}$ must be continuously differentiable. However, in porous media applications q can be a point sink/source, and the permeability is in general only piecewise constant. Therefore, the equation is often casted into in a weak form, and we seek a $week\ solution$ of the problem. The weak, or variational, formulations are starting points for many numerical methods,

see Section 4.7. The control volume methods investigated in this work are based on an integral formulation, however, they are closely related to approximations derived from the variational formulations [137].

- Symmetry: The differential operator $-\nabla \cdot (\mathbf{K}\nabla\cdot)$ is self adjoint in the L^2 inner product. The analogy for a discrete method is a symmetric system matrix.

- Positive definiteness: The eigenvalues of the differential operator are positive. For a numerical method to mimic this property, it should render a positive definite system matrix for the potential. This can be considered as a stability condition for the discretisation.

- Maximum principles: The solution obeys a maximum principle. The analogy for numerical methods is covered by the consideration of $monotonicity$ properties. These issues are thoroughly investigated in Section 4.5.

- Global domain of dependence: A point sink/source will influence the solution everywhere in the computational domain. Discretisations of elliptic problems therefore render systems of algebraic equation where all cells are connected. Hence, it can be computationally demanding to solve the equations.

The literature on elliptic equations is extensive, we refer to [6, 90] for more information.

4.2 Control Volume Methods

Let Ω_i be a cell in our computational domain. We integrate Equation (4.1) over Ω_i and use the divergence theorem to get

$$-\int_{\Omega_i} \nabla\cdot(\mathbf{K}\nabla u)dV = -\int_{\partial\Omega_i} \mathbf{n}\cdot(\mathbf{K}\nabla u)dS = \int_{\partial\Omega_i} \mathbf{n}\cdot\mathbf{q}dS = \int_{\Omega_i} qdV \,. \quad (4.2)$$

Here we have introduced the flux variable $\mathbf{q} = -\mathbf{K}\nabla u$. Equation (4.2) is a conservation law, the flux out of Ω_i is equal to the sinks/sources inside the cell. The control volume methods approximate the gradient of u by the pressure values in nearby cells. Let $\partial\Omega_{i,j}$ be an edge of Ω_i. The numerical flux f_j through $\partial\Omega_{i,j}$, is given by

$$\int_{\partial\Omega_{i,j}} \mathbf{n}\cdot(\mathbf{K}\nabla u)\, dS \approx f_j = \sum_k t_{j,k}u_k \,, \quad (4.3)$$

where u_k is the potential in cell k, and the sum is taken over all cells contributing to the flux expression. The quantities $t_{j,k}$ are called $transmissibilities$. They depend on both permeability and grid geometry. The fluxes are approximated for all edges $\partial\Omega_{i,j}$, and conservation of mass is obtained by requiring

$$\sum_j f_j = \sum_j \sum_k t_{j,k} u_k = \int_{\Omega_i} q \, dV \, . \tag{4.4}$$

There is a large number of control volume methods, see [93] for a recent overview. In the sequel, we will discuss some methods that are relevant for reservoir simulations.

4.3 Two Point Flux Approximations

The two-point flux approximation (TPFA) is one of the simplest control volume methods. As the name indicates, the flux over $\partial\Omega_{i,j}$ is approximated by using the pressure in the two cells sharing the edge. Consider Figure 4.1(a). The flux through the edge seen from cell number 1, f_1, can be expressed as

$$f_1 = -\int_{\partial\Omega_{i,j}} \boldsymbol{n} \cdot \left(\mathbf{K}_1 \cdot \frac{\boldsymbol{v}_1}{\|\boldsymbol{v}_1\|} (u_e - u_1) \right) dS \, , \tag{4.5}$$

where $\mathbf{n}$ is the normal vector out of cell 1, see Figure 4.1(a). The gradient is approximated by a normalised vector $\boldsymbol{v}_1$, pointing from the cell centre $\boldsymbol{x}_1$ to the midpoint of the edge $\boldsymbol{x}_e$, scaled by the potential difference between $u_e = u(\boldsymbol{x}_e)$ and $u_1 = u(\boldsymbol{x}_1)$. Similarly, the flux can be seen from cell number 2 as

$$f_2 = -\int_{\partial\Omega_{i,j}} \mathbf{n} \cdot \left(\mathbf{K}_2 \cdot \frac{\boldsymbol{v}_2}{\|\boldsymbol{v}_2\|} (u_2 - u_e) \right) dS \, . \tag{4.6}$$

Here $\boldsymbol{v}_2$ represents a vector from $\boldsymbol{x}_e$ to $\boldsymbol{x}_2$, cell centre of cell 2, and $u_2 = u(\boldsymbol{x}_2)$. By requiring continuity of the flux we obtain

$$f_1 = f_2 = t(u_1 - u_2) \, . \tag{4.7}$$

The transmissibility can be found by combining Equations (4.5) and (4.6). Note that we have implicitly required continuity of the potential in $\boldsymbol{x}_e$.

TPFA does not render a consistent flux approximation, e.g. [5, 7, 82]. It is only convergent in the special case where the grid is aligned with the principle axes of the permeability tensor. Such grids are said to be $\mathbf{K}$-orthogonal.

Figure 4.1(b) shows two Voronoi cells with a primary triangular grid. The vector $\boldsymbol{\nu}$ is normal to the straight line that connects the cell centres, and $\mathbf{n}$ is normal to the edge between the cells. A sufficient condition for $\mathbf{K}$-orthogonality

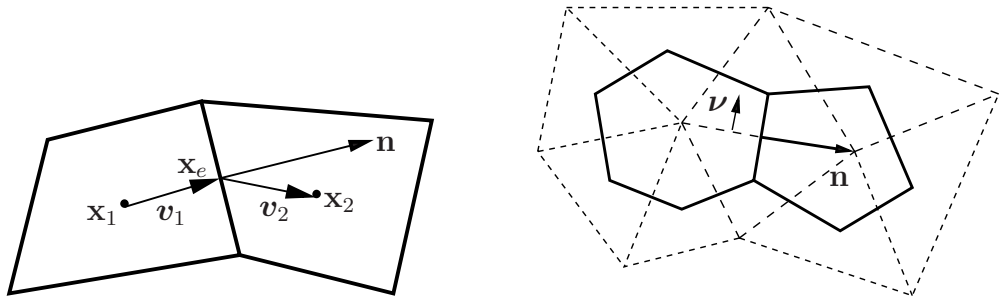

(a) TPFA (b) $\mathbf{K}$-orthogonality of Voronoi grids

Figure 4.1: To the left, the flux stencil for TPFA. To the right, a primal triangular (stippled) and a dual grid. The vector $\boldsymbol{\nu}$ is orthogonal to the line connecting the cell centres.

reads $\boldsymbol{\nu}^T \mathbf{K}\mathbf{n} = 0$. We see that dual grids are $\mathbf{K}$-orthogonal if the permeability is isotropic, and the triangles have the Delaunay property. However, Voronoi grids can yield good results also for anisotropic media. Dual grids for reservoir simulations are studied in i.e. [109, 133, 184].

Even though TPFA is not convergent, and in many cases not capable of resolving the flow field accurately, it is widely used in industrial simulations [204]. There are several reasons for this, apart from historical ones. The method is easy to formulate and apply. The resulting system matrix is symmetric with small bandwidth, and it is an M-matrix provided all transmissibilities are positive. This renders possible design of efficient linear solvers. Moreover, since the system matrix is an M-matrix, TPFA does not suffer from artificial oscillations related to monotonicity issues. This makes it more robust than the multi-point methods studied in Section 4.4.

4.3.1 Non-Linear Methods

Despite the shortcomings of the TPFA method, its small cell stencil is appealing. Before we introduce methods with larger stencil, we will therefore mention some schemes that keep a two-point approximation of the fluxes, but consider the transmissibilities as functions of the solution u, as well as of permeability and grid geometry. This yields a significant improvement of the traditional TPFA method, to the price of increased computational complexity. We denote the resulting schemes non-linear two point flux approximation (NTPFA) methods.

An Upscaling-Related Approach

For the two-point flux approximation to be good, the grid must be aligned with the permeability field. The fine scale geological models often have isotropic permeability, but anisotropies and heterogeneities are introduced by grid effects and upscaling. Still, upscaling procedures based on TPFA can provide accurate results. This motivated Chen et. al. to develop a NTPFA method applicable both to upscaling and as a single level method [55].

The main idea is to compute a reference solution by multi-point flux approximations; either globally or locally in combination with a global TPFA. Then, transmissibilities are computed based on a local two-point flux approximation. The aim is to tune the transmissibilities so that the reference flow field is reproduced as accurately as possible. To accomplish this, iterations might be necessary, hence the transmissibilities depend on u. If more than one phase is present, the flow pattern and thereby the reference potential solution will gradually change as components are transported. The transmissibilities, which are tuned to mimic the reference flow pattern, must thus be updated regularly. Compared to the computational cost of a multiphase simulation, the update is not a significant burden.

The results obtained with this method are promising, and indicate that in many cases, a two-point method might be sufficient, provided the transmissibilities are carefully computed.

An Unconditionally Monotone NTPFA Scheme

In [152], LePotier introduced an unconditional monotone NTPFA method. The scheme has later been extended to a class of methods, see [159, 161, 234]. The methods approximate the potential in collocation points that need not coincide with the cell barycentres. In most of the methods, auxiliary unknowns are introduced in the vertices of the grid. The flux through an edge from one cell can then be approximated by the potential values in the collocation point of the cell and the vertices of the edge. A similar expression is found for the other cell sharing the edge. Requiring continuity of the flux gives a two point flux expression, i.e. the auxiliary unknowns are eliminated. However, the transmissibility becomes a function of the potential in the vertex nodes, thus the method is non-linear. Further, the vertex values are computed by interpolation from values in the collocation points, and the choice of interpolation scheme affects the accuracy of the scheme. An interpolation-free method is presented in [161].

The framework described here provides methods that are provably monotone, also in cases where linear methods with increased cell stencils cannot be monotone (see Section 4.5). The methods render algebraic systems of non-linear equations. To guarantee positivity of the potentials in each iteration step, the system is solved

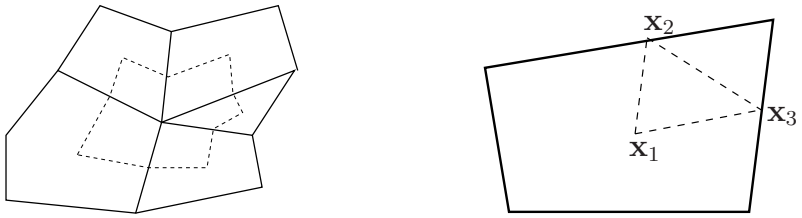

(a) An interaction region (b) A variational triangle

Figure 4.2: To the left, an interaction region (stippled) for a cluster of cells. To the right, a variational triangle used to construct basis functions.

by Piccard iterations instead of by Newton's method. The number of iterations needed is quite high, partly because not much effort has been put into solving the system efficiently yet. It has been suggested that the schemes are best suited for non-linear problems [205].

We are not aware of any applications of the method to multiphase flow. Therefore, it is an open question how the non-linear transmissibilities will behave in difficult scenarios such as counter-current flow and potentials close to the bubble point. We also remark that if rock compressibility is significant, the permeability is no longer constant in time. Hence the transmissibilities must be recomputed anyhow, and the overburden due to the non-linear flux approximation is easier to justify.

4.4 Multi-Point Flux Approximations

So far, we have stated that the flux over an edge cannot be approximated consistently by a linear combination of the potentials in the two adjacent cells. One possible remedy is to introduce a non-linear approximation. Another way to amend to the TPFA, is to modify the flux expression (4.7) to include more points in the flux stencil. The result is the so called multi-point flux approximations (MPFA), which were developed independently by Aavatsmark et. al. [8], and Edwards and Rogers [80], and further studied in i.e. [9, 10, 11, 12, 81, 82, 153].

To obtain a local flux expression, MPFA methods introduce $interaction\ regions$. For most methods we are aware of, these are cells or subcells in the dual grid, see Figure 4.2(a). The only exception is the rarely used Z-method. The shape of the interaction region differs from method to method. However, the construction of the schemes have many similarities. We will therefore describe the general procedure before we go on to discuss the two most commonly applied methods. All considerations in this thesis are in two dimensions.

From Figure 4.2(a), we see that the interaction regions divide each cell into

several subcells. In each of these subcells, the potential is approximated by a linear function. The function is determined by the values in the cell centre, and in one point on each edge, see Figure 4.2(b). These three points span a $variational\ triangle$. Thus, on subcell i, the potential approximation can be expressed as

$$u_i = \sum_{j=1}^{3} u_{i,j}\phi_{i,j}\,. \tag{4.8}$$

Here $u_{i,j}$ is the potential values in the cell centre and the points at the edge, see Figure 4.2(b). The basis functions $\phi_{i,j}$ are linear, with value 1 in one vertex of the variational triangle, and 0 in the others. The gradient of the potential can be used to find an approximation of the flux through a half-edge seen from one cell. The flux through the half-edge can also be approximated by the potential in the adjacent cell. This can be done for all half-edges in the interaction region. By requiring continuity of all the fluxes, we get a linear system of equations

$$\mathbf{A}\bar{\mathbf{u}} = \mathbf{B}\mathbf{u}\,, \tag{4.9}$$

where $\bar{\mathbf{u}}$ and $\mathbf{u}$ are potential values at the edges and at the cell centres, respectively. We invert $\mathbf{A}$ to get $\bar{\mathbf{u}} = \mathbf{A^{-1}B}\mathbf{u}$. The flux over the edges can be expressed as

$$f = \mathbf{C}\bar{\mathbf{u}} + \mathbf{D}\mathbf{u}\,, \tag{4.10}$$

and by substituting the expression for $\bar{\mathbf{u}}$, we get

$$f = (\mathbf{C}\mathbf{A}^{-1}\mathbf{B} + \mathbf{D})\mathbf{u} = \mathbf{T}\mathbf{u}\,. \tag{4.11}$$

The elements in $\mathbf{T}$ are the transmissibilities for the half-edges in the interaction region. The fluxes over the edges are found by summing the half-edge fluxes. The set of all cells contributing to the flux over an edge form a $flux\ stencil$, see Figure 4.3(a), whereas the $cell\ stencil$ of a cell is the union of the flux stencils for all the cell's edges, confer Figure 4.3(b). Requiring conservation of mass yields a global system of linear equations with the potentials in the cell centres as unknowns. The bandwidth of the resulting system matrix equals the size of the cell stencils.

Boundary conditions can be handled by modifying the Equations (4.9)-(4.10). In reservoir simulation, homogeneous Neumann conditions are prevailing. They can easily be implemented by applying ghost cells with zero permeability. Ghost cells can also be used to implement interpolated Dirichlet conditions. For handling of non-homogeneous Neumann conditions and non-interpolated Dirichlet conditions, we refer to [50, 87, 171].

We also remark that the use of interaction regions based on the dual grid allows for assigning different permeability tensors to each subcell, and thus incorporate more information from the geological model. However, this approach is rarely used in practice.

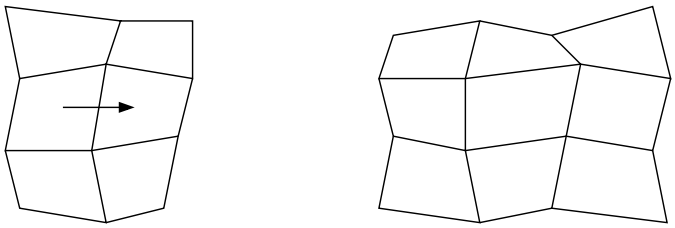

(a) Flux stencil (b) Cell stencil

Figure 4.3: A flux stencil and a cell stencil for the MPFA O-method on a quadrilateral grid.

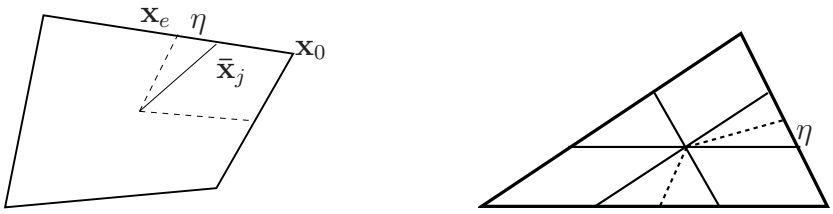

(a) The continuity point (b) The O(1/3)-method for triangles

Figure 4.4: The continuity point for the O-method is determined by η, as shown to the right. To the left, the O(1/3)-method on triangles. Note that the variational triangles are part of parallelograms.

4.4.1 The O-Method

The O(η)-method can be considered the basic MPFA scheme. It can be applied both in two and three dimensions, and for most grid topologies. However, it has problems with handling hanging nodes, see [17].

The interaction region for the O-method consists of all cells sharing a vertex, yielding an O-shaped region like the one showed in Figure 4.2(a). Thus there are $3\,n_c$ degrees of freedom, where n_c is the number of cells in the interaction region. We use $2\,n_c$ degrees of freedom to impose continuity of the fluxes, and to lock the values in the cell centres. With the remaining n_c degrees of freedom, continuity of the potential is enforced in one point on each half-edge. The location of the continuity point is determined by the parameter η, by the relation

$$\bar{\mathbf{x}}_j = \eta\,\mathbf{x}_0 + (1-\eta)\mathbf{x}_e\,, \tag{4.12}$$

where $\mathbf{x}_e$ is the midpoint of the edge, and $\mathbf{x}_0$ is the vertex in the centre of the interaction region. Hence, η measures the relative distance from the midpoint of the edge to the continuity point for the potential, see Figure 4.4(a). On quadrilateral grids, the two common choices for η are 0 and 0.5, see e.g. [5] and [81],

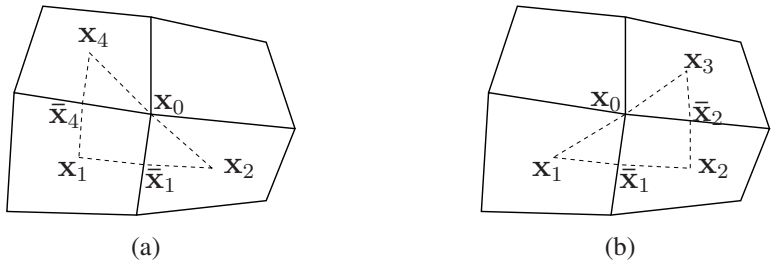

Figure 4.5: The two possible variational triangles for the L-method.

respectively. On triangular grids $\eta = 1/3$ has been investigated in [95, 135].

For quadrilateral grids in two dimensions, the O-method in general yields a 9-point cell stencil. In three dimensions, the cell stencil consists of 27 cells. Note that for $\mathbf{K}$-orthogonal grids, the O(0)-method will reduce to TPFA. For quadrilateral grids, $\boldsymbol{K}$-orthogonality is also the only case in which the system matrix yields an M-matrix for this choice of η.

If the transmissibilities are computed in physical space, the O-method applied to a quadrilateral grid will be symmetric only if the cells are parallelograms. Symmetry can be obtained by a mapping to reference space, however, to this is achieved to the price of deteriorated the convergence properties [13]. On triangular grids, the O(1/3)-method with discretisation in physical space will always be symmetric. This is due to the variational triangles being parallelograms, see Figure 4.4(b).

4.4.2 The L-Method

For high anisotropy ratios, the O-method is known to suffer from spurious internal oscillations. This will be further discussed in Section 4.5. The shortcomings of the O-method have motivated development of other MPFA methods. The L-method was introduced for quadrilateral grids in [17], although it was originally discovered in [177] as a method with optimal properties with respect to avoiding internal oscillations. Further, the L-scheme can handle hanging nodes, thus it is a natural choice for local grid refinement. A method for three dimensional problems was introduced in [15].

In two dimensions, the interaction region for the L-method consists of three cells. This gives us 9 degrees of freedom, out of which 3 are used to lock the values in the cell centres. The remaining degrees of freedom are sufficient to ensure continuity of both the potential and the flux over the entire half-edges. Consider Figure 4.5(a). The flux over half-edge $\mathbf{x}_0\bar{\mathbf{x}}_1$ can be computed by using the cells 1,2, and 4. However, as indicated by Figure 4.5(b), we can also use the cells 1,2,

and 3. The two possible interaction regions give two sets of transmissibilities for the half-edge $\mathbf{x}_0\bar{\mathbf{x}}_1$. Let t_1 and t_2 be the transmissibilities for the half-edge computed with cell 1 and 2 as the central cell in the interaction region, respectively. If $|t_1| < |t_2|$, we use the values computed with cell 1 as the central cell, if not use cell 2. For a uniform grid in a homogeneous medium, this selection criterion will chose cells aligned with directions of high conductivity. The selection criterion is defined so that the system matrix will be an M-matrix for a large range of grid parameters, confer Section 4.5.3. A further motivation can be found in [17].

The cell stencil of the L-method consists of 7 cells if the cells are uniform parallelograms and the medium homogeneous, and increases to 9 for general quadrilaterals and permeabilities. In three dimensions, the stencil has 13 cells. We also remark that if the grid is $\mathbf{K}$-orthogonal, the L-method reduces to a two-point flux approximation. The L-method does not render a symmetric system matrix.

4.4.3 Convergence

There is no independent theory of convergence for MPFA methods. However, the schemes can be considered as either mixed finite element methods or mimetic finite difference methods (see Section 4.7), with numerical quadrature. Analytical convergence results based on this relation can be found in [138, 135, 136, 139, 226] for the O-method, and [209] for the L-method. Numerical convergence of MPFA methods is studied in e.g. [17, 14, 16, 86, 182]. For smooth solutions and rough grids, these numerical investigations indicate second order convergence for the potential, and first order convergence for the edge flux. However, the half-edge fluxes are known to exhibit a reduced convergence rate [139]. For solutions with low regularity, the convergence rates are in agreement with finite element theory.

4.4.4 Other Multi-Point Methods

For completeness, we mention some MPFA methods and related schemes that are not discussed here. The MPFA Z-method, is constructed by using parts of two cells in the dual grid, see [178]. This improves the monotonicity properties of the O-method in highly anisotropic media. The U-method was introduced together with the O-method [8] to reduce the size of the cell stencils, and thereby the bandwidth of the system matrix. There is also an Enriched MPFA method [53], which is an extension of the O-method, with improved monotonicity properties. Similar work is also done in [85].

The notion of multi-point methods used in this thesis can somewhat loosely be defined as methods that are formulated with an interaction-region framework, and use more than two cell values to approximate the flux. A more straightforward interpretation of the name could consider all schemes that yield flux stencils

with more than two points, which would include a vast number of methods. The definition used here is, however, commonly used in the reservoir simulation community.

4.5 Monotonicity

As mentioned in the beginning of this chapter, the solution of elliptic equations fulfils a maximum principle (for a precise definition, see below). This guarantees that the solution will be free of internal oscillations, and the maximum principle should be preserved when the equation is discretised. Questions related to preservation of maximum principles and to avoid spurious internal oscillations for elliptic equations have become known as *monotonicity* issues. A major part of the present work has been devoted to investigations related to monotonicity and control volume methods, with special emphasis on MPFA methods. The results are given in Papers A and B, and also the additional Paper F. In the following, we give background information on monotonicity for elliptic equations.

4.5.1 Motivation

We say that a numerical method is monotone if it fulfils the discrete maximum principle stated below. The importance of applying monotone methods is illustrated in Figure 4.6. The figure shows two solutions of Equation (4.1), where the right hand side is a point source, and the boundary conditions are $u = 0$. The transition from the peak at the source to the minima on the boundary should be smooth, as seen in Figure 4.6(a). However, if the numerical solution scheme is non-monotone, we can get internal oscillations, and false global extrema, see Figure 4.6(b).

Monotonicity issues also arise for the Multiscale Finite Volume method discussed in Section 4.7.3. False internal oscillations in the potential can also cause problems for streamline methods. Further, reordering methods for non-linear problems [145] and transport methods [172] also show sensitivity to monotonicity issues.

It is important to notice that since the MPFA methods by construction reproduce uniform flow exactly, they tend to robust even if applied to problems outside their region of monotonicity. One example of this can be seen to the end of Paper B. In other words, even if a discretisation violates necessary conditions for monotonicity, this is not sufficient to yield oscillating solutions when the discretisation is applied to a specific problem. Non-monotone behaviour is most often seen in highly non-linear flow regimes, e.g. near wells.

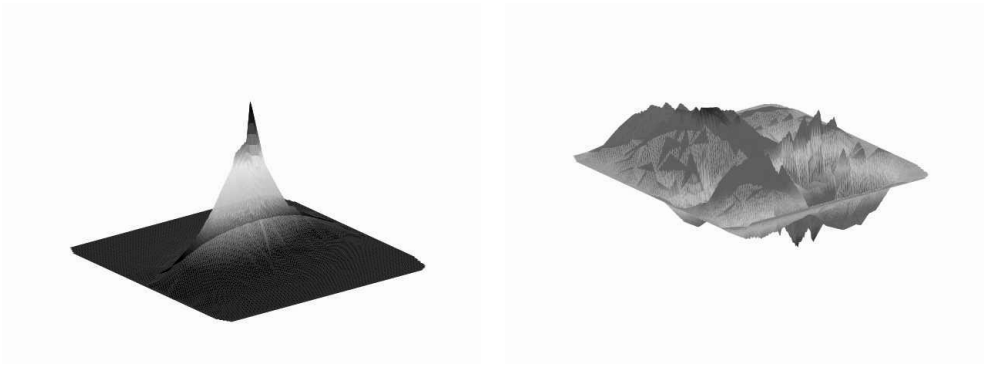

(a) Monotone (b) Non-monotone

Figure 4.6: The figure shows two numerical solutions of a problem with a point source in the middle of a domain, and homogeneous Dirichlet boundary conditions. The smooth solution to the right is obtained from a monotone method. To the left, a highly oscillatory solution produced by a non-monotone method. Note that the entire setup (including the grid) is identical for the two figures.

4.5.2 Maximum Principles

We consider the elliptic model equation (4.1), stated for a domain Ω. This solution then fulfils a maximum principle, which can be stated as follows [115]:

Hopf's first lemma
Let the permeability tensor be continuously differentiable and let the boundary be sufficiently smooth. Further, let the source/sink term q be non-negative in a domain $\omega \subseteq \Omega$. The, the solution u of Equation (4.1) has no local minima in ω, i.e., there is no point $\boldsymbol{x}_0 \in \omega$ such that $u(\boldsymbol{x}_0) < u(\boldsymbol{x})$ for all other $\boldsymbol{x}$ in a neighbourhood of $\boldsymbol{x}_0$.

The maximum principle, or equivalently Hopf's first lemma, should be preserved in the discretisation. Since the term internal oscillation is not defined for a discrete solution, it is not straightforward to define a discrete analogue of Hopf's lemma. To motivate the definition, we introduce a Green's function $G(\boldsymbol{\xi}, \mathbf{x})$ to express the solution of the elliptic equation. To test if the solution is free of local minima on a domain ω, we impose homogeneous Dirichlet conditions on $\partial\omega$. Then, the solution of Equation (4.1) can be written

$$u(\mathbf{x}) = \int_{\omega} G(\boldsymbol{\xi}, \mathbf{x}) q(\boldsymbol{\xi}) \, d\tau_{\boldsymbol{\xi}} \,. \tag{4.13}$$

If the solution has no internal oscillations, it should decrease from a maximum at the sources to 0 at the boundary, i.e. the solution is positive inside ω. Hence, we see that if a non-negative q is to imply a non-negative u, G must be everywhere non-negative;

$$G(\boldsymbol{\xi}, \mathbf{x}) \geq 0\,. \tag{4.14}$$

A linear discretisation method will give a system of linear equations

$$\mathbf{A}\mathbf{u} = \mathbf{q}\,, \tag{4.15}$$

where $\mathbf{A}$ is the discretised operator, and $\mathbf{u}$ and $\mathbf{q}$ are the solution and the sink/source term in the grid blocks, respectively. The solution of the linear system reads $\mathbf{u} = \mathbf{A}^{-1}\mathbf{q}$, thus $\mathbf{A}^{-1}$ can be considered a discrete Green's function. Now, a positive right hand side should render a positive solution. This is fulfilled if the discrete equivalent of Eq. (4.14)

$$\mathbf{A}^{-1} \geq 0\,, \tag{4.16}$$

where the inequality is interpreted in the element-wise sense. When the inequality (4.16) holds, we say that the matrix $\mathbf{A}^{-1}$ is monotone, while $\mathbf{A}$ is inverse monotone.

To impose homogeneous Dirichlet conditions on a subdomain gets a bit involved. The boundary conditions are implemented using ghost cells. Thus, the boundary is defined as a set of cell centres, and the linear interpolation between them. This curve resembles a possible iso-contour for the solution. If there is a positive source/sink inside the curve, and the curve happens to be an iso-contour, we want our numerical solution to honour Hopf's lemma; it should be positive inside the curve. This is achieved if the restricted system matrix is inverse monotone. However, for Hopf's lemma to be valid on the domain bounded by this piecewise linear curve, the boundary must have certain properties specified below. Thus we get the following definition of the discrete maximum principle, formulated in Paper A:

A discrete maximum principle
For any subgrid bounded by a closed Jordan curve, with homogeneous Dirichlet conditions, the discretisation must yield a system matrix, whose inverse has no negative elements. The boundary conditions are implemented by using ghost cells. The boundary of the subgrid is defined by the linear interpolation of the cell centres of the surrounding cells.

We call numerical schemes which have this property *monotone methods*. It is important to note that violations of the discrete maximum principle does not rule out convergence of the numerical solution and vice versa. Indeed, a convergent solution can exhibit spurious oscillations on every refinement level.

The discrete maximum principle does not involve discretisation of boundary conditions on $\partial\Omega$. That is partly covered by the following result [116]

Hopf's second lemma
If the solution of Equation (4.1) with a smooth boundary and continuously differentiable $\mathbf{K}$ has a maximum on the boundary, there must be a non-zero flow through the boundary.

From a physical point of view, it is obvious that a stationary solution (no time dependency) cannot have a maximum on a no-flow boundary. However, by Hopf's second lemma, non-physical values on the boundary are related to the maximum principles. Moreover, in reservoir simulation, homogeneous Neumann conditions are prevailing. Investigations of whether discretisations fulfill discrete maximum principles should therefore involve tests with no-flow boundaries.

4.5.3 Sufficient Condition for Monotonicity of Control Volume Methods

To test directly whether a discretisation of Equation (4.1) fulfils the discrete maximum principle we must invert system matrices for all subgrids fulfilling the requirements. The computational complexity makes this task undesirable. Therefore, there has in recent years been an effort to derive sufficient conditions for a control volume method to yield a monotone discretisation of the elliptic model equation.

One class of matrices that are inverse monotone is the *M-matrices*. An M-matrix is an invertible matrix with positive diagonal elements and non-positive off-diagonal elements [102]. The TPFA method always yields an M-matrix on the main grid, as well as on subgrids, hence it is always monotone. For MPFA methods, the situation is more complex. For instance, the O(0)-method on quadrilaterals does not render an M-matrix unless the grid is $\mathbf{K}$-orthogonal, when the discretisation reduces to a TPFA. Still, the system matrix for the O(0)-method is inverse monotone for more general grids. M-matrix analysis for other choices of η can be found in e.g. [81]. Thus, we need criteria that take into account matrices with positive off-diagonal elements, and still fulfill the discrete maximum principle.

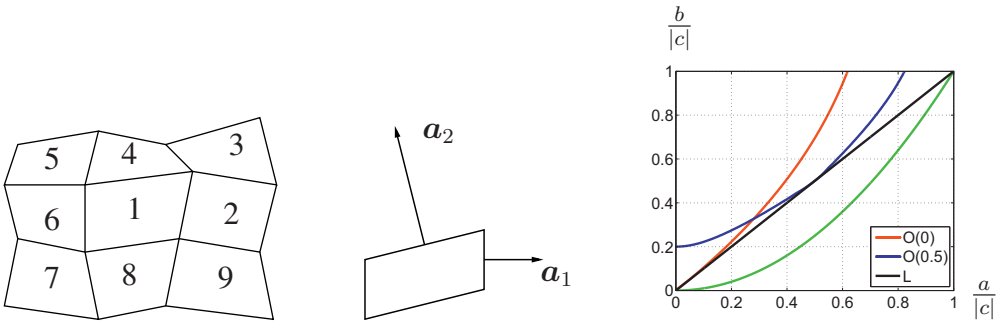

(a) Local numbering (b) Parameters (c) Monotonicity regions

Figure 4.7: To the left, the local numbering for the monotonicity conditions is shown. The figure in the middle shows the parameters in Equation (4.18). To the right, monotonicity regions for three MPFA methods for a parallelogram grid in a homogeneous medium are shown. The green line shows the elliptic bound $\sqrt{ab} = |c|$.

In [175] Nordbotten and Aavatsmark derived sufficient conditions for monotonicity on uniform parallelogram grids in homogeneous media. The derivation is based on constructing the discrete Green's function (i.e. $\mathbf{A}^{-1}$) in a dimension by dimension manner. Their arguments are, however, quite complicated and extensions of the technique to more general media and grid topologies seem out of reach.

By utilising a splitting of the system matrix, Nordbotten et. al. [177] extended the results from [175] to general quadrilateral grids. The splitting follows the grid topology, based on the two natural directions in a quadrilateral grid. The analysis holds for all linear control volume methods that lead to a 9-point cell stencil. Let m_i be the contribution to the system matrix corresponding to cell i, the local numbering is shown in Figure 4.7(a). The results in [177] require $m_1 > 0$ and $\max(m_2, m_4, m_6, m_8) < 0$. Further, the contribution from the corner cell 3 must obey an inequality of the form

$$m_2^{i,j} m_4^{i,j-1} - m_3^{i,j-1} m_1^{i,j} > 0\,. \tag{4.17}$$

Here, the superscripts (i, j) refer to grid row and column index. Similar constraints apply to m_5, m_7, and m_9. Thus, the system matrix can be inverse monotone even if the elements corresponding to corner cells are positive.

The analysis in [177] also considered the special case of MPFA methods applied to uniform grids in homogeneous media. Let $\mathbf{K}$ denote the permeability in the medium. Further, let $\boldsymbol{a}_1$ and $\boldsymbol{a}_2$ be normal vectors to the cells, with length equal to their respective edges, see Figure 4.7(b). Then the monotonicity properties of the MPFA methods can be visualised by quantities a, b, and c, defined

by

$$\begin{bmatrix} \boldsymbol{a}_1 & \boldsymbol{a}_2 \end{bmatrix}^T \boldsymbol{K} \begin{bmatrix} \boldsymbol{a}_1 & \boldsymbol{a}_2 \end{bmatrix} = \frac{1}{V} \begin{bmatrix} a & c \\ c & b \end{bmatrix} , \tag{4.18}$$

where V is the area of the cell. Note that for $\boldsymbol{K}$ to be positive definite, we must have $ab > c^2$. The monotonicity regions are shown in Figure 4.7(c). The sufficient conditions seem to indicate that no linear methods are monotone below the line $a/|c| = b/|c|$. The MPFA L-method is ideal in the sense that it is monotone whenever $b \geq a$, whereas both the O-methods have reduced monotonicity regions. We remark that the L-method yields an M-matrix whenever it is monotone.

The analysis and numerical experiments in [177] did not, however, include tests on convex subgrids. Such grids were considered in Paper A, with the result that most of the conditions derived in [177] are necessary as well as sufficient. Monotonicity for MPFA methods on triangular grids are considered in Paper B.

We also remark that for Voronoi grids, all cells that share a vertex will also share an edge. By imposing the discrete maximum principle on subgrids consisting of two cells sharing an edge, it can be shown that for the discretisation to be monotone, it must yield a system matrix that is an M-matrix.

Monotonicity for Parabolic Equations

The elliptic model Equation (4.1) was derived from the equation for single phase flow (2.12) under an assumption of incompressibility. The flow of a weakly compressible fluid is governed by a linear parabolic equation, see Section 2.2. Monotonicity properties for discretisations of such equations were studied in [120]. The compressibility terms impose additional restrictions for the solution to be free of spurious oscillations. The corner-elements $m_3, m_5, m_7,$ and m_9 can still be positive, but their magnitudes must be smaller than what is sufficient for incompressible flow. Also worth noticing is that the region where the discretisation is monotone increases when the time step is increased.

4.6 Near-Well Discretisations

In our presentation of control volume methods, we have barely touched upon how to handle sink/source terms. Obviously, all the recovered hydrocarbons must flow through wells, thus a proper representation of the sink/source terms is crucial for the simulations. The importance of the well terms can be illustrated by considering the pressure equation; for a reservoir with no-flow conditions on the outer boundary, the flow pattern will to a large extent be determined by the wells. Data on the flow rate through a well, and the pressure at the well bore are among the

few sources to knowledge of what happens in the reservoir that are available in real time. This information is utilised in day-to-day reservoir management. Thus, there are many reasons why an accurate description of flow in the vicinity of wells is a key issue.

A part of this work has been devoted to investigations of control volume discretisations for flow in near-well regions. In the following, we give background information for numerical modelling of processes near wells. Results from the investigations can be found in Paper D.

4.6.1 Characteristics of Near-Well Regions

To illustrate the nature of near-well flow, we consider Equation (4.1) in a homogeneous reservoir. The reservoir contains a single well with flow rate q. If the medium is isotropic, the solution of Equation (4.1) reads

$$u = u_w + \frac{q}{2\pi k} \ln\left(\frac{r}{r_w}\right). \tag{4.19}$$

Here u_w is the pressure at the well bore, k is the (scalar) permeability, r is a radial coordinate, and r_w is the well radius. We note that the flow is purely radial, there is no angular dependency in the solution. Further, the solution varies logarithmically in the radial direction.

Equation (4.1) should be equipped with appropriate boundary conditions. On the well bore, either the pressure or the flux must be specified. For an isotropic medium, it seems evident that the well boundary condition should be uniform. If the permeability is anisotropic, the situation becomes somewhat more complicated. In a work addressing modelling of horisontal wells, Babu and Odeh apply a point sink/source representation of the well [27]. They argue that in an anisotropic medium, the iso-potential curves are ellipsis, and therefore the pressure varies along the well bore. According to Babu and Odeh, a uniform flux condition is the most correct boundary condition [28, 29].

Peaceman disagreed with the sink/source representation of the well, and argued in favour of assigning uniform pressure along the well bore. The anisotropic medium can be transformed to an isotropic medium. The relation between the physical coordinates (x, y) and (ρ, η) in the isotropic space reads

$$x = b\Big(\frac{k_x}{k_y}\Big)^{1/4} \sinh\rho \sin\eta\,, \tag{4.20}$$

$$y = b\Big(\frac{k_y}{k_x}\Big)^{1/4} \cosh\rho \cos\eta\,. \tag{4.21}$$

Here, we have assumed $k_x > k_y$. The constant b is given by

$$b^2 = \frac{r_w^2(k_x - k_y)}{\sqrt{k_x k_y}}\,. \tag{4.22}$$

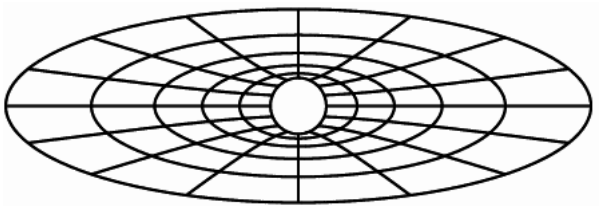

Figure 4.8: The flow pattern near a well in an anisotropic medium. The potential is uniform along the well bore, but the iso-contours turn ellipses away from the well. The streamlines are hyperbolas which are orthogonal to the potential contours.

Now, the potential is given by [187, 188]

$$u = u_w + \frac{q}{2\pi\sqrt{k_x k_y}}(\rho - \rho_w)\,, \tag{4.23}$$

where $\tanh^2(\rho_w) = k_x/k_y$. Further, Peaceman showed that on the well bore, uniform pressure and uniform flux are in fact equivalent. The iso-contours for the potential are circular at the well bore, but turn into ellipsis away from the well bore, as shown in Figure 4.8. The streamlines are orthogonal to the potential iso-contours, and thus are hyperbolas. The difference between the sink/source approach of Babu and Odeh and Peaceman's finite well bore model decreases rapidly as the distance from the well bore increases [190].

So far, we have tacitly assumed a homogeneous permeability field all the way up to the well bore. In reality, the rock near the well can be damaged during drilling. The permeability near the well can also be altered by injection of acids and/or hydraulic fracturing, both aimed at increasing the conductivity near the well. Such effects will modify the potential distribution described by (4.19), and the equation becomes [65]

$$u = u_w + \frac{q}{2\pi k}\Big(\ln\Big(\frac{r}{r_w}\Big) + S\Big)\,, \tag{4.24}$$

where S is called a skin factor. The modification of (4.23) is similar. For simplicity, we will set $S = 0$.

We consider the well bore as the boundary of our domain, that is, we assume infinite conductivity inside the well. In reality this is not true, and it might be necessary to couple the porous media model to a hydraulic model for flow inside the well. These issues will not be pursued further in this work.

4.6.2 Well Index Approaches

The main challenge in modelling near-well flow is the difference in scale. The radius of the well bore will normally some centimetres, while the size of the reservoir can be several kilometres. For a well block with a size of meters, it may be

reasonable to consider the well as geometric point. The numerical scheme itself is not adapted to the flow in the near-well region. We emphasis that representing the well as a point sink/source in the numerical scheme is not equivalent to the point sink/source solution to the analytical problem, presented by Babu and Odeh. Indeed, models for the interaction between the well and the surrounding grid can be constructed both from Babu and Odeh's point-source method, and Peaceman's finite well bore approach.

When the well is represented as a point sink/source, the computed pressure in the grid block containing the well, u_b, can differ significantly from the well bore pressure. The relation between the pressure difference $u_b - u_w$ and the well flow rate is usually calculated according to

$$q = \frac{WI}{\mu}(u_b - u_w)\,. \tag{4.25}$$

Here, WI is the *well index*, which depend on cell geometry, permeability field, well radius etc. For multiphase flow, (4.25) becomes

$$q_\alpha = WI\frac{k_{r,\alpha}}{\mu_\alpha}(u_b - u_w)\,. \tag{4.26}$$

The above expressions are commonly applied in commercial simulators, with an appropriate value of WI. Thus, the dynamics in the near-well region is represented by a well index, which is computed by upscaling.

Several authors have addressed the question of how to calculate the well index for various well configurations. The first thorough investigation of these matters was done by Peaceman in a series of papers. He defined an equivalent radius, r_e, where the steady state flow pressure is equal to the well block pressure. In an infinite, isotropic reservoir, with a uniform Cartesian grid with cell size h, the equivalent radius for an isolated well is given by [186]

$$r_e = 0.2h\,. \tag{4.27}$$

Now, let the medium be anisotropic with permeabilities k_x and k_y in the x and y direction, respectively. Further Δx and Δy represent the grid spacing. Then, r_e is defined by [187]

$$r_e = 0.28\frac{\left((k_y/k_x)^{1/2}(\Delta x)^2 + (k_x/k_y)^{1/2}(\Delta y)^2\right)^{1/2}}{(k_y/k_x)^{1/4} + (k_x/k_y)^{1/4}}\,. \tag{4.28}$$

In an anisotropic medium, the pressure at the equivalent radius is given by

$$u_e = u_w + \frac{q}{2\pi\sqrt{k_x k_y}}\ln\left(\frac{r_e}{r_w}\right). \tag{4.29}$$

Thus, (4.25), (4.28) and (4.29) together give us (with viscosity set to unity)

$$WI = \frac{q}{u_e - u_w} = \frac{2\pi\sqrt{k_x k_y}}{\ln(\frac{r_e}{r_w})}\,. \tag{4.30}$$

Peaceman's approach builds upon several simplifying assumptions. The grid blocks are assumed to be rectangular, and aligned with the principle permeability directions. The wells must be vertical and isolated, although an extension to the case of multiple wells within one grid block is considered in [189]. Despite these shortcomings, Peaceman's equivalent radii approach is applied in commercial simulators [204].

To increase the recovery factor, wells are drilled with highly complex trajectories. In onshore production, vertical wells are still predominating, partly due to low drilling costs. However, for offshore production, skew and horisontal wells with multiple branches are commonly drilled. Such *non-conventional* wells can intersect with grid blocks in an arbitrary manner. To upscale the near-well dynamics for such wells, more involved models are required. For general media, we have no analytical expressions for the potential near non-conventional wells. Instead, it is common to either consider simplified physical configurations where analytical solutions can be found, or resort to semi-analytical techniques, or even numerically computed solutions. Babu and Odeh proposed an analytical model to compute the well index in [27, 30]. Their method applies to horisontal wells in anisotropic, but homogeneous media. For more complex scenarios, a semi-analytical approach based on Green's functions was proposed in [229, 230]. Ding studied upscaling for heterogeneous near-well regions [71]. He found the classical upscaling methods that assume a linear flow regime inappropriate in the near-well region. Instead he proposed to adapt the upscaling to the non-linearity in the near-well dynamics. He applied a fine-scale pressure solve to compute equivalent coarse-scale transmissibilities and well indices. This approach was later developed in e.g. [72, 79]. Similar considerations can also be found in for instance [228].

We emphasis that the above presentation of approaches to near-well modelling by no means is a complete survey of the available schemes. Our intention is rather to point out that this is an unsolved topic, and thus there is a need for a more general and robust framework.

4.6.3 Applications of MPFA Methods to Near-Well Modelling

We here present a methodology for application of local grid refinement and control volume methods in near-well regions. The common numerical methods, such as

the control volume methods previously introduced, employ a linear reconstruction of the potential. In near-well regions, we expect the potential to be dominated by the well, and thus exhibit a logarithmic behaviour. Ding and Jeannin perform a truncation error analysis near singularities of control volume methods based on linear reconstruction [73]. They split the error into a 'regular' term, e_r, and a 'singular' term, e_s, stemming from the well, and the overall error, e, can be written

$$e = e_r + e_s = \mathcal{O}(h^2) + \mathcal{O}\Big(\frac{h^2}{r_w^2}\Big)\,, \tag{4.31}$$

where h is a measure of the grid block size. Near the well, we expect e to be dominated by e_s, and hence the truncation error will be small only if the grid blocks are smaller than the well radius.

To improve the performance of the control volume methods, Ding and Jeannin proposed to adapt the discretisation to the logarithmic potential profile. They introduce a mapping from the physical space $\mathcal{P}$ to a logarithmic reference space $\mathcal{R}$, according to

$$x = \quad e^{\rho}\cos\theta\,, \tag{4.32}$$

$$y = \quad e^{\rho}\sin\theta\,. \tag{4.33}$$

Here, (x, y) and (ρ, θ) are the coordinates in $\mathcal{P}$ and $\mathcal{R}$, respectively. A logarithmic potential in physical space will vary linearly in reference space, thus numerical methods based on linear reconstruction are appropriate. Moreover, the transformation is of polar-type, honouring the radial nature of near-well flow. The potential in $\mathcal{R}$ is the solution of an elliptic equation similar to (4.1), but with a transformed permeability $\hat{\mathbf{K}}$. Further, let $e_{\mathcal{P}}$ be an edge in physical space, and let $e_{\mathcal{R}}$ be its curvilinear image in reference space. Then the flux over the edge is preserved, that is

$$f = \int_{e_{\mathcal{P}}} \boldsymbol{n}\cdot(\mathbf{K}\nabla u)\,dS = \int_{e_{\mathcal{R}}} \hat{\boldsymbol{n}}\cdot(\hat{\mathbf{K}}\nabla u)\,dS\,. \tag{4.34}$$

where $\hat{\mathbf{n}}$ is normal to $e_{\mathcal{R}}$.

Since fluxes are conserved in the transformation between $\mathcal{P}$ and $\mathcal{R}$, and further the potential varies linearly in $\mathcal{R}$, it is natural to consider discretisation in reference space instead of physical space. In [73], Ding and Jeannin investigate this approach for a Cartesian grid. They show that if the transmissibilities are computed in $\mathcal{R}$ by an MPFA method, the total error is $\mathcal{O}(h^2/r)$. The well is considered a point sink/source inside the well block in $\mathcal{R}$. However, the numerically computed potential in the cell containing the block is a good approximation to the actual pressure at the well bore. That is, the transmissibilities computed in reference space can be considered a well index.

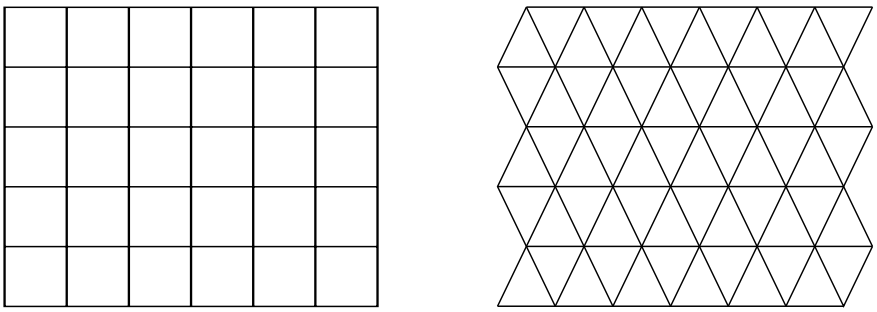

(a) Quadrilaterals (b) Triangles

Figure 4.9: Illustration of the near-well grids in $\mathcal{R}$. The spacing in radial direction is equidistant.

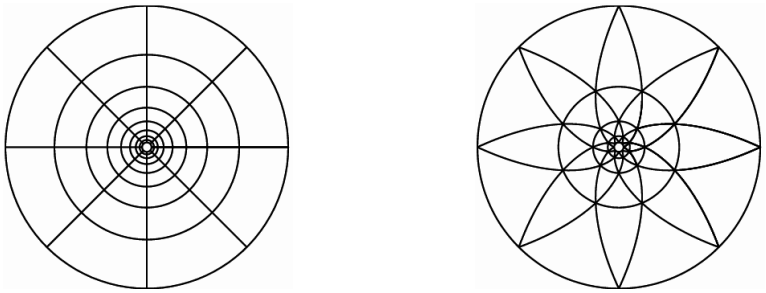

(a) Quadrilaterals (b) Triangles

Figure 4.10: Illustration of near-well grids with logarithmic refinement shown in physical space. The transmissibilities are computed in $\mathcal{R}$, and the edges are mapped to curved lines in $\mathcal{P}$.

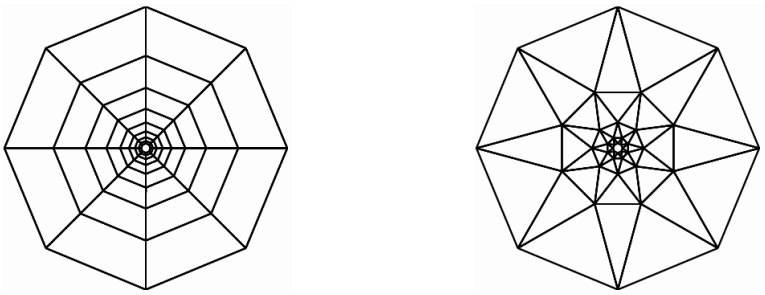

(a) Quadrilaterals (b) Triangles

Figure 4.11: Illustration of near-well grids with logarithmic refinement, and discretisation in physical space. The edges are straight lines in $\mathcal{P}$. Note that the well bore is approximated by a polygon.

Another approach to well modelling is to create a grid that follows the well bore itself, and describe the physical parameters at there. Thus, the boundary condition on the well bore is treated as a boundary condition also in the numerical scheme. This is in contrast to all previously discussed methods, where the well is discretised as a point sink/source. Ding and Jeannin suggested this approach using flexible grids, i.e. triangles or general polyhedra, in the near-well region [74]. In Paper D, we follow up their work with a systematic test of different options for near-well modelling with radial-like grids. We adapt to the logarithmic potential profile by creating grids with equidistant spacing in the radial direction in $\mathcal{R}$, thus when transformed to $\mathcal{P}$, the grids adapt to the logarithmic potential profile. The grid cells can be either isosceles triangles or quadrilaterals, see Figure 4.9(a) and 4.9(b). On both grids, the elliptic equation is discretised by MPFA methods, with the transmissibility calculation performed either in reference space, or in physical space. Since the potential varies linearly in $\mathcal{R}$, we expect discretisations in reference space to do well. A discretisation in physical space apply a linear reconstruction of the potential, which was shown insufficient by Ding and Jeannin for uniform Cartesian grids. However, since the grid cells are distributed according to the logarithmic behaviour, the drop in the potential between cells aligned in the radial directions is approximately constant. Therefore, we hope that a linear reconstruction suffice to capture the flow pattern.

The grid edges are straight lines in the discretisation space. If the the transmissibilities are computed in $\mathcal{R}$, the grid has curved edges in physical space, as shown in Figure 4.10(a) and 4.10(b). If the elliptic equation is discretised in $\mathcal{P}$, the edges will be non-curved, see Figure 4.11(a) and 4.11(b). Note that when discretising in $\mathcal{P}$, we approximate the well bore by a polygon.

When local grid refinement is applied in the near-well region, the near-well grid must be coupled with the surrounding global grid. In Paper D, the global grid is triangular, and the near-well region is considered a constraint in the global triangulation. Note that if the global grid was quadrilateral, say, the transition zone between the near-well grid and the surrounding grid can still be covered by triangles. In this way, we can ensure a smooth transition from logarithmic to linear gridding. Another way to handle the coupling can be found in [192].

4.7 Other Locally Conservative Methods

In addition to the control volume methods, there are several other locally conservative methods that handle discontinuous permeability tensors. A recent overview and comparison of some methods can be found in [137]. We here briefly discuss some choices that are commonly considered in the reservoir simulation community.

4.7.1 Mixed Finite Elements

As mentioned in Section 4.1, the elliptic model equation (4.1) can be written in weak form that reads; find $u \in L^2$ and $\mathbf{q} \in H(\mathrm{Div}, \Omega)$ such that

$$\int_\Omega \mathbf{p}^T \mathbf{K}^{-1} \mathbf{q} + u(\nabla \cdot \mathbf{p})\, dV = 0\,, \qquad \forall\, \mathbf{p} \in H(\mathrm{Div}, \Omega)\,, \tag{4.35}$$

$$\int_\Omega v(\nabla \cdot \mathbf{q} - q)\, dV = 0\,, \qquad \forall\, v \in L^2\,. \tag{4.36}$$

For a derivation of the weak form, and definition of the *Sobolev space* $H(\mathrm{Div}, \Omega)$ confer e.g. [41, 194].

The *mixed finite element* (MFE) method seeks for approximations $(u_h, \mathbf{q}_h)$ to u and $\mathbf{q}$ in finite dimensional subspaces $V_h \subset L^2$ and $W_h \subset H(\mathrm{Div}, \Omega)$, respectively. Here, u_h is associated with pressure values in the cells, while $\mathbf{q}_h$ represents fluxes over the edges. For first order methods, there is one pressure unknown for each cell, and one flux unknown for each edge. Higher order methods have more degrees of freedom. For stability of the MFE method, the approximation spaces V_h and W_h must be chosen such that a *coersivity* and an *inf-sup* condition hold, see e.g. [37, 44]. In two dimensions, families of approximation spaces are constructed for triangles and quadrilaterals, for definitions and consideration see e.g. [24, 42, 195]. For three-dimensional problems the MFE method is defined for tetrahedral and hexahedrals, see e.g. [43, 173], and also [179] and the references therein. Note, however, that if the hexahedral cells are more irregular than slightly perturbed parallelepipeds, no approximation spaces have been published so far.

The MFE method has a good theoretical foundation, see e.g. [76]. Applications to reservoir simulation can be found in for instance [56, 78]. However, the method has drawbacks that so far have limited the usage in industry. The Equations (4.35)-(4.36) form a saddle-point problem, and the discretisation renders an indefinite symmetric linear system with both pressure and velocity variables as unknowns. Local flux expressions for MFE methods are only known in special cases [224]. Because of its high computational complexity, the MFE method is mostly applied in IMPES formulations.

4.7.2 Mimetic Finite Differences

The *mimetic finite difference* (MFD) methods provide a framework to obtain discretisations that preserve, or mimic, certain properties of the continuous operator. For elliptic conservation laws, the MFD methods define approximation spaces P_h for the scalar variables (potentials) and F_h for the edge fluxes. In P_h we define an

inner product by

$$[\boldsymbol{p}, \boldsymbol{q}]_{P_h} = \sum_i |V_i| p_i q_i \,, \qquad \boldsymbol{p}, \boldsymbol{q} \in P_h \,, \tag{4.37}$$

where the sum is taken over all cells, $|V_i|$ represents the volume of cell i, and p_i and q_i contain the cell values. The construction of the inner product in F_h is somewhat involved. For each cell C, we define

$$[\mathbf{f}, \mathbf{g}]_C = \mathbf{f}^T \mathbf{M}_C \mathbf{g} \,. \tag{4.38}$$

Here $\mathbf{M}_C$ is a symmetric, positive definite matrix of dimension $n_e \times n_e$, where n_e is the number of edges for the cell C. Further, $\boldsymbol{f}$ and $\boldsymbol{g}$ store fluxes over the edges of C. The construction of the matrix $\mathbf{M}_C$ is non-trivial. Sufficient conditions for existence are given in [45]. Details on how to construct the matrix and analysis of the resulting schemes can be found in [47, 158]. Note that the construction is not unique. The inner product in F_h is now defined as

$$[\mathbf{f}, \mathbf{g}]_{F_h} = \sum_C [\mathbf{f}, \mathbf{g}]_C \,, \qquad \mathbf{f}, \mathbf{g} \in F_h \,, \tag{4.39}$$

with summation over all cells. The divergence operator DIV is readily defined as a sum over edge fluxes;

$$(DIVG)_C = \frac{1}{|V_C|} \sum_{i=1}^{n_e} G_i |e_i| \,, \tag{4.40}$$

where the sum is taken over the edges of the cell, G_i is the edge flux, and e_i is the length of the edges. Finally, we can write a discrete Green's formula as

$$[\mathbf{f}, GRADp]_{F_h} = [p, DIV\mathbf{f}]_{P_h} \,, \qquad \forall\, \mathbf{p} \in V_n \,, \forall\, \mathbf{f} \in W_n \,. \tag{4.41}$$

This gives an implicit definition of the discrete gradient $GRAD$. The MFD discretisation of Equation (4.1) now reads; find $\mathbf{u}_h \in P_h$ and $\mathbf{q}_h \in F_h$ such that

$$\mathbf{q}_h = GRAD\mathbf{u}_h \,, \tag{4.42}$$

$$DIV\mathbf{q}_h = \mathbf{b} \,, \tag{4.43}$$

where $\mathbf{b}$ represents the sink/source terms.

The MFD method is appealing due to its applicability to general grids, and a solid theoretical foundation for single phase problems. Convergence proofs for the method are given in [45, 46]. However, like in the mixed finite element formulation, the flux in the MFD method is a global function of the potential, and the resulting linear system is of saddle point type. One notable exception is the local method presented in [160], which is identical to the MPFA O(1/3)-method. Regarding extensions to multiphase flow, the only applications we are aware of are the multiscale methods mentioned next.

4.7.3 Multiscale Methods

The flow in porous media have characteristic features on a multiple of length scales, and information on geological properties such as permeability is available on a much finer resolution than what can be handled by standard techniques. The computational cost is especially severe for the pressure equation, due to its global domain of dependence. We touched upon this problem in Chapter 1, where we mentioned upscaling techniques as a tool to represent the parameters on a scale that can be handled by the computer resources available. However, this approach leaves much of the fine-scale information available unused after the upscaling.

In multiscale (MS) methods, coarse and fine scale descriptions of the medium are combined in ways that attempt to combine the computational efficiency of a coarse scale algorithm and the accuracy of the fine scale. A vast number of multiscale methods have been proposed, and we describe only some of the methods studied in the reservoir simulation community. For simplicity, we will stick to a two-level method in our outline. In the methods we consider, both a fine and a coarse grid are constructed, so that the coarse grid cells define subdomains for the fine grid. By solving local fine scale problems, one can obtain a coarse scale operator for the pressure that incorporates fine scale features. The coarse scale problem has fewer degrees of freedom than the original fine scale problem, and its solution can be found faster. So far, the procedure resembles upscaling of the pressure equation. However, contrary to an upscaling method, a MS method provides a way to obtain the pressure and, for the methods applied to reservoir simulation, mass conservative fluxes on the fine scale. The velocity field can be used to solve transport equations on the fine scale.

Since MS methods for elliptic problems were introduced in [118], a vast number of different methods have been introduced, see e.g. [131]. There are MS methods that applies techniques from MFE [1, 58] and MFD [4, 157]. The control volume methods that have been the primal focus of this work have their multiscale extension in the Multiscale Finite Volume (MSFV) method [121, 122]. The MSFV method has been formulated to handle a large range of physical problems [123, 154, 162, 163]. Also, since it is based on control volume methods, it is a natural candidate for incorporation into industrial codes. However, the monotonicity issues discussed in Section 4.5 may limit the applicability to realistic problems.

The idea of considering the problem on multiple levels, and dividing the fine scale grid into subdomains is also found in the domain decomposition (DD) methods. Indeed, links between multiscale methods and DD are studied in [2, 3, 176].

Chapter 5

Hyperbolic Discretisation Principles

In Chapter 2 we saw that the mass variables are governed by equations that have an hyperbolic nature. This chapter is devoted to techniques for discretising hyperbolic equations. Like in the previous chapter, we mainly consider schemes that are used in the mainstream commercial simulators of today, i.e. control volume methods. At the end of the chapter, we will briefly review alternative approaches.

5.1 Preliminaries

Hyperbolic equations have a quite different nature from the elliptic equations considered in the last chapter. They propagate information with finite speed, allowing for explicit time stepping methods, cf Chapter 3. The solution of hyperbolic equations can exhibit discontinuities, or $shocks$. Consider the prototype hyperbolic model equation for an unknown c in one dimension

$$\frac{\partial c}{\partial t} + \frac{\partial f(c)}{\partial x} = 0\,. \tag{5.1}$$

Here, $f(c)$ is a possibly non-linear flux function. Now, assume that the solution experience a discontinuity, with value $c = c_R$ on one side, and $c = c_L$ on the other. The speed of the discontinuity, σ, can be found by the $Rankine-Hugoniot$ shock condition

$$\sigma = \frac{f(c_R) - f(c_L)}{c_R - c_L}\,. \tag{5.2}$$

However, there are two types of solutions that honours the Rankine-Hugoniot condition. One is a shock, where the solution jumps from one state to another.

The other is a continuous transition between c_R and c_L in rarefaction wave. For the solution to exhibit a proper shock, it must honour Oleinik's *entropy* condition

$$\frac{f(c) - f(c_L)}{c - c_L} \geq \sigma \geq \frac{f(c) - f(c_R)}{c - c_R} \,. \tag{5.3}$$

This holds for all c between c_L and c_R, no matter which of the initial values are largest. For a general flux function f, the solution can consist of multiple shocks and rarefaction waves.

5.1.1 Riemann Problems

A fundamental building block in many numerical methods for hyperbolic problems is the much studied *Riemann problem*. The Riemann problem consist of a non-linear hyperbolic equation like (5.1) with initial condition

$$c(x,0) = \begin{cases} c_L & x < 0\,, \\ c_R & x > 0\,. \end{cases} \tag{5.4}$$

A numerical method that approximates the flux over an edge using only function values in the two adjacent cells, must in practice solve a Riemann problem for each edge. The analytical flux for a Riemann problem with a general shaped flux function is given by

$$f(c) = \begin{cases} \min\limits_{c_L \leq c \leq c_R} f(c)\,, & \text{if } c_L \leq c_R\,, \\ \max\limits_{c_R \leq c \leq c_L} f(c)\,, & \text{if } c_R \leq c_L\,. \end{cases} \tag{5.5}$$

We remark that for a monotone f, the flux is simply either $f(c_L)$ or $f(u_R)$, depending on the initial data.

5.1.2 Hyperbolic Formulations

We now develop two formulations of the hyperbolic transport equations introduced in Chapter 2. For simplicity, we focus on flow of two incompressible, immiscible phases. The governing equations for this case were introduced in Section 2.3. If we define the concentration of phase α as $c_\alpha = \rho_\alpha S_\alpha$, and for simplicity set the porosity to 1 everywhere and ignore capillary forces, Equation (2.17) can be written

$$\frac{\partial c_\alpha}{\partial t} - \nabla \cdot (\rho_\alpha \lambda_\alpha \mathbf{K} \nabla (p - \rho_\alpha g z)) = q_\alpha \,. \tag{5.6}$$

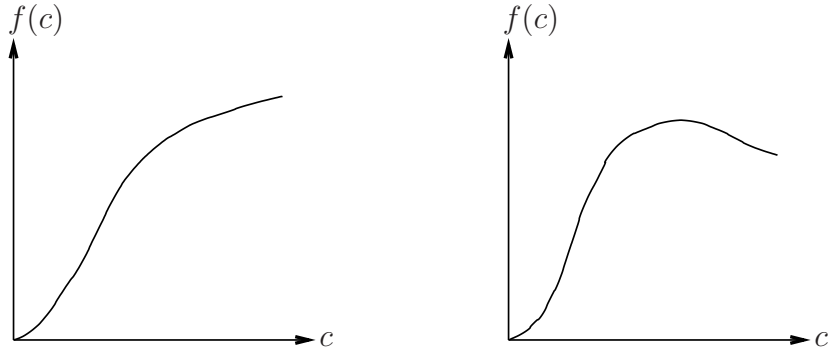

(a) Monotonic (b) Non-monotonic

Figure 5.1: Two possible flux functions. The function to the left is monotonic. The function to the right has a sonic point.

This is a hyperbolic transport equation for the concentrations. We refer to Equation (5.6) as the phase-based approach.

In the absence of capillary forces, the total velocity $\mathbf{q}_T$ can be written

$$\mathbf{q}_T = -\sum_\alpha \lambda_\alpha \mathbf{K} \nabla (p - \rho_\alpha g z) \,. \tag{5.7}$$

Now, we can rewrite Equation (5.6) to read

$$\frac{\partial c_\alpha}{\partial t} - \nabla \cdot (\rho_\alpha f_\alpha (\mathbf{q}_T - \mathbf{K} \nabla (p - \rho_{\beta \neq \alpha} g z) \lambda_{\beta \neq \alpha})) = q_\alpha \,. \tag{5.8}$$

Here we have introduced the fractional flow function $f_\alpha = \frac{\lambda_\alpha}{\lambda_T}$. Hereafter, we will refer to Equation (5.8) as the fractional flow or total velocity formulation.

The total velocity field will normally vary slower in time than the phase velocities. Therefore, the fractional flow might be the more robust formulation, however, it might be more difficult to apply. Consider the methods in one spatial dimension, written on the form of Equation (5.1). The monotonic flux function ($f' > 0$) shown in Figure 5.1(a) is representative for the phase based formulation both for horisontal and vertical flow. The flux function for the fractional flow formulation will only be monotonic if the flow is horisontal. For vertical flow, the flux function can have a shape as shown in Figure 5.1(b). Note that it has a point where $f' = 0$, and thus the solution of the Riemann problem becomes non-trivial. In two dimensions, the phase formulation can be written in the form

$$\frac{\partial c}{\partial t} + \nabla \cdot (\zeta(c)(\sigma_x \mathbf{e}_x + \sigma_z \mathbf{e}_z) = q \,, \tag{5.9}$$

where ζ is some generally non-linear function, and the velocity vector

$$\boldsymbol{\sigma} = \sigma_x \mathbf{e}_x + \sigma_z \mathbf{e}_z \,, \tag{5.10}$$

is independent of c. Due to the gravity term, this will not be true for the fractional flow formulation.

To ease the presentation, we have neglected capillary forces. The character of the phase formulation is not altered if capillary forces are introduced, although the phase velocities will change. On the contrary, the fractional flow formulation turns into an advection-diffusion equation, which has a parabolic nature. In the control volume framework presented next, the parabolic terms will naturally be treated with elliptic discretisation principles as discussed in the previous chapter. To ensure stability the diffusive terms should be treated implicitly. Treatment of diffusion terms in Lagrangian methods will be discussed at the end of this chapter.

5.2 Control Volume Methods

For a multi-dimensional problem, a generic hyperbolic equation can be written

$$\frac{\partial c}{\partial t} + \nabla \cdot \mathbf{f}(c) = q\,. \tag{5.11}$$

As in the previous chapter, let Ω_i be a cell in the grid, and write the edges of the cell as $\partial\Omega_{i,j}$, so that $\partial\Omega_i = \bigcup_j \partial\Omega_{i,j}$. Integration in space over Ω_i and in time from t^n to t^{n+1} yields

$$\int_{\Omega_i} (c^{n+1} - c^n) dV + \frac{1}{V_i} \sum_j \int_{t^n}^{t^{n+1}} \int_{\partial\Omega_{i,j}} \mathbf{f}(c) \cdot \mathbf{n} dS dt = \int_{t^n}^{t^{n+1}} \int_{\Omega_i} q dV dt, \tag{5.12}$$

where we have used the divergence theorem, V_i is the area of Ω_i, and $\mathbf{n}$ is the outer normal vector of $\partial\Omega_{i,j}$. By replacing c and q by cell centred variables, we get a numerical scheme

$$c^{n+1} - c^n = \frac{1}{V_i} \sum_j \int_{t^n}^{t^{n+1}} \int_{\partial\Omega_{i,j}} \mathbf{f}(c) \cdot \mathbf{n} dS dt + \int_{t^n}^{t^{n+1}} q_i dt\,. \tag{5.13}$$

Our main focus is to construct approximations, f_{num} to the flux integral

$$f_{num} \approx \int_{\partial\Omega_{i,j}} (\mathbf{f}(c) \cdot \mathbf{n}) dS\,. \tag{5.14}$$

However, before we do so, we need to introduce a concept from the theory for scalar transport schemes. If the approximation (5.13) only depends on values at time t^n, the scheme can be written in the generic form

$$C_i^{n+1} = \Phi_i^n(C_1^n, \ldots, C_{n_e}^n)\,, \tag{5.15}$$

where n_e is the number of cells in the grid. The scheme is said to be *monotone* if [155]

$$\frac{\partial C_i^{n+1}}{\partial C_j^n} = \frac{\partial \Phi_i^n(C_1^n, \ldots, C_{n_c}^n)}{\partial C_j^n} \geq 0 \qquad \forall j \,. \tag{5.16}$$

A monotone scheme cannot generate spurious oscillations in the computed solution, and requiring monotonicity may seem natural. This will be sufficient to guarantee convergence to the correct entropy solution [62, 105]. However, as shown in [99], monotone methods are at most first order accurate. Thus, it is natural to require monotonicity for first order schemes, whereas higher-order schemes must meet other criteria. We will briefly come back to this in Section 5.4.

5.2.1 Upstream Weighting

The perhaps simplest way to approximate the flux integral (5.14) is to consider a Riemann problem with the discontinuity at the edge $\partial\Omega_{i,j}$, and the initial values equal to the cell values in the adjacent cells. Now, the *upstream* method, hereafter denoted SPU (single point upstream) evaluate the direction of the flux over the edge based on the local velocity field $\boldsymbol{v}$, and define the flux according to

$$f_{num}(c_u) = \begin{cases} |\partial\Omega_{i,j}| f(u_i) \,, & \mathbf{v} \cdot \mathbf{n} > 0 \,, \\ |\partial\Omega_{i,j}| f(u_j) \,, & \mathbf{v} \cdot \mathbf{n} < 0 \,, \end{cases} \tag{5.17}$$

where the normal vector of the edge $\mathbf{n}$ points from cell i into cell j, and $|\partial\Omega_{i,j}|$ denotes the length of the edge.

The prevailing solution technique in industrial reservoir simulators is to solve the phase based formulation with upstream weighting [26]. The upstream approach is monotone, and proof of convergence for this approach to one-dimensional problems and homogeneous media can be found in [40, 203]. The upstream method suffers from some problems near discontinuities in the flux function (i.e. discontinuous permeability) [19]. The difficulty stems from how the upstream direction is found. SPU defines the upstream direction according to the local velocity field. However, the analytical solution of the Riemann problem applies upstreaming with respect to waves defined by the flux function. For complex flux functions, the two approaches are not necessarily equal.

The standard upstream method as presented above is essentially a one-dimensional method; it computes the flux based on the values in the two adjacent cells only. This methodology can readily be extended to multi-dimensional problems by doing a dimensional splitting, and this is the common approach in industrial simulations. The convergence proof for monotone methods given in [62] also holds for dimensional splitting on Cartesian grids.

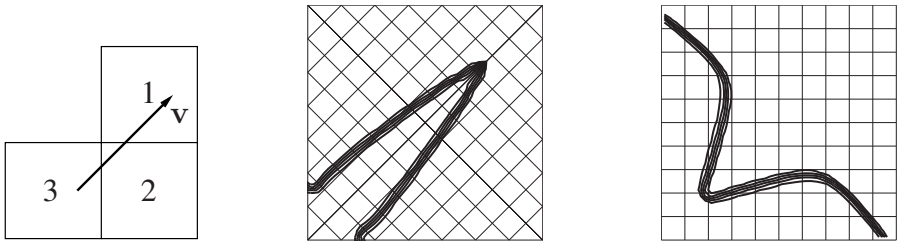

(a) (b) (c)

Figure 5.2: Figure a) illustrates cells involved in multi-dimensional upstream weighting. Figure b) and c) show saturation contours for a quarter-five spot simulation. The direction of the grid orientation is indicated in the figures. Except from grid orientation, the parameters for the simulations are identical.

However, in displacement processes with adverse mobility ratios, i.e. the intruding fluid is more mobile than the displaced fluid, dimensional splitting can lead to *grid orientation effects* (GOE), first observed in [215]. Consider Figure 5.2(a). The upstream method approximates the flow over the edge between cells 1 and 2 by using cell 2 as the upstream cell. Any contribution from cell 3 is ignored. A possible result of this can be seen in the Figures 5.2(b) and 5.2(c). These shows saturation profiles from a simulation on a Cartesian grid. There is an injection in the lower left corner, and a producer well in the upper right corner. The displacing fluid has lower viscosity than the displaced fluid, and the mobility functions are taken from [232]. The saturation front tends to follow the coordinate lines, rendering solutions that completely depend upon grid geometry.

GOE in reservoir simulation is a much studied topic, see for instance [38] and the references therein. The fundamental difficulty is that the displacement process is unstable on the level it is discretised; that is, the mathematical model is not well posed. Therefore, the instability does not disappear with grid refinement. Parameters such as grid size, mobility ratio, and truncation errors for the discretisation schemes play an important role in triggering the instabilities. Several remedies have been proposed for reducing GOE, including applying higher order methods for transport [54], and constructing pressure discretisations aimed at capturing the flow over corners [207, 232].

5.3 A Framework for Truly Multi-Dimensional Upstream Weighting

Here we present a framework for upstream methods that preserve the multi-dimensionality of the problem better than dimensional splitting approaches. The

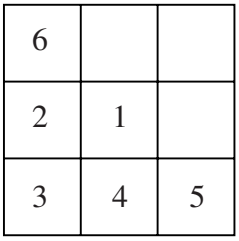

Figure 5.3: The figure shows local numbering of cells that are possible candidates for a transport scheme for the central cell.

intention is to amend to SPU, and thereby reduce biasing with respect to the grid. The methods apply to all problems that can be written on the form (5.9) - (5.10). The framework was originally developed and studied by Kozdon and coworkers in [141, 142, 143]. To ease the presentation, we restrict ourselves to Cartesian grid. Extensions to other grids are considered in Paper E.

5.3.1 Multi-Dimensional Transport

The reason for the poor performance of SPU shown in Figure 5.2(b) and 5.2(c), is that the scheme neglects flow over corners, that is, from cell 3 to cell 1, referring to Figure 5.2(a). To formulate better schemes, we thus need to define methods with larger stencils. Consider the cells shown in Figure 5.3, and assume for the time being that both the velocity components are positive, i.e. the flow is more or less from the lower left to the upper right corner. Then, the four cells that are most significant for the state in cell 1 are number 1, 2, 3, and 4. We will formulate a framework which utilise schemes consisting of these four most important cells. We remark that also cell number 5 and 6 are in the upstream direction to cell 1, and thus it is possible to define stencils with five and six cells. This will not be pursued here, more information can be found in [222].

One of the simplest hyperbolic problems is that of linear transport. Referring to Equation (5.11), this corresponds to $\boldsymbol{f} = (c\boldsymbol{v}_1, c\boldsymbol{v}_2)$, where $\boldsymbol{v}_1$ and $\boldsymbol{v}_2$ are the velocity components in the x- and y-direction, respectively. In [197], Roe and Sidilkover found that the linear four-point schemes on Cartesian grids can be described by a single parameter. Further, due to the simple structure of the problem, it is possible to gain insight in the properties of the methods by a modified equation analysis. Details can be found in [142, 197], and also in Paper E, where the analysis is extended to parallelogram grids. Even though our transport problem of interest is non-linear, we would like to base our framework upon the linear theory.

As we saw in Chapter 2, the variables that are governed by hyperbolic equations typically represents mass or concentrations. Obviously, negative values of

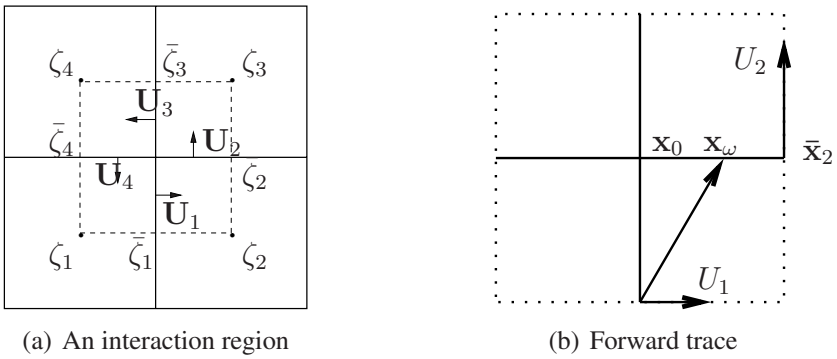

(a) An interaction region (b) Forward trace

Figure 5.4: To the right, an interaction region for the multi-dimensional transport framework. The arrows show the positive directions of the velocities. The forward trace is shown to the left, $\omega^* = \|\mathbf{x}_\omega - \mathbf{x}_0\|/\|\bar{\mathbf{x}}_2 - \mathbf{x}_0\|$.

these variables make no sense from a physical point of view, and the numerical schemes should be designed to avoid this situation. For two-phase systems, we can avoid such numerical artifacts by requiring the schemes to be monotone. That is, Definition (5.16) will be imposed for each cell in the grid. In general, all cells are included in several cell stencils, and hence the positivity requirement might yield a global coupling of the coefficients in the transport scheme, which must be solved for each time step. In addition to being a cumbersome solution procedure, this can impose strong restrictions on the schemes. Moreover, the global coupling is in conflict with the local nature of hyperbolic problems. To avoid these issues, the numerical schemes are formulated with the help of interaction regions, which were presented in Section 4.4. As we will see, this framework allows for the coefficients in the transport scheme to be defined locally. The desire to use interaction regions is also the reason why we only seek inspiration from methods with four-point cell stencils.

We now first describe how the schemes constructed for linear transport can be formulated by interaction regions. Applications to two-phase flow will be considered next. Assume that a velocity field is known, and let the fluxes over a half-edge i be represented by U_i. Moreover, denote by ζ_i cell centred values of a quantity to be treated with upstreaming. For the time being we do not assign any physical meaning to ζ, but instead emphasis the generality of the framework presented here. Later, we will let the upstreamed quantities be phase mobilities. Consider the interaction region shown in Figure 5.4(a). The transport over half-edge i is given by

$$F_i = U_i \bar{\zeta}_i \,, \tag{5.18}$$

where the function value at the half-edge, $\bar{\zeta}_i$, is to be determined. Consider the

case shown in Figure 5.4(b), when both U_1 and U_2 are positive. Then, a forward trace of the characteristic from the midpoint of edge 1 suggests that $\bar{\zeta}_2$ can be expressed as a combination of the value of ζ in the centre of cell 2, $\zeta_2 = \zeta(C_2)$, and $\bar{\zeta}_1$. This can be achieved if we define $\bar{\zeta}_2$ by

$$\bar{\zeta}_2 = (1 - \omega_2)\zeta_2 + \omega_2 \bar{\zeta}_1 \,, \tag{5.19}$$

where ω_2 will be defined below. For a general velocity field, the edge concentrations can be written as

$$\bar{\zeta}_i = \begin{cases} (1 - \omega_i)\zeta_i + \omega_i \bar{\zeta}_{i-1} \,, & \text{if } U_i \geq 0 \,, \\ (1 - \omega_i)\zeta_{i+1} + \omega_i \bar{\zeta}_{i+1} \,, & \text{if } U_i < 0 \,, \end{cases} \tag{5.20}$$

where $i \pm 1$ is defined cyclically on $i = 1 \ldots 4$. This is of course not the only way to define edge quantities $\bar{\zeta}_i$. It is however convenient, since Definition (5.20) allows the parameter ω_i to describe the family found by Roe and Sidilkover of all possible linear, monotone four-point schemes for a constant velocity field. Moreover, we can apply these schemes to more general cases as well.

Equation (5.20 can be set up for all half-edges in the interaction region. Let $\boldsymbol{\zeta} = (\zeta_1, \ldots, \zeta_4)$ and $\bar{\boldsymbol{\zeta}} = (\bar{\zeta}_1, \ldots, \bar{\zeta}_4)$. Then $\bar{\boldsymbol{\zeta}}$ can be found from the linear system

$$\bar{\boldsymbol{\zeta}} = \mathbf{S}\boldsymbol{\zeta} + \mathbf{T}\bar{\boldsymbol{\zeta}} \,. \tag{5.21}$$

In this way, the coefficients in the transport scheme are computed locally within each interaction region, thus, we avoid the issues with a global coupling. If the concentrations are positive, $\zeta'(C) > 0$, and $\omega_i < 1$ for at least one i, the scheme will be monotone [141, 142].

What remains is to define the parameter ω so that flow not aligned with the grid is properly represented. Again, consider Figure 5.4(b). We do a local reconstruction of the velocity field inside cell 2, based on U_1 and U_2. A vector aligned with the velocity field, starting in the midpoint of edge 1, $\bar{\mathbf{x}}_1$, will intersect with half-edge 2 in a point $\mathbf{x}_\omega$. Then define ω^* as the relative distance between $\mathbf{x}_\omega$ and the centre in the interaction region $\mathbf{x}_0$, compared to the length of the half-edge,

$$\omega^* = \frac{\|\mathbf{x}_\omega - \mathbf{x}_0\|}{\|\bar{\mathbf{x}}_2 - \mathbf{x}_0\|} \,. \tag{5.22}$$

The functional relationship between ω^* and $\omega = \omega(\omega^*)$ is inspired by methods designed for linear adevection. To guarantee monotonicity of the schemes, the weights of both ζ and $\bar{\zeta}$ should be positive. Therefore, we need $0 \leq \omega \leq 1$. Moreover, the schemes are not monotone unless $\omega \leq \omega^*$ [141]. For Cartesian grids,

we consider three choices, single point upstream (SPU), tight multi-dimensional upstream (TMU), and smooth multi-dimensional upstream (SMU), given by

$$\begin{aligned} \omega_{SPU}(\omega^*) &= 0\,, \\ \omega_{TMU}(\omega^*) &= \begin{cases} \min(\omega^*, 1)\,, & \omega^* > 0 \\ 0\,, & \omega^* < 0 \end{cases}\,, \\ \omega_{SMU}(\omega^*) &= \begin{cases} \frac{\omega^*}{1+\omega^*}\,, & \omega^* > 0 \\ 0\,, & \omega^* < 0 \end{cases}\,. \end{aligned} \tag{5.23}$$

The schemes are motivated by the standard SPU scheme, the Narrow scheme [197] and Koren's scheme [140], respectively. The reason for defining the limiter functions in this way can most easily be seen from a modified equation analysis, confer [142] and Paper E.

We point out that in [142], the method was formulated as a traceback instead of a forward trace. For Cartesian grids, the two approaches are equivalent. However, on an unstructured grid, forward tracing is conceptually somewhat easier to formulate than tracing backwards. In practice, the two different formulations yield approximately the same results.

5.3.2 Discretisation of Two-Phase Flow

So far, we have only considered transport schemes for a single time step. We will now outline how the scheme presented above can be applied to two-phase flow. As we saw in Section 2.3, the mobilities render a hyperbolic behaviour for the mass or saturation variables, thus they are treated with upstream weighting. We remark that we could have treated the mass variables with upstreaming instead of the mobilities. However, it has been found difficult to obtain schemes that are provably monotone within such a framework [141].

Flow of two immiscible phases was studied in Section 2.3, where we derived the governing equation

$$\int_\Omega \phi \frac{\partial(\rho_\alpha S_\alpha)}{\partial t}\, dV + \int_{\partial\Omega} \mathbf{n} \cdot (\rho_\alpha \lambda_\alpha \mathbf{K} \nabla (p_\alpha - \rho_\alpha g z))\, dS = \int_\Omega q_\alpha\, dV\,. \tag{5.24}$$

Throughout this section, we for simplicity consider the density to be constant. Now, let the control volume be a cell Ω_i, and split the surface integral into one for each edge. We then recognise

$$\int_{\partial\Omega_{i,j}} \mathbf{n} \cdot (\rho_\alpha \lambda_\alpha \mathbf{K} \nabla (p_\alpha - \rho_\alpha g z)) dS\,, \tag{5.25}$$

as a two-phase version of Equation (4.3). For each edge j, we therefore split the flux term into a fluid term $\bar{\lambda}_{\alpha,j}$ and a geometric term

$$\sigma_{\alpha,j} = \int_{\partial\Omega_{i,j}} \mathbf{n} \cdot (\mathbf{K}\nabla(p_\alpha - \rho_\alpha g z))dS\,, \tag{5.26}$$

where $\sigma_{\alpha,j}$ is a phase flux over edge j. This phase flux should not be confused with the mass flux of phase α, which is $f_\alpha = \rho_\alpha \bar{\lambda}_\alpha \sigma_\alpha$. For simplicity, the densities are considered constant in this section.

The geometric term can thus be treated by the control volume techniques from the previous chapter, and a discretisation of Equation (5.26) for all edges gives us

$$\boldsymbol{\sigma}_\alpha = \mathbf{T}(\mathbf{p} - \rho_\alpha g \mathbf{H}))\,. \tag{5.27}$$

Here $\boldsymbol{\sigma}_\alpha$ is a vector of phase velocities for each edge, $\mathbf{T}$ is a transmissibility matrix, and the vectors $\mathbf{p}$ and $\mathbf{H}$ contain cell centre pressures and heights.

The phase velocity field can be used to define mobilities on the edges by the method previously presented. The vector of edge mobilities, $\bar{\boldsymbol{\lambda}}_\alpha$, can be written as

$$\bar{\boldsymbol{\lambda}}_\alpha = \boldsymbol{C}_\alpha \boldsymbol{\lambda}_\alpha\,, \tag{5.28}$$

where $\mathbf{C}_\alpha$ is a matrix that takes cell values to edge values, based on Equation (5.21), and $\boldsymbol{\lambda}_\alpha$ is a vector of cell mobilities. Note that $\mathbf{C}_\alpha$ depend on $\boldsymbol{\sigma}_\alpha$, hence the edge mobilities are functions of the pressure. The flux over all edges can now be written on the form

$$\boldsymbol{f}_\alpha = \bar{\boldsymbol{\lambda}}_\alpha \cdot \boldsymbol{\sigma}_\alpha\,, \tag{5.29}$$

where $\cdot$ denotes component wise multiplication. Each component in $\boldsymbol{f}_\alpha$ can be considered a flux approximation f_{num} to its respective edge, confer Section 5.2.

As long as the mobilities are non-decreasing functions of saturation, the phase formulation yield a flux function with no sonic points. For more complex physical processes, this will no longer be the case. A strategy for how to handle sonic points is presented in [141]. The basic idea is to apply upstreaming to fluxes instead of mobilities. We remark that this approach requires knowledge of the sonic points of the flux functions.

Explicit Time Stepping

The schemes introduced in the previous section are provably monotone, and thereby free of spurious oscillations. For a consistent scheme, monotonicity is sufficient to guarantee non-negative values of the transported variable c_α [141].

However, we have no means to impose an upper bound on the variable. The common approach for a two-phase simulation would be to let the mass be represented by one saturation variable, and define the saturation of the other phase according to (2.6); $\sum_\alpha S_\alpha = 1$. However, the pressure equation for the multi-dimensional framework derived below has non-linearities which require an iterative solution approach, i.e. Newton's method. In practice, the pressure solution will therefore not be exact, and transport of saturations according to the corresponding velocity field may yield non-physical values, i.e. they do not honour the constraints $0 \leq S_\alpha \leq 1$, and $\sum_\alpha S_\alpha = 1$. One remedy is to use phase masses as primary variables. Let $M_{\alpha,i}$ be the average mass in cell i,

$$M_{\alpha,i} = \int_{\Omega_i} \rho_\alpha S_\alpha \, dV \,, \tag{5.30}$$

where the phase can be aqueous or liquid. The discrete saturation of phase α in cell i is then defined by

$$S_{\alpha,i} = \frac{M_{\alpha,i}/\rho_\alpha}{M_{a,i}/\rho_a + M_{l,i}/\rho_l} \,. \tag{5.31}$$

This definition guarantees positive saturations if the masses are so, moreover, the physical constraints are satisfied. However, the discrete saturation concept, means we have in fact introduced a framework which allows for a volume residual. Another way to think of this is that we have added a small, artificial compressibility to the system.

Again considering Equation (5.24), we now have a strategy for discretising all the surface integrals for all the edges. Moreover, we recognise the first term as the time derivative of the discrete mass in cell i. We integrate in time from t^n to t^{n+1}, and apply the fundamental theorem of calculus to get the discrete conservation equation for phase α as

$$\begin{aligned} \mathbf{M}_\alpha^{n+1} &= \mathbf{M}_\alpha^n \\ &\quad -\Delta t \mathbf{V}^{-1}(\mathrm{Div}((\rho_\alpha \bar{\boldsymbol{\lambda}}_\alpha(\mathbf{S}_\alpha^n, \mathbf{p}^{n+1}) \cdot \boldsymbol{\sigma}_\alpha(\mathbf{p}^{n+1}))) - \rho_\alpha \mathbf{Q}_\alpha(\mathbf{S}_\alpha^n, \mathbf{p}^{n+1})) \,. \end{aligned} \tag{5.32}$$

Here, $\mathbf{M}_\alpha$ is a vector of cell averaged masses, $\boldsymbol{V}$ is a diagonal matrix with cell volumes on the diagonal, and Div is a discrete divergence operator. Further $\mathbf{S}_\alpha$ is a vector of phase saturations, and (volumetric) source terms are represented by $\mathbf{Q}_\alpha$. Superscripts indicate time steps and Δt is the time step size. Note that we have employed an IMPES strategy; pressure is discretised implicitly, while masses and saturations are treated explicitly.

If we divide by the densities, and sum the conservation equations for the two phases, we get a pressure equation which reads

$$\sum_{\alpha=a,l} \frac{\mathbf{M}_\alpha^{n+1}}{\rho_\alpha} = \sum_{\alpha=a,l} \frac{\mathbf{M}_\alpha^{n}}{\rho_\alpha} \tag{5.33}$$
$$-\Delta t \mathbf{V}^{-1} \sum_{\alpha=a,l} \left(\mathrm{Div}((\bar{\boldsymbol{\lambda}}_\alpha(\mathbf{S}_\alpha^n, \mathbf{p}^{n+1}) \cdot \boldsymbol{\sigma}_\alpha(\mathbf{p}^{n+1}))) - \boldsymbol{Q}_\alpha(\mathbf{S}_\alpha^n, \mathbf{p}^{n+1}) \right).$$

If the volume balance is exact, we have

$$\sum_{\alpha=a,l} \frac{\mathbf{M}_\alpha^{n+1}}{\rho_\alpha} = \sum_{\alpha=a,l} \frac{\mathbf{M}_\alpha^{n}}{\rho_\alpha}\,. \tag{5.34}$$

However, within the volume relaxed framework, this is not necessarily true. We aim for volume balance at time step $n+1$ by setting

$$\sum_{\alpha=a,l} \frac{M_{i,\alpha}^{n+1}}{\rho_\alpha} = 1\,. \tag{5.35}$$

Now, the pressure equation can be written in residual form, $\mathbf{F} = \mathbf{0}$, where

$$\mathbf{F}(\mathbf{p}^{n+1}) = \mathbf{e} - \sum_{\alpha=a,l} \frac{\mathbf{M}_\alpha^{n}}{\rho_\alpha} \tag{5.36}$$
$$+\Delta t \mathbf{V}^{-1} \sum_{\alpha=a,l} \left(\mathrm{Div}((\bar{\boldsymbol{\lambda}}_\alpha(\mathbf{S}_\alpha^n, \mathbf{p}^{n+1}) \cdot \boldsymbol{\sigma}_\alpha(\mathbf{p}^{n+1}))) - \boldsymbol{Q}_\alpha(\mathbf{S}_\alpha^n, \mathbf{p}^{n+1}) \right),$$

where $\mathbf{e}$ is a vector of ones. This is a non-linear equation for $\mathbf{p}^{n+1}$, which can be solved by Newton's method. The Jacobian matrix, $\mathbf{J}_{p,p}$, is also needed in the fully implicit method, and is presented below.

The above equations represent a truly multi-dimensional framework for two-phase transport. The computational cost of the scheme is somewhat increased compared to a standard two phase method with pressure and saturation as primary variables. First, more than one iteration might be needed to solve the pressure equation, although, in practice a residual tolerance of 10^{-3} has been sufficient for the tests done so far. This is normally achieved after 1-3 iterations on the pressure equation, depending on how important role gravitational forces play. Second, we need to update two mass equations variables instead of one saturation equation. However, solving an explicit transport equation is cheap, and this does not add a significant computational burden to the simulation.

Implicit Time Stepping

The multi-dimensional framework can also be used for fully implicit methods. Since the transport equation now is solved implicitly, it is tempting to use water saturation as our mass variable to limit the number of equations. We therefore abandon the volume relaxed framework. Treatment of non-physical saturation values is discussed in Paper E.

Our governing equations are now one equation for pressure, and one for transport of the saturation of water. The discretised pressure equation can be written as

$$\mathbf{F}_p(\mathbf{S}_w, \mathbf{p}) = \Delta t \mathbf{V}^{-1} \sum_{\alpha=a,l} \Big(\mathrm{Div}(\bar{\boldsymbol{\lambda}}_\alpha(\mathbf{S}_\alpha, \mathbf{p}) \cdot \boldsymbol{\sigma}_\alpha(\mathbf{p})) - \boldsymbol{Q}_\alpha(\mathbf{S}_\alpha, \mathbf{p}) \Big) . \quad (5.37)$$

Similarly, the saturation equation is discretised by

$$\mathbf{F}_S(\mathbf{S_w}, \mathbf{p}) = \mathbf{S}_w - \mathbf{S}_w^n + \Delta t \mathbf{V}^{-1} \mathrm{Div}(\bar{\boldsymbol{\lambda}}_w(\mathbf{S}_w, \mathbf{p}) \cdot \boldsymbol{\sigma}_w(\mathbf{p})) - \boldsymbol{Q}_\alpha(\mathbf{S}_w, \mathbf{p})) . \quad (5.38)$$

We solve the equations by casting them into residual form, $(\mathbf{F}_p, \mathbf{F}_S) = \mathbf{0}$, and apply Newton's method. The Jacobian matrix reads

$$\mathbf{J}(S, p) = \begin{bmatrix} \mathbf{J}_{S,S} & \mathbf{J}_{S,p} \\ \mathbf{J}_{p,S} & \mathbf{J}_{p,p} \end{bmatrix} , \quad (5.39)$$

where $\mathbf{J}_{a,b} = \frac{\partial \mathbf{F}_a}{\partial \mathbf{b}}$. The elements in the Jacobian are defined as follows

$$\mathbf{J}_{S,S} = \mathbf{I} + \Delta t \mathbf{V}^{-1} \Big(\mathrm{Div} \Big(\mathrm{diag}(\sigma_w(\mathbf{p})) \frac{\partial \bar{\boldsymbol{\lambda}}_w}{\partial \mathbf{S}_w} \Big) - \frac{\partial \mathbf{Q}_w}{\partial \mathbf{S}} \Big) , \quad (5.40)$$

$$\mathbf{J}_{S,P} = \Delta t \mathbf{V}^{-1} \Big(\mathrm{Div} \Big(\mathrm{diag}(\bar{\boldsymbol{\lambda}}_w) \mathbf{T} + \mathrm{diag}(\sigma_w(\mathbf{p})) \frac{\partial \bar{\boldsymbol{\lambda}}_w}{\partial \mathbf{p}} \Big) - \frac{\partial \mathbf{Q}_w}{\partial \mathbf{p}} \Big) , \quad (5.41)$$

$$\mathbf{J}_{P,S} = \Delta t \mathbf{V}^{-1} \sum_{\alpha=a,l} \Big(\mathrm{Div} \Big(\mathrm{diag}(\sigma_\alpha(\mathbf{p})) \frac{\partial \bar{\boldsymbol{\lambda}}_\alpha}{\partial \mathbf{S}_w} \Big) - \frac{\partial \mathbf{Q}_\alpha}{\partial \mathbf{S}} \Big) , \quad (5.42)$$

$$\mathbf{J}_{P,P} = \Delta t \mathbf{V}^{-1} \sum_{\alpha=a,l} \Big(\mathrm{Div} \Big(\mathrm{diag}(\bar{\boldsymbol{\lambda}}_\alpha) \mathbf{T} + \mathrm{diag}(\sigma_\alpha(\mathbf{p})) \frac{\partial \bar{\boldsymbol{\lambda}}_\alpha}{\partial \mathbf{p}} \Big) - \frac{\partial \mathbf{Q}_\alpha}{\partial \mathbf{p}} \Big) . \quad (5.43)$$

The multi-dimensional upstream formulation adds terms involving $\frac{\partial \bar{\boldsymbol{\lambda}}_\alpha}{\partial \mathbf{p}}$ to the Jacobian matrix. Differentiation of Equation (5.21) with respect to the pressure, gives a linear system that can be solved for $\frac{\partial \bar{\boldsymbol{\lambda}}_\alpha}{\partial \mathbf{p}}$.

The methods presented in this section have been applied to Cartesian grids in [141, 143], and they have been shown to reduce grid orientation dependency. Development of the method presented above is in a starting phase, and only very simplified cases have been considered so far. Some thoughts on the road ahead are given in Chapter 7.

5.4 Other Approaches

There are many methods developed for solving transport equations apart from the simple first order upstream strategy. The aim of this section is to give an overview of some of the alternatives to the upstreaming presented above. There are two distinct groups of schemes for hyperbolic problems: control volume methods and Lagrangian methods. However, we first discuss Riemann solvers in general, and present front tracking methods, which can be applied both in control volume and Lagrangian frameworks.

5.4.1 Riemann Solvers and Front Tracking

In Section 5.2, we formulated control volume methods in terms of a set of Riemann problems that must be solved for each edge. Godunov proposed a method based on solving the Riemann problem exactly for each edge. For scalar equations, he also showed that this strategy gives a method with less artificial diffusion than any other monotone method. If this strategy is applied to problems with more than one hyperbolic conservation law, we need to solve systems of equations of the form

$$\frac{\partial \boldsymbol{c}}{\partial t} + \nabla \cdot (\boldsymbol{f}(\boldsymbol{c})) = \boldsymbol{q}\,, \tag{5.44}$$

with initial data

$$\boldsymbol{c}(x,0) = \begin{cases} \boldsymbol{c}_L & x < 0\,, \\ \boldsymbol{c}_R & x > 0\,. \end{cases} \tag{5.45}$$

The solution will in general contain multiple shocks, rarefaction waves and contact discontinuities. One key difficulty for Riemann solvers is that the theory for hyperbolic systems is not fully developed, and we only know the solution in certain special cases, see for instance [127, 130]. If an analytical solution is not available, approximate Riemann solvers must be applied to find the wave-structure, see for instance [181, 196, 216]. These procedure can be cumbersome, and this partly explains why reservoir simulators often use upstream evaluation based on the phase velocity field instead of the Riemann waves.

The Riemann solvers can be applied to reservoir simulations in (at least) two different ways. The edge fluxes in a control volume method can be considered as solutions of Riemann problems. Another possibility is to represent the solution as a set of discontinuities, and propagate them in time. This is the philosophy of the *front tracking methods*. An important point here is that the flux function is approximated by a piecewise linear function, while the initial data is piecewise constant [63, 112]. Thus, the speed of the shocks can be computed by the Rankine-Hugoniot condition. Further, rarefaction waves are approximated by a sequence of small shocks. As the name indicates, the methods are especially well suited to follow fronts in the solution, e.g. the water front during secondary production. Now, the fronts can either be tracked on a Cartesian grid, with some dimensional splitting, e.g. [106], or a streamline method (explained below) can be applied [129, 156].

5.4.2 Control Volume Methods

Higher Order Upstream Methods

So far, all methods presented have solved problems with constant initial data in each cell. As a result, the methods are only first order accurate. Higher order methods can be constructed in a *Reconstruct - Solve - Average* fashion. Based on the solution from one time step, a higher order representation of the data is computed, often in the form of polynomials. These polynomials serve as initial data for the next time step. The solution is propagated, and an average value in each cell is computed for use in the next time step. As previously mentioned, a monotone method cannot be more than first order accurate. A naive approach to the reconstruction of the solution may lead to self-sharpening, and eventually development of spurious oscillation in areas where the solution gradient is steep. This can be avoided by a careful reconstruction step that ensures that the method is only first order accurate near shocks. Well known higher order methods are of TVD-, ENO-, or WENO-type, we refer to the reviews [206, 211] and the references therein. Applications to porous media flow can be found in e.g. [166, 198, 212].

Multi-Dimensional Upstreaming

Most control volume methods are essentially designed for one spatial dimensional, although multi-dimensional problems can be solved by dimensional splitting. However, Hurtado et.al. [119] presented a methodology with strong similarities to the framework presented here. They define edge mobilities based on forward tracing on a dual grid. However, the pressure equation is solved by a control volume finite element method, and this also mean the concepts of primal

and dual grid is flipped compared to the present method.

Another genuinely multi-dimensional approach which is quite similar to the one outlined in this chapter was presented by Edwards in [83, 84], and further developed by Lamine and Edwards in [150, 151]. The main focus of the work is to develop higher order methods for transport. Their methods combine an MPFA pressure solver with multi-dimensional transport. However, the upstream quantities are either fluxes or saturations, and they do not explicitly introduce an interaction region framework for transport. Moreover, the transport method is based on the fractional flow formulation instead of phase velocities. So far, no extension to problems with gravity included (i.e. fractional flow functions with sonic points) has been published.

Central Schemes

All the schemes mentioned above can be considered as upstreaming methods. An alternative is the class of central schemes. The simplest method is the first order Lax-Friedrichs scheme, which suffers from high levels of numerical viscosity. Nessyahu and Tadmor proposed to use higher order central methods, and showed that the higher accuracy reduce the artificial smearing [174]. The scheme was further improved in e.g. [125, 144]. Multi-dimensional problems can be handled without dimensional splitting [126]. An application to multiphase flow is presented in [18]. A major concern for these methods is how much artificial smearing they will introduce in areas with sharp discontinuities in the permeability.

Discontinuous Galerkin Methods

The higher order methods mentioned above construct a polynomial from the function value in multiple cells, rendering a system of equations with some bandwidth. Moreover, extensions to multiple dimensions can be difficult if the grid is irregular, even if dimensional splitting is applied. In the *Discontinuous Galerkin* (DG) framework, a higher order finite element method is applied in the interior of the elements. The finite element framework allows for a high resolution in the interior of the cells, and since the approximation on the interior is decoupled from other cells, parallelising is easy. We let $V_h(\Omega_i)$ denote the approximation space on an element Ω_i. A DG discretisation of Equation (5.11) on Ω_i reads: Find $u_h \in V_h(\Omega_i)$ such that for all $v_h \in V_h(\Omega_i)$

$$\int_{\Omega_i} \frac{\partial u_h}{\partial t} v_h - \boldsymbol{f}(u_h) \cdot \nabla v_h dV + \int_{\partial\Omega_i} (\widehat{\boldsymbol{f} \cdot \boldsymbol{n}}) v_h dS = q\,. \tag{5.46}$$

Here, v_h are basis functions in a finite element space $V_h(\Omega_i)$, and $\widehat{\boldsymbol{f} \cdot \boldsymbol{n}}$ denotes the numerical flux over the cell boundary. A finite element solution will in general not

preserve mass over the element edges. Therefore, the interaction between the elements is approximated by a numerical method, usually a lower order method such as Godunov, Enquist-Osher, or Lax-Friedrichs. To prevent artificial oscillations, some slope limiting is necessary. Time integration is commonly done by Runge-Kutta methods. The flux approximation is one-dimensional, however, the high resolution on the interior means the method is able to capture multi-dimensionality better than traditional control volume method. For more information, confer [60] and the references therein. Usage of DG in porous media flow is reported in e.g. [88, 117].

5.4.3 Lagrangian Methods

The control volume methods considered in this chapter can be considered Eulerian, in the sense that the grid is constant in time, and fluid is transported between grids cells. Explicit time stepping is computationally cheap, but for stability the schemes must honour a CFL-criterion that limits the size of the time step [61]. In some sense, this is an artificial constraint imposed by the computational grid. If the transport scheme is implicit in time, the time step can be taken larger, but the computational overhead from solving linear systems can be severe. Moreover, control volume methods suffer from grid orientation effects.

By employing a Lagrangian frame of reference that follows the path of fluid particles, the time step restriction can be relaxed . If capillary forces are included, we must consider advection-diffusion equations on the form

$$\frac{\partial c}{\partial t} + \nabla \cdot (\boldsymbol{v} f(c)) - \nabla \cdot (\boldsymbol{D} \nabla c) = q \,, \tag{5.47}$$

where $\boldsymbol{D}$ is a diffusion tensor, which can be a function of c. For simplicity, we will sometimes consider a simplified model problem (on non-conservative form) instead;

$$\frac{\partial c}{\partial t} + \boldsymbol{v} \cdot \nabla c - \nabla \cdot (\boldsymbol{D} \nabla c) = q \,, \tag{5.48}$$

where we have ignored compressibility effects ($\nabla \cdot \boldsymbol{v} = 0$), and assumed a linear flux function f. We go to a Lagrangian frame of reference by introducing the material derivative

$$\frac{D}{Dt} = \frac{\partial}{\partial t} + \boldsymbol{v} \cdot \nabla \,. \tag{5.49}$$

Now, Equation (5.48) can be written

$$\frac{Dc}{Dt} - \nabla \cdot (\boldsymbol{D} \nabla c) = q \,, \tag{5.50}$$

which is a parabolic equation without an advective first order term. Thus, in a Lagrangian frame of reference there are no steep fronts, and the resulting solution is much smoother than in an Eulerian framework; hence the stability restrictions on time step size is correspondingly less restrictive [91]. Also, Lagrangian methods will be far less sensitive to grid orientation errors than Eulerian techniques.

Application of Lagrangian methods to complex recovery processes (tertiary production) is in an early stage of development compared to the control volume framework primarily studied in this work, and thus there are many issues that should be investigated further. Also, implementation of Lagrangian methods is non-trivial compared to Eulerian methods. However, if these methods can be improved on, Lagrangian transport schemes may offer a robust and computationally cheap alternative to control volume approaches [97]. We therefore briefly review some methods that have shown promising results.

Characteristic Methods

In an advection dominated process, information is mainly transported along characteristic curves, and the *characteristic methods* are based upon tracing these lines. The classical approach would be to trace characteristics forward with a finite difference method. However, if we trace forward from time t^n, there may be cells that contain no characteristics at time t^{n+1}, thus some interpolation scheme must be applied. Therefore backward tracing is often preferred. A technique well known in reservoir simulation is the method of modified characteristics (MMOC) presented in [77], and extended in i.e. [89, 202], with emphasis on porous media flow. An MMOC discretisation of Equation (5.48) read

$$\int_\Omega \frac{c(\boldsymbol{x}, t^{n+1})(\boldsymbol{x}^*, t^n)}{\Delta t} w(\boldsymbol{x}) dV + \int_\Omega \nabla w(\boldsymbol{x}) \boldsymbol{D} \nabla c(\boldsymbol{x}, t^{n+1}) dV = \int_\Omega q(\boldsymbol{x}, t^{n+1}) dV \,, \tag{5.51}$$

where w is a finite element method basis function. The point $(\boldsymbol{x}^*, t^{n+1})$ is defined by back tracing from $(\boldsymbol{x}, t^n)$ along the path described by the material derivative $\frac{Dc}{Dt}$.

Even though MMOC outperforms forward tracing, it does in general not conserve mass, since it is based on backward tracing. An adjusted version of MMOC that preserves mass is presented in [75]. To maintain conservation of mass and volume in backward tracing is a challenge for characteristic methods in general, see [22]. The advection and diffusion terms are handled by operator splitting, which may lead to artificial diffusion near shocks, as shown in [134], where a

remedy is also presented. Moreover, there are also issues with handling of boundary conditions.

The *Euler-Lagrange localised adjoint method* (ELLAM), first introduced in [51, 111] can be viewed as an improvement of MMOC. Again, we consider the linear problem (5.48), for non-linear problems confer [64]. For backward tracing from time t^{n+1}, we let w_{ADJ} be a test function satisfying the system of equations

$$\frac{\partial w_{ADJ}}{\partial t} - \boldsymbol{v} \cdot \nabla w_{ADJ} = 0\,, \tag{5.52}$$

$$\nabla \cdot (\boldsymbol{D} \nabla w_{ADJ}) = 0\,. \tag{5.53}$$

This is a splitting of the adjoint equation of (5.48), see e.g. [200]. Note that in general, both $\boldsymbol{v}$ and $\boldsymbol{D}$ can be time dependent, thus the basis functions must be redefined for each time step. Equation (5.53) is elliptic, suggesting that a finite element basis is appropriate for w_{ADJ}. To honour Equation (5.52), w_{ADJ} should be defined as constant along the characteristics $\frac{\partial \boldsymbol{x}}{\partial t} = \boldsymbol{v}$. This will also assure a Lagrangian treatment of transport, allowing for large time steps. Then, a discretisation of Equation (5.48) will result in an equation

$$\begin{aligned}\int_\Omega c(\boldsymbol{x}, t^{n+1})\, dV + \Delta t \int_\Omega (\nabla w_{ADJ} \boldsymbol{D} \nabla c)(\boldsymbol{x}, t^{n+1})\, dV \\ = \int_\Omega c(\boldsymbol{x}, t^n) w_{ADJ}(\boldsymbol{x}, t^n_+)\, dV + \int_\Omega q w_{ADJ}\, dV\,.\end{aligned} \tag{5.54}$$

Here, $w_{ADJ}(\boldsymbol{x}, t^n_+)$ is interpreted as the limit value when $t \to t^n$ from above. ELLAM methods have been formulated for a large range of problems with promising results, we refer to [92, 200] and the references therein for an overview. Other methods such as Characteristic mixed finite elements can also be considered ELLAM methods [23].

Streamline Methods

The *streamline* methods represent the flow pattern by tracing a set of streamlines starting at different spatial points. In each time step, the pressure equation is solved implicitly. After the pressure solve, the velocity field is used to trace streamlines. Along the streamlines, we must solve a one-dimensional hyperbolic problem of the form

$$\frac{\partial c}{\partial t} + \nabla \cdot (\boldsymbol{v} f(c)) = q\,. \tag{5.55}$$

The streamlines usually varies on a much slower time scale than the transport along the streamlines. Therefore, streamline methods allow for time step sizes

that can be several times the CFL-restriction. After the transport solve, the mass variables must be mapped back to the grid for a new pressure update.

A major advantage of streamline methods is that problems in multiple dimensions are reduced to a set of one dimensional problems. These can be solved by for instance front tracking, or higher order methods. Thus, streamlines offer a way to reduce the dimensionality without applying dimensional splitting. However, there are some issues related to the methods. The mapping from the grid to the streamline, known as streamline tracing, is non-trivial, see [104]. Also, in the mapping from streamlines back to the grid, mass is usually not conserved. Moreover, gravity is treated by operator splitting [39], and it is an open question how this can be done properly. For more information of streamline methods, we refer to [67, 103, 165] and the references therein.

Chapter 6

Summary of the Papers

As a part of the work with this thesis, a number of scientific papers have been produced. The previous chapters have provided theory and background for the investigations. Here, we further outline the process leading to the papers, and present the main results.

Paper A: Sufficient criteria are necessary for monotone control volume methods

Eirik Keilegavlen, Jan Martin Nordbotten, and Ivar Aavatsmark

Published in *Applied Mathematics Letters*, Vol. 22 (8), Pages 1178-1180, 2009

In Section 4.5, we gave background information on monotonicity for elliptic equations. Sufficient conditions for monotonicity of control volume methods on quadrilateral grids were found in [177]. These criteria were derived by a global analysis, requiring inverse monotonicity of the entire system matrix. However, as stated in Section 4.5, the maximum principle is valid also on subgrids. The present paper considers monotonicity on subdomains consisting of no more than 3 cells. These considerations show that most of the criteria from [177] are necessary as well as sufficient. The importance of the subdomains are reflected in a definition of a discrete maximum principle more precise than what stated in [177]. The main conclusion from this paper is that no linear nine-point control volume method can be constructed that satisfies a discrete maximum principle for all media and quadrilateral grids. Referring to the special case of parallelogram grids in homogeneous media shown in Figure 4.7(c), no methods can be monotone below the line $b < a$.

Paper B: Monotonicity for MPFA methods on triangular grids

Eirik Keilegavlen and Ivar Aavatsmark

Submitted to *Computational Geosciences*, April 2009

This paper attempts to establish monotonicity properties for MPFA methods on unstructured grids. The aim of the work was to follow up the results in [177] with a similar analysis as for quadrilateral grids. However, as the work in Paper F shows, the techniques applied to quadrilaterals come cannot provide sharp results for triangular grids. The topology of the grid makes splitting of the system matrix inappropriate. Therefore, it seems out of reach to obtain results for general methods on general grids based on a global analysis, i.e. which focus on properties on the entire grid. We therefore have to restore to considering specific methods, and rely heavily upon numerical experiments.

For the special case of uniform triangular grids in homogeneous media, Paper B provides a characterisation of the monotonicity properties of some MPFA methods, namely the O(η)-method for $\eta = 0, 1/3,$ and 0.5, and the L-method. The regions cover quite a large part of the entire parameter space, apart from the O(0)-method, which has considerably worse properties than the other methods.

On genuinely unstructured grids, the failure to obtain sharp sufficient monotonicity constraints limits the analytical results. Numerical simulations on several realisations of randomly perturbed grids are used to give an indication of the properties of the methods. Based on the insight from Paper A, special attention is given to subgrids composed by clusters of cells sharing a vertex. Indeed, for a genuinely unstructured grid, subgrids consisting of all but one cell sharing a vertex prove to yield the most restrictive monotonicity constraints. The main result of these test is that an MPFA discretisation on an unstructured grid cannot be expected to be monotone. The methods prove even more vulnerable when anisotropies are introduced in the permeability tensor. If an MPFA method still is to be applied, the O(1/3)-method seems to be the best choice.

In the last part of the paper, simple two-phase experiments are performed. This serves as a test of the role of monotonicity for non-linear problems. Even though the pressure discretisation is not monotone, the saturation profiles produced bear no signs of irregularities.

Paper C: Non-hydrostatic pressure in sigma-coordinate ocean models.

Eirik Keilegavlen and Jarle Berntsen

Published in *Ocean Modelling*, Vol 28 (4), Pages 240-249, 2009

This paper explores computation of pressure in an ocean modelling setting. Numerical ocean modelling is computationally very expensive, and traditionally, many approximations are done to ease the computational burden. One of these simplification is to neglect the non-hydrostatic pressure, stemming from dynamical processes. For coarse grids, this is a good approximation, however, it becomes questionable with the increasing grid resolutions now available. Processes such as mixing of water masses take place on a rather small scale, and is greatly influenced by non-hydrostatic pressure. Therefore accurate modelling of these effects is vital.

For Cartesian grids, equations governing the non-hydrostatic pressure was given in [168]. These were transformed to the terrain-following σ-coordinate system in [132]. However, the σ-coordinate system is not orthogonal unless the bottom is flat. Thus, the classical 5-point stencil used to solve elliptic equations is transformed into a 9-point stencil in terrain following coordinates. In three dimensions, we get a stencil of 15 points instead of 7 [132]. The increased bandwidth can result in a significant overhead when solving the linear system.

In [36], a new set of governing equations for the non-hydrostatic pressure was proposed, modelling the pressure directly in the non-orthogonal σ-coordinate system. This leads to a 5 or 7 point stencil in 2 and 3 dimensions, respectively. Essentially, the approach of [36] is to replace a multi-point approximation of the flux with a two-point estimate. Paper C explores the differences between the two systems presented in [132] and [36]. It is shown that except from the trivial case of a flat bottom (i.e. the grid is orthogonal) the two approaches are not equal. To investigate the differences by analytical means is out of reach because of the complexity of the systems of equations. Instead, the two approaches are explored by numerical experiments. The differences due to computation of the non-hydrostatic pressure are influenced by feedback from the rest of the simulation procedure. However, the difference in the primary variables obtained with the two approaches is of comparable size with other well-known sources of errors in ocean modelling. The test cases involve a broad range of physical regimes. Thus, in this application, it seems justifiable to use a TPFA-method instead of the more expensive multi-point estimates.

Paper D: Simulation of Anisotropic Heterogeneous Near-well Flow using MPFA Methods on Flexible Grids

Sissel Mundal, Eirik Keilegavlen, and Ivar Aavatsmark

Accepted for publication in Computational Geosciences.

In this work, we explore different strategies for local grid refinement in near-well regions. The local grids are radial-like, and they (mostly) apply logarithmic refinement towards the well to adapt to the expected behaviour of the pressure. The cells are both triangular and quadrilateral, and we test discretisation both in physical and reference space.

Simple tests for a single well in an anisotropic medium show that a two-point flux approximation is inadequate to get a convergent solutions; thus multi-point methods must be applied. Further, if the grid spacing in radial direction is not logarithmic, the convergence rate deteriorates. A comparison between the two different cell types shows that triangles yield a much smaller error than quadrilateral. Moreover, discretisation in physical space is sufficient, the logarithmic behaviour of the solution is well captured by the adjustments in the grid. For a heterogeneous test case, the convergence rate is reduced, in agreement with finite element theory.

If more than one well is present, or if the near-well grid do not cover the entire domain, a transition grid is needed in the zone between the near-well grids and the boundary of the domain. In this paper, we apply a triangulation algorithm to construct the transition grid. A test case with three wells indicate a smooth transition between the near-well region and the surrounding grid.

To support the single phase test, we also do two-phase simulations for a horisontal well. There are only minor differences in saturation profiles and water cut curves for the different discretisation choices. In the two-phase simulation, there is a kink in the saturation in the transition from the near-well grid to the surrounding grid. However, the size of the kink is reduced as the grids are refined. We also test the sensitivity of the solutions with respect to grid resolution in the near-well region. These simulations show that a fairly large number of cells is needed to capture the flow accurately.

Paper E: Multi-dimensional upstream weighting on general grids for flow in porous media

Eirik Keilegavlen, Jeremy Kozdon, and Bradley Mallison

Draft manuscript

In Section 5.3 a framework for multi-dimensional upstream weighting was presented. The methods have only been formulated for Cartesian grids, though. This paper addresses extensions of the methodology to more general grids.

The edge mobilities are defined according to the description in Section 5.3. Since the grid no longer is Cartesian, the definition of edge parameters should be reconsidered. On uniform parallelogram grids, the linear advection problem can be studied by a modified equation analysis. The schemes considered for Cartesian grids seem to be fairly well behaved also on more general grids. The usefulness of the analysis is however limited due to a lack of understanding of how performance for linear problems are carried over to non-linear cases. Some possible guidelines for adapting the interpolation parameters to grid geometry are also given.

Since the grids are no longer $\boldsymbol{K}$-orthogonal, TPFA methods can no longer be applied. Due to the similarities between the multi-dimensional framework presented in Chapter 5 and MPFA methods, we apply the latter schemes to discretise the elliptic parts of the problem. An MPFA discretisation provides fluxes for each half-edge. In general, the fluxes over the two halves of an edge are not equal. The trace forward in the hyperbolic scheme can be based on either the half-edge fluxes, or the total edge fluxes. The latter option will, however, lead to a prohibitively large cell molecule, and we are forced to consider the half-edge fluxes.

To assess the applicability and robustness of the multi-dimensional schemes, numerical tests are performed on a series of grids. Both parallelogram grids and general perturbed quadrilaterals are considered, as well as triangular and dual grids. Overall, the new schemes reduce the bias in the solutions compared to SPU. When multi-dimensional upstream weighting is applied in combination with fully implicit time stepping, the number of non-linear iterations decreases significantly.

Chapter 7

Conclusions and Future Directions

In this final chapter of the background, we draw conclusions, and point out directions for further work.

7.1 Control Volume Methods for Elliptic Problems

An major part of this work has been devoted to preservation of maximum principles for elliptic equations when constructing control volume discretisations. For quadrilateral grids, sufficient and necessary conditions for monotonicity are now known. These allow us to tell whether a method is monotone based on the discretisation coefficients. For unstructured grids, however, we have no means to tell if a discretisation fulfils the discrete maximum principle without inverting a large number of matrices. The main problem is a lack of understanding of which parameters control monotonicity. This issue should be investigated further. In principle, it should be possible to derive the sufficient conditions for monotonicity found in [177] starting with subdomains similar to those studied in Paper A. If such a link between the local and global criteria can be found, this may also inform the analysis for triangular grids.

In real field applications, much of the computational efforts are spent on solving non-linear, and thereby linear systems. Development of fast solvers for MPFA methods is of major importance for the schemes to gain popularity outside academia. Of special importance is cases where the system matrix is not an M-matrix. This is again related to monotonicity issues.

Another open issue regarding MPFA methods is to formulate a proper mathematical framework for analysis of the methods. So far, convergence analysis has

been based on relations between MPFA methods and MFE or MFD discretisations. However, there are indications that the estimates obtained in this way are too conservative, see e.g. [139]. Further research is thus needed to know when the methods are applicable.

As we have seen in Chapter 4, the transmissibilities in control volume methods are determined by both the permeability field, and the cell geometry. Hence, the methods may be improved by appropriate adjustments in the grid. This way of thinking has led to development of state of the art triangulation algorithms that are optimised with respect to convergence of finite element simulations. In the same way, grid generation algorithms that pay special attention to control volume methods should be explored. An example of grid optimisation with respect to monotonicity constraints can be found in [169]. A more radical option is to put more weight on discretisation techniques when the geo-model is built and upscaled. Today, grids are constructed with representation of geology in mind, more than discretisation of flow equations. However, to change this would require a major change in the work flow, which might be difficult to achieve in practise.

Control volume methods are of great interest for industrial applications due to their the local flux expressions and applicability to general grids. In Chapter 4, we mentioned three methods or classes of methods; TPFA, non-linear TPFA, and MPFA. Of these, TPFA is not consistent, and will in many cases not be sufficient to capture the flow pattern accurately. MPFA methods will often render a better representation of the flow, however, they suffer from spurious oscillations in the pressure solution. The non-linear TPFA requires iterations on the numerical scheme even for linear problems. Methods with larger cell stencil can be expected to have better properties due to their greater flexibility, but to the price of an increased computational cost when solving linear systems. The question then becomes how to deal with problems where we cannot preserve both convergence, monotonicity, and linearity of the solution scheme. In some cases, we may be forced to let go of one of the properties, thus guidelines for what to do should be developed. Another possibility is to apply 'hybrid' methods, that attempt to achieve a compromise between robustness and accuracy, see [149] for an example. Which method is best, or more generally, which schemes provide reasonable results, is probably case dependent, and theoretical analysis of simplified cases can only give limited insight. It may be necessary to perform systematic studies of the performance of control volume schemes for elliptic problems under different physical circumstances, as was done in Paper C. Due to the broad range in processes of interest (cf Chapter 1), this is an enormous task.

7.2 Simulation in Near-Well Regions

In Paper D, we considered grids and discretisations adapted to the flow pattern in near-well regions. The single phase simulations indicated that the near-well grid should be triangular, and that the transmissibilities can be computed in physical space, provided the grid has logarithmic spacing in the radial direction. Further, the methods are applicable also for multiphase flow. However, the presented numerical simulations are far from realistic, thus there is a long way to go before the methods can be applied to real cases. We now discuss two possible bottlenecks; extensions to three dimensions and reduction of the computational cost of the methods.

A non-conventional well can have several branches, each of which can be horisontal or skew. The well can also perforate multiple geological layers. To create a grid that adapts to the logarithmic pressure variation and also honour the main geological features near the well is a challenging task. The results in Paper D suggest that the grid should be based upon triangles, possibly by applying a prismatic extension to three dimensions. However, creating a 2 1/2-D grid that can adapt to a realistic well trajectory and reservoir geometry will be difficult. On the other hand, simulations will be computationally more expensive on tetrahedral grids than on prismatic extensions of triangles. Also, the coupling between the near-well grid and the global grid becomes much more complicated when going from 2D to non-conventional 3D wells. Some ideas on how this can be done can be found in e.g. [34, 94, 124].

Even though the two-phase experiments in Paper D were far from realistic, a fairly large number of grid cells was needed near the well to capture the dynamics somewhat accurately. For a realistic field, with at least tens of (non-conventional) wells, each with a length of hundreds of meters, the number of grid cells needed can be severely high. Moreover, to enhance recovery, wells are frequently opened and shut down. To apply local grid refinement around a well that has been closed for a while may be a waste of computational resources. These topics need to be addressed before the techniques developed in Paper D are applicable to field-cases. One possible solution is to apply a local time stepping in the near-well region. The mapping between the local and global grid can be handled by the windowing technique presented in [70, 170]. However, conservation of mass in the mapping might be an issue. Another option would be to use the fine-scale solution obtained by the methods presented in Paper D as a basis for upscaling to a coarser grid. This will be similar to the upscaling techniques mentioned in Section 4.6.2.

An alternative to compute a well index based on upscaling might be to apply the MSFV method presented in Section 4.7.3 Treatment of wells in the MSFV method is based on introducing an extra basis function to capture the singularity

in the solution, see [164, 231]. Another possible strategy is to consider the MSFV method as a domain decomposition method as outlined in [176], and assign a separate subdomain for each near-well region. This can allow for a good resolution of flow in the vicinity of the well, and still ease the computational burden of solving the pressure equation for large system matrices. Similar considerations can be found in [21].

7.3 Multi-Dimensional Upstream Weighting

As we have seen in this thesis, there has been a considerable effort to construct robust and accurate schemes for elliptic equations for use in reservoir simulation. In the same way, it is natural to consider more advanced transport schemes that can be applied within today's framework. The multi-dimensional upstream methods introduced in Chapter 5 can be considered analogous to MPFA methods for hyperbolic equations. Since the upstream schemes are based on a control-volume methodology, they fit naturally into mainstream simulators, and they might yield improvements in accuracy as well as performance. However, several aspects to the methods should be further investigated.

In this work, we have only considered two-phase problems. Grid orientation effects are especially severe for adverse mobility ratios. These situations often arise when heavy oil is produced with the help of EOR-techniques. During tertiary production, compositional modelling is appropriate. Therefore, the framework introduced in Chapter 5 should be extended to three phases and compositional flow. Several challenges can be expected for such extensions. The distribution of masses in a two-phase problem can be described by a single variable that fulfil a comparison principle. This motivates us to require monotonicity of numerical schemes. For three-phase or compositional problems, we do not have such a property. Therefore, it is not clear what a robust and rigorous scheme should be based on.

We have only considered FIM and IMPES time stepping strategies. For a compositional problem, the high number of unknowns makes fully implicit methods too expensive, while the IMPES time step restriction may be severe. Therefore, more flexible methods should be considered. One natural candidate is an adaptive implicit scheme. For AIM, it is an interesting question what are appropriate primary variables; saturations or component masses. Other options are asynchronous time stepping, or maybe multiscale methods.

Except from very simplified cases, the strength of the non-linearities in the pressure equation mean only an approximate solution can be found, and thus the resulting velocity field will be inexact. As an consequence, if volume-related variables (i.e. saturations) are transported according to the velocity field, unphysical

values may arise. In Chapter 5 and Paper E, we circumvented this problem by using mass variables instead of saturations. The incompressible two-phase simulations performed in [141] and Paper E show no sign of problem with this approach. However, it is an open question how the volume relaxed framework will affect more difficult physical problems such as large differences in component densities, highly compressible fluids, and phase equilibrium calculations. We emphasis that the inexactness of the pressure solution must be treated somehow; the volume relaxed framework has proven to be robust and provide physical values for the mass variables for the tests performed so far.

The upstream strategies mainly considered in this work are only first order accurate. It is thus natural to consider higher order methods in space, that is, to treat hyperbolic problems with the same order of accuracy as the elliptic equations. A higher order reconstruction of data would require a cell stencil that is larger than the scheme presented in Chapter 5. The reconstruction should be done in a way that minimise bias with respect to grid orientation, furthermore, spurious oscillations should be avoided.

All investigations done so far are for two-dimensional flow. An extension of the trace forward methodology to three dimensions should be possible. In practice, however, the hexahedral cells which are prevailing in reservoir grids, most often follow the geological layering, and thus be thin in the vertical direction. As a consequence, all the schemes considered in this work become very similar to the standard SPU-method for transport orthogonal to the layering. The reason why the cells are long and thin is that we expect the flow to a large extent to be confined within the layers. Thus, for hexahedral cells it might be sufficient to apply the multi-dimensional schemes to transport aligned with the geological layers. For other cells, i.e. tetrahedral and their duals, further investigations are needed.

On the theoretical side, there is a lack of understanding of what are the crucial properties for solving non-linear problems. For linear problems, the TMU scheme [197] is ideal, whereas this is not the case for non-linear transport. A better understanding can hopefully also help construction of limiters for more general grids.

Bibliography

[1] J.E. Aarnes. On the use of a mixed multiscale finite element method for greater flexibility and increased speed or improved accuracy in reservoir simulation. *Multiscale Model. Simul.*, 2(3):421–439, 2004.

[2] J.E. Aarnes. Efficient domain decomposition methods for elliptic problems arising from flows in heterogeneous porous media. *Computing and Visualization in Science*, 8(2):93–106, 2005.

[3] J.E. Aarnes and T.Y. Hou. Multiscale domain decomposition methods for elliptic problems with high aspect ratios. *Acta Math. Appl. Sin.*, 18(1):63–76, 2002.

[4] J.E. Aarnes, S. Krogstad, and K.-A. Lie. Multiscale mixed/mimetic methods on corner-point grids. *Comput. Geosci.*, 12(3):297–315, 2008.

[5] I. Aavatsmark. An introduction to multipoint flux approximations for quadrilateral grids. *Comput. Geosci.*, 6(3-4):405–432, 2002.

[6] I. Aavatsmark. Bevarelsesmetoder for elliptiske differensialligninger. University of Bergen, 2005. Lecture note.

[7] I. Aavatsmark. Interpretation of a two-point flux stencil for skew parallelogram grids. *Comput. Geosci.*, 11(3):199–206, 2007.

[8] I. Aavatsmark, T. Barkve, Ø. Bøe, and T. Mannseth. Discretization on non-orthogonal, curvilinear grids for multi-phase flow. *Proc. of the 4th European Conf. on the Mathematics of Oil Recovery*, 1994.

[9] I. Aavatsmark, T. Barkve, Ø. Bøe, and T. Mannseth. Discretization on non-orthogonal, quadrilateral grids for inhomogeneous, anisotropic media. *J. Comput. Phys.*, 127(1):2–14, 1996.

[10] I. Aavatsmark, T. Barkve, Ø. Bøe, and T. Mannseth. Discretization on unstructured grids for inhomogeneous, anisotropic media. I. Derivation of the methods. *SIAM J. Sci. Comput.*, 19(5):1700–1716, 1998.

[11] I. Aavatsmark, T. Barkve, Ø. Bøe, and T. Mannseth. Discretization on unstructured grids for inhomogeneous, anisotropic media. II. Discussion and numerical results. *SIAM J. Sci. Comput.*, 19(5):1717–1736, 1998.

[12] I. Aavatsmark, T. Barkve, and T. Mannseth. Control-volume discretization methods for 3D quadrilateral grids in inhomogeneous, anisotropic reservoirs. *SPE J*, 3:146–154, 1998. SPE 38000.

[13] I. Aavatsmark, G. T. Eigestad, R. A. Klausen, M. F. Wheeler, and I. Yotov. Convergence of a symmetric MPFA method on quadrilateral grids. *Comput. Geosci.*, 11(4):333–345, 2007.

[14] I. Aavatsmark and G.T. Eigestad. Numerical convergence of the MPFA O-method and U-method for general quadrilateral grids. *Int. J. Numer. Methods Fluids*, 51(9-10):939, 2006.

[15] I. Aavatsmark, G.T. Eigestad, B.O. Heimsund, B.T. Mallison, J. Nordbotten, and E. Øian. A new finite-volume approach to efficient discretization on challenging grids. *Proc. of the SPE Symposium on Reservoir Simualtion*, 2007. SPE 106435.

[16] I. Aavatsmark, G.T. Eigestad, and R.A. Klausen. Numerical convergence of the MPFA O-method for general quadrilateral grids in two and three dimensions. In *Compatible spatial discretizations*, volume 142 of *IMA Vol. Math. Appl.*, pages 1–21. 2006.

[17] I. Aavatsmark, G.T. Eigestad, B.T. Mallison, and J.M. Nordbotten. A compact multipoint flux approximation method with improved robustness. *Numer. Methods Partial Differ. Equations*, 24(5):1329–1360, 2008.

[18] E.C. Abreu, L.F.F. Pereira, and S.S. Ribeiro. Central schemes for porous media flow. *Comput. Appl. Math.*, 28(1):87–110, 2009.

[19] Adimurthi, J. Jaffré, and G.D. Veerappa Gowda. Godunov-type methods for conservation laws with a flux function discontinuous in space. *SIAM J. Numer. Anal.*, 42(1):179–208, 2004.

[20] J.R. Appleyard and I.M. Cheshire. The cascade method for accelerated convergence in implicit simulators. *Proc. of the European Petroleum Conference*, pages 113–122, 1982. SPE 12804.

[21] T. Arbogast. Implementation of a locally conservative numerical subgrid upscaling scheme for two-phase Darcy flow. *Comput. Geosci.*, 6:453–481, 2002.

[22] T. Arbogast and C.-S. Huang. A fully mass and volume conserving implementation of a characteristic method for transport problems. *SIAM J. Sci. Comput.*, 28(6):2001–2022, 2006.

[23] T. Arbogast and M.F. Wheeler. A characteristics-mixed finite element method for advection-dominated transport problems. *SIAM J. Numer. Anal.*, 32(2):404–424, 1995.

[24] D.N. Arnold, D. Boffi, and R.S. Falk. Quadrilateral H(div) finite elements. *SIAM J. Numer. Anal.*, 42(6):2429–2451, 2005.

[25] K. Aziz. Reservoir simulation grids: opportunities and problems. *J. Petrol. Technol.*, 45(7):658–663, 1993. SPE 25233.

[26] K. Aziz and A. Settari. *Petroleum Reservoir Simulation*. Chapman & Hall, 1979. ISBN: 0-85334-787-5.

[27] D.K. Babu and A.S. Odeh. Productivity of a horizontal well. *SPE Reserv. Eng.*, 4(4):417–421, 1989. SPE 18298.

[28] D.K. Babu and A.S. Odeh. Author's reply to discussion of productivity of a horizontal well. *SPE Reserv. Eng.*, 5(2):256, 1990. SPE 20403.

[29] D.K. Babu and A.S. Odeh. Author's reply to further discussion of productivity of a horizontal well. *SPE Reserv. Eng.*, 5(3):438, 1990. SPE 21307.

[30] D.K. Babu, A.S. Odeh, A.J. Al-Khalifa, and R.C. McCann. The relation between wellblock and wellbore pressures in numerical simulation of horizontal wells. *SPE Reserv. Eng.*, 6(3):324–328, 1991. SPE 20161.

[31] R. Barrett, M. Berry, T. F. Chan, J. Demmel, J. Donato, J. Dongarra, V. Eijkhout, R. Pozo, C. Romine, and H. van der Vorst. *Templates for the Solution of Linear Systems: Building Blocks for Iterative Methods*. SIAM, 2nd edition, 1994. ISBN: 0-89871-328-5.

[32] J. Bear and A. Verruijt. *Modeling Groundwater Flow and Pollution*. Reidel, 1987. ISBN: 1-55608-014-X.

[33] J.B. Bell, J.A. Trangenstein, and G.R. Shubin. Conservation laws of mixed type describing three-phase flow in porous media. *SIAM J. Appl. Math.*, 46(6):1000–1017, 1986.

[34] C. Bennis, H. Borouchaki, and N. Flandrin. 3D conforming power diagrams for radial LGR in CPG reservoir grids. *Eng. Comput.*, 24(3):253–265, 2008.

[35] M. Benzi. Preconditioning techniques for large linear systems: a survey. *J. Comput. Phys.*, 182(2):418–477, 2002.

[36] J. Berntsen and G. Furnes. Internal pressure errors in sigma-coordinate ocean models- sensitivity of the growth of the flow to the time stepping method and possible non-hydrostatic effects. *Cont. Shelf Res.*, 25:829–848, 2005.

[37] D. Braess. *Finite elements: Theory, fast solvers, and applications in solid mechanics*. Cambridge University Press, 3rd edition, 2007. ISBN: 0-521-70518-5.

[38] C.W. Brand, J.E.Heinemann, and K. Aziz. The grid orientation effect in reservoir simulation. *Proc. of the SPE Symposium on Reservoir Simualtion*, 1991. SPE 21228.

[39] F. Bratvedt, T. Gimse, and C. Tegnander. Streamline computations for porous media flow including gravity. *Transp. Porous Med.*, 25(1):63–78, October 1996.

[40] Y. Brenier and J. Jaffré. Upstream differencing for multiphase flow in reservoir simulation. *SIAM J. Numer. Anal.*, 28(3):685–696, 1991.

[41] S.C. Brenner and L.R. Scott. *The mathematical theory of finite element methods*. Springer Verlag, 2002. ISBN: 0-387-95451-1.

[42] F. Brezzi, , J. Douglas, and L.D. Marini. Two families of mixed finite elements for second order elliptic problems. *Numer. Math.*, 47(2):217–235, 1985.

[43] F. Brezzi, J. Douglas, R. Durn, and M. Fortin. Mixed finite elements for second order elliptic problems in three variables. *Numer. Math.*, 51(2):237–250, 1987.

[44] F. Brezzi and M. Fortin. *Mixed and Hybrid Finite Element Methods*. Springer, 1991. ISBN: 3540975829.

[45] F. Brezzi, K. Lipnikov, and M. Shashkov. Convergence of the mimetic finite difference method for diffusion problems on polyhedral meshes. *SIAM J. Numer. Anal.*, 43(5):1872–1896, 2005.

[46] F. Brezzi, K. Lipnikov, and M. Shashkov. Convergence of mimetic finite difference method for diffusion problems on polyhedral meshes with curved faces. *Math. Models Methods Appl. Sci.*, 16(2):275–298, 2006.

[47] F. Brezzi, K. Lipnikov, and V. Simoncini. A family of mimetic finite difference methods on polygonal and polyhedral meshes. *Math. Models Methods Appl. Sci.*, 15(10):1533–1553, 2005.

[48] H. Cao. *Development of Techniques for General Purpose Simulators*. PhD thesis, Stanford University, 2002.

[49] H. Cao, H.A. Tchelepi, J. Wallis, and H. Yardumian. Parallel scalable unstructured CPR-type linear solver for reservoir simulation. *Proc. of SPE Annual Technical Conference and Exhibition*, 2005. SPE 96809.

[50] Y. Cao, R. Helmig, and B.I. Wohlmuth. Geometrical interpretation of the multi-point flux approximation L-method. *Int. J. Numer. Methods Fluids*, 60(11):1173–1199, 2008.

[51] M.A. Celia, T.F. Russell, I. Herrera, and R.E. Ewing. An Eulerian-Lagrangian localized adjoint method for the advection-diffusion equation. *Adv. Water Resour.*, 13(4):187 – 206, 1990.

[52] G. Chavent and J. Jaffre. *Mathematical models and finite elements for reservoir simulation: single phase, multiphase, and multicomponent flows through porous media*. North Holland, 1986. ISBN: 0-444-70099-4.

[53] Q.-Y. Chen, J. Wan, Y. Yang, and R.T. Mifflin. Enriched multi-point flux approximation for general grids. *J. Comput. Phys.*, 227(3):1701–1721, 2008.

[54] W.H. Chen, L.J. Durlofsky, B. Engquist, and S. Osher. Minimization of grid orientation effects through use of higher-order finite difference methods. *SPE Adv. Tech. Ser.*, 1:43–52, 1993. SPE 22887.

[55] Y. Chen, B.T. Mallison, and L.J. Durlofsky. Nonlinear two-point flux approximation for modeling full-tensor effects in subsurface flow simulations. *Comput. Geosci.*, 12(3):317–335, 2008.

[56] Z. Chen and R.E. Ewing. From single-phase to compositional flow: Applicability of mixed finite elements. *Transp. Porous Med.*, 27(2):225–242, 1997.

[57] Z. Chen and R.E. Ewing. Fully discrete finite element analysis of multiphase flow in groundwater hydrology. *SIAM J. Numer. Anal.*, 34(6):2228–2253, 1997.

[58] Z. Chen and T.H. Hou. A mixed multiscale finite element method for elliptic problems with oscillating coefficients. *Math. Comput.*, 72(242):541–576, 2003.

[59] Z. Chen, G. Huan, and Y. Ma. *Computational methods for multiphase flows in porous media*. SIAM, 2006. ISBN: 0-89871-606-3.

[60] B. Cockburn and C.-W. Shu. Runge-Kutta discontinuous Galerkin methods for convection-dominated problems. *J. Sci. Comput.*, 16(3):173–261, 2001.

[61] R. Courant, K. Friedrichs, and H. Lewy. Über die partiellen Differenzengleichungen der mathematischen Physik. *Math. Ann.*, 100(1):32–74, 1928.

[62] M.G. Crandall and A. Majda. Monotone difference approximations for scalar conservation laws. *Math. Comput.*, 34(149):1–21, 1980.

[63] C.M. Dafermos. Polygonal approximations of solutions of the initial value problem for a conservation law. *J. Math. Anal. Appl*, 38:33–41, 1972.

[64] H.K. Dahle, R.E. Ewing, and T.F. Russell. Eulerian-Lagrangian localized adjoint methods for a nonlinear advection-diffusion equation. *Comput. Methods Appl. Mech. Eng.*, 122(3-4):223 – 250, 1995.

[65] L.P. Dake. *Fundamentals of Reservoir Engineering*. Elsevier, 1978. ISBN: 0-444-41667-6.

[66] E.I. Dale. *Modelling om immiscible WAG with emphasis on the effect of capillary pressure*. PhD thesis, University of Bergen, 2008.

[67] A. Datta-Gupta and M.J. King. *Streamline simulation: Theory and practice*. SPE, 2007. ISBN: 978-1555631116.

[68] R. de Loubens. Construction of high-order adaptive implicit methods for reservoir simulation. Master's thesis, Stanford University, 2007.

[69] R. de Loubens, A. Riaz, and H.A. Tchelepi. Error analysis of an adaptive implicit scheme for hyperbolic conservation laws. *SIAM J. Sci. Comput.*, 31(4):2890–2914, 2009.

[70] F.X. Deimbacher and Z.E. Heinemann. Time-dependent incorporation of locally irregular grids in large reservoir simulation models. *Proc. of the SPE Symposium on Reservoir Simulation*, 1993. SPE 25260.

[71] Y. Ding. Scaling-up in the vicinity of wells in heterogeneous field. *Proc. of the SPE Symposium of Reservoir Simulation*, 1995. SPE 29137.

[72] Y. Ding. Upscaling on distorted gridblocks for simulation of advanced wells. *J. Petrol. Sci. Eng.*, 43(1-2):87 – 97, 2004.

[73] Y. Ding and L. Jeannin. A new methodology for singularity modelling in flow simulations in reservoir engineering. *Comput. Geosci.*, 5(2):93–119, 2001.

[74] Y. Ding and L. Jeannin. New numerical schemes for near-well modeling using flexible grid. *SPE J*, 9(1):109–121, 2004. SPE 87679.

[75] J. Douglas, F. Furtado, and F. Pereira. On the numerical simulation of waterflooding of heterogeneous petroleum reservoirs. *Comput. Geosci.*, 1(2):155–190, 1997.

[76] J. Douglas and J.E. Roberts. Global estimates for mixed methods for second order elliptic equations. *Math. Comput.*, 44(169):39–52, 1985.

[77] J. Douglas and T.F. Russel. Numerical methods for convection-dominated diffusion problems based on combining the method of characteristics with finite element or finite difference procedures. *SIAM J. Numer. Anal.*, 19(5):871–885, 1982.

[78] L.J. Durlofsky. A triangle based mixed finite element–finite volume technique for modeling two phase flow through porous media. *J. Comput. Phys.*, 105(2):252 – 266, 1993.

[79] L.J. Durlofsky, W.J. Milliken, and A. Bernath. Scaleup in the near-well region. *SPE J*, 5(1):110–117, 2000. SPE 61855.

[80] M. G. Edwards and C. F. Rogers. A flux continuous scheme for the full tensor pressure equation. In *Proc. of the 4th European Conf. on the Mathematics of Oil Recovery*, 1994.

[81] M. G. Edwards and C. F. Rogers. Finite volume discretization with imposed flux continuity for the general tensor pressure equation. *Comput. Geosci.*, 2(4):259–290, 1998.

[82] M.G. Edwards. Unstructured, control-volume distributed, full-tensor finite-volume schemes with flow based grids. *Comput. Geosci.*, 6(3-4):433–452, 2002.

[83] M.G. Edwards. Higher-resolution hyperbolic-coupled-elliptic flux-continuous cvd schemes on structured and unstructured grids in 2-D. *Int. J. Numer. Methods Fluids*, 51(9-10):1059–1077, 2006.

[84] M.G. Edwards. Higher-resolution hyperbolic-coupled-elliptic flux-continuous cvd schemes on structured and unstructured grids in 3-D. *Int. J. Numer. Methods Fluids*, 51(9-10):1079–1085, 2006.

[85] M.G. Edwards and H. Zheng. A quasi-positive family of continuous Darcy-flux finite-volume schemes with full pressure support. *J. Comput. Phys.*, 227(22):9333 – 9364, 2008.

[86] G. T. Eigestad and R. A. Klausen. On the convergence of the multi-point flux approximation O-method: numerical experiments for discontinuous permeability. *Numer. Methods Partial Differential Equations*, 21(6):1079–1098, 2005.

[87] G.T. Eigestad. *Reservoir simulation with imposed flux continuity conditions on heterogeneous and anisotropic media for general geometries, and the inclusion of hysteresis in forward modeling*. PhD thesis, University of Bergen, 2003.

[88] B. Eikemo, K.-A. Lie, G.T. Eigestad, and H.K. Dahle. Discontinuous Galerkin methods for advective transport in single-continuum models of fractured media. *Adv. Water Resour.*, 32(4):493 – 506, 2009.

[89] M.S. Espedal and R.E. Ewing. Characteristic Petrov-Galerkin subdomain methods for two-phase immiscible flow. *Comput. Methods Appl. Mech. Eng.*, 64(1-3):113 – 135, 1987.

[90] L.C. Evans. *Partial Differential Equations*. AMS, 1998. ISBN: 0-8218-0772-2.

[91] R. E. Ewing and H. Wang. A summary of numerical methods for time-dependent advection-dominated partial differential equations. *J. Comput. Appl. Math.*, 128(1-2):423 – 445, 2001.

[92] R.E. Ewing, O. Iliev, and R. Lazarov. A modified finite volume approximation of second-order elliptic equations with discontinuous coefficients. *SIAM J. Sci. Comput.*, 23(4):1335–1351, 2001.

[93] R. Eymard and J.-M. Herard, editors. *Finite Volumes for Complex Applications V*. Wiley, 2008.

[94] N. Flandrin, H. Borouchaki, and C. Bennis. 3D hybrid mesh generation for reservoir simulation. *Int. J. Numer. Methods Eng.*, 65(10), 2006.

[95] H.A. Friis, M.G. Edwards, and J. Mykkeltveit. Symmetric positive definite flux-continuous full-tensor finite-volume schemes on unstructured cell-centered triangular grids. *SIAM J. Sci. Comput.*, 31(2):1192–1220, 2008.

[96] A. Fuchs. Almost regular Delaunay-triangulations. *Int. J. Numer. Methods Eng.*, 40(24), 1997.

[97] M.G. Gerritsen and L.J. Durlofsky. Modeling fluid flow in oil reservoirs. *Annu. Rev. Fluid Mech.*, 37:211–238, 2005.

[98] J.G. Gluyas and R.E. Swarbrick. *Petroleum geoscience*. Blackwell Pub, 2004. IBSN: 0-632-03767-9.

[99] S.K. Godunov. A difference method for numerical calculation of discontinuous solutions of the equations of hydrodynamics. *Matematicheskii Sbornik*, 89(3):271–306, 1959.

[100] R. Guzman and F. Fayers. Mathematical properties of three-phase flow equations. *SPE J*, 2(3):291–300, 1997. SPE 35154.

[101] R. Guzman and F. Fayers. Solutions to the three-phase Buckley-Leverett problem. *SPE J*, 2(3):301–311, 1997. SPE 35156.

[102] W. Hackbusch. *Iterative solution of large sparse systems of equations*. Springer, 1985. ISBN: 978-0387940649.

[103] H. Hægland. *Streamline methods with application to flow and transport in fractured media*. PhD thesis, University of Bergen, 2009.

[104] H. Hægland, H.K. Dahle, G.T. Eigestad, K.A. Lie, and I. Aavatsmark. Improved streamlines and time-of-flight for streamline simulation on irregular grids. *Adv. Water Resources*, 30(4):1027–1045, 2007.

[105] A. Harten, J.M. Hyman, and P.D. Lax. On finite-difference approximations and entropy conditions for shocks. *Commun. Pur. Appl. Math.*, 29:297–319, 1976.

[106] V. Haugse, K. H. Karlsen, K.-A. Lie, and J. R. Natvig. Numerical solution of the polymer system by front tracking. *Transp. Porous Med.*, 44(1):63–83, July 2001.

[107] J. Haukas. *Compositional reservoir simuation with emphasis on the IMPSAT formulation*. PhD thesis, University of Bergen, 2006.

[108] B.O. Heimsund. *Mathematical and Numerical Methods for Reservoir Fluid Flow Simulation*. PhD thesis, University of Bergen, 2005.

[109] Z.E. Heinemann, C.W. Brand, M. Munka, and Y.M. Chen. Modeling reservoir geometry with irregular grids. *SPE Reserv. Eng.*, 6(2):225–232, 1991.

[110] R. Helmig. *Multiphase Flow and Transport Processes in the Subsurface: A contribution to the modeling of hydrosystems*. Springer, 1997. ISBN: 3-540-62703-0.

[111] I. Herrera, R. Ewing, M. A. Celia, and T.F. Russel. Eulerian-Lagrangian localized adjoint method: The theoretical framework. *Numer. Methods Partial Differ. Equations*, 9:431–457, 1993.

[112] H. Holden and N.H. Risebro. *Front tracking for hyperbolic conservation laws*. Springer, 2002. ISBN: 3-540-43289-2.

[113] R. Holm. *Modelling of Three-Phase Flow Functions for Applications in Enhanced Oil Recovery*. PhD thesis, University of Bergen, 2009.

[114] R. Holm, R. Kaufmann, B.O. Heimsund, E. Øian, and M.S. Espedal. Meshing of domains with complex internal geometries. *Numer. Linear Algerbr.*, 13(9):717 – 731, 2006.

[115] E. Hopf. Elementare Bemerkungen über die Lösungen partieller Differentialgleichungen zweiter Ordnung vom elliptischen Typus. *Preuss. Akad. Wiss*, 19:147–152, 1927.

[116] E. Hopf. A remark on linear elliptic differential equations of second order. *Proc. Am. Math. Soc.*, 3(5):791–793, 1952.

[117] H. Hoteit and A. Firoozabadi. Multicomponent fluid flow by discontinuous Galerkin and mixed methods in unfractured and fractured media. *Water Resour. Res*, 41(11):1–15, 2005.

[118] T.Y. Hou and X.-H.Wu. A multiscale finite element method for elliptic problems in composite materials and porous media. *J. Comput. Phys.*, 134(1):169–189, 1997.

[119] F.S.V. Hurtado, C.R. Maliska, A.F.C. da Silva, and J. Jordazzo. A quadrilateral element-based finite-volume formulation for the simulation of complex reservoirs. *Proc. of the Latin American & Caribbean Petroleum Engineeringi Conference*, 2007. SPE 107444.

[120] H.K. Hvidevold. Monotonicity conditions for discretization of parabolic conservation laws. Master's thesis, University of Bergen, 2009.

[121] P. Jenny, S. H. Lee, and H. A. Tchelepi. Multi-scale finite-volume method for elliptic problems in subsurface flow simulation. *J. Comput. Phys.*, 187(1):47–67, 2003.

[122] P. Jenny, S. H. Lee, and H. A. Tchelepi. Adaptive multiscale finite-volume method for multiphase flow and transport in porous media. *Multiscale Model. Simul.*, 3(1):50–64, 2005.

[123] P. Jenny, S.H. Lee, and H.A. Tchelepi. Adaptive fully implicit multi-scale finite-volume method for multi-phase flow and transport in heterogeneous porous media. *J. Comput. Phys.*, 217(2):627 – 641, 2006.

[124] P. Jenny, C. Wolfsteiner, S.H. Lee, and L.J Durlofsky. Modeling flow in geometrically complex reservoirs using hexahedral multi-block grids. *SPE J*, 7(2):149–157, 2002. SPE 78673.

[125] G.-S. Jiang, D. Levy, C.-T. Lin, S. Osher, and E. Tadmor. High-resolution non-oscillatory central schemes with non-staggered grids for hyperbolic conservation laws. *SIAM J. Numer. Anal.*, 35:2147–2168, 1998.

[126] G.-S. Jiang and E. Tadmor. Non-oscillatory central schemes for multidimensional hyperbolic conservation laws. *SIAM J. Sci. Comput.*, 19:1892–1917, 1998.

[127] T. Johansen and R. Winther. The solution of the Riemann problem for a hyperbolic system of conservation laws modeling polymer flooding. *SIAM J. Math. Anal.*, 19(3):541–566, 1988.

[128] R. Juanes. *Displacement theory and multiscale numerical modeling of three-phase flow in porous media*. PhD thesis, University of Berkley, 2003.

[129] R. Juanes and K.-A. Lie. A front-tracking method for efficient simulation of miscible gas injection processes. *Proc. of the SPE Symposium on Reservoir Simulation*, 2005. SPE 93298.

[130] R. Juanes and T.W. Patzek. Analytical solution to the Riemann problem of three-phase flow in porous media. *Transp. Porous Med.*, 55(1):47–70, April 2004.

[131] R. Juanes and H.A. Tchelepi. Special issue on multiscale methods for flow and transport in heterogeneous porous media. *Comput. Geosci.*, 12(3), 2008.

[132] Y. Kanarska and V. Maderich. A non-hydrostatic numerical model for calculating free-surface stratified flows. *Ocean Dynam.*, 53:176–185, 2003.

[133] M. Karimi-Fard. Grid optimization to improve orthogonality of two-point flux approximation for unstructured 3D fractured reservoirs. *Proc. of the 11th European Conf. on the Mathematics of Oil Recovery*, 2008.

[134] K.H. Karlsen and N.H. Risebro. Corrected operator splitting for nonlinear parabolic equations. *SIAM J. Numer. Anal.*, 37(3):980–1003, 2000.

[135] R. A. Klausen, F.A. Radu, and G.T. Eigestad. Convergence of MPFA on triangulations and for Richards' equation. *Int. J. Numer. Methods Fluids*, 58(9):1327 – 1351, 2008.

[136] R. A. Klausen and R. Winther. Robust convergence of multi point flux approximation on rough grids. *Numer. Math.*, 104(3):317–337, 2006.

[137] R.A. Klausen and T.F. Russell. Relationships among some locally conservative discretization methods which handle discontinuous coefficients. *Comput. Geosci.*, 8(4):341–377, 2004.

[138] R.A. Klausen and A.F. Stephansen. Convergence of the MPFA O-method on general grids. *Numer. Methods Partial Differ. Equations*, Sumbitted, 2009.

[139] R.A. Klausen and R. Winther. Convergence of multipoint flux approximations on quadrilateral grids. *Numer. Methods Partial Differential Equations*, 22(6):1438–1454, 2006.

[140] B. Koren. Low-diffusion rotated upwind schemes, multigrid and defect corrections for steady, multi-dimensional Euler flows. *Int. Ser. Numer. Math.*, 98:265–276, 1991.

[141] J. Kozdon. *Numerical Methods with reduced grid dependency for enhanced oil recovery*. PhD thesis, Stanford University, 2009.

[142] J. Kozdon, B.T. Mallison, and M. Gerritsen. Robust multi-D transport schemes with reduced grid orientation effects. *Transp. Porous Med.*, 78(1):47–75, 2009.

[143] J. Kozdon, B.T. Mallison, M. Gerritsen, and W. Chen. Multi-D upwinding for multi phase transport in porous media. *Proc. of the SPE Symposium on Reservoir Simulation*, 2009. SPE 119190.

[144] A. Kurganov and E. Tadmor. New high-resolution central schemes for nonlinear conservation laws and convection-diffusion equations. *J. Comput. Phys.*, 160(1):241 – 282, 2000.

[145] F. Kwok and H.A. Tchelepi. Potential-based reduced newton algorithm for nonlinear multiphase flow in porous media. *J. Comput. Phys.*, 227(1):706 – 727, 2007.

[146] F. Labelle and J.R. Shewchuk. Anisotropic Voronoi diagrams and guaranteed-quality anisotropic mesh generation. *Proc. of the 19th Annual Symposium on Computational Geometry*, pages 191–200, 2003.

[147] F. Labelle and J.R. Shewchuk. Isosurface stuffing: Fast tetrahedral meshes with good dihedral angles. *ACM T. Graphic.*, 26:57.1–57.10, 2007.

[148] S. Lacroix, Y.V. Vassilevski, and M.F. Wheeler. Decoupling preconditioners in the implicit parallel accurate reservoir simulator (IPARS). *Numer. Linear Algerbr.*, 8(8):537 – 549, 2001.

[149] J.V. Lambers, M.G. Gerritsen, and B.T. Mallison. Accurate local upscaling with variable compact multipoint transmissibility calculations. *Comput. Geosci.*, 12(3):399–416, 2008.

[150] S. Lamine and M.G. Edwards. Higher-resolution convection schemes for flow in porous media on highly distorted unstructured grids. *Int. J. Numer. Methods Eng.*, 76(8):1139–1158, 2008.

[151] S. Lamine and M.G. Edwards. Higher order multidimensional wave oriented upwind schemes for flow in porous media on unstructured grids. *Proc. of the SPE Symposium on Reservoir Simulation*, 2009. SPE 119187.

[152] C. Le Potier. Schema volumes finis monotone pour des operateurs de diffusion fortement anisotropes sur des maillages de triangle non structures. *CR Math. Acad. Sci. Paris*, 341(12):787–792, 2005.

[153] S. Lee, H.A. Tchelepi, J. Patrick, and L. DeChant. Implementation of a flux-continuous finite-difference method for stratigraphic, hexahedron grids. *SPE J*, 7(3):267–277, 2002. SPE 80117.

[154] S.H Lee, C. Wolfsteiner, and H.A.. Tchelepi. Multiscale finite-volume formulation for muliphase flow in porous media; black oil formulation of compressible, three-phase flow with gravity. *Comput. Geosci.*, 12(3):351–366, 2008.

[155] R.J. LeVeque. *Finite volume methods for hyperbolic problems*. Cambridge University Press, 2002. ISBN: 978-0-521-00924-9.

[156] K.-A. Lie and R. Juanes. A front-tracking method for the simulation of three-phase flow in porous media. *Comput. Geosci.*, 9(1):29–59, 2005.

[157] K. Lipnikov, J.D. Moulton, and D. Svyatskiy. A multilevel multiscale mimetic (m3) method for two-phase flows in porous media. *J. Comput. Phys.*, 227(14):6727 – 6753, 2008.

[158] K. Lipnikov, M.Shashkov, and D.Svyatskiy. The mimetic finite difference discretization of diffusion problem on unstructured polyhedral meshes. *J. Comput. Phys.*, 211(2):473 – 491, 2006.

[159] K. Lipnikov, M. Shashkov, D. Svyatskiy, and Y. Vassilevski. Monotone finite volume schemes for diffusion equations on unstructured triangular and shape-regular polygonal meshes. *J. Comput. Phys.*, 227(1):492–512, 2007.

[160] K. Lipnikov, M. Shashkov, and I. Yotov. Local flux mimetic finite difference methods. *Numer. Math.*, 112(1):115–152, 2009.

[161] K. Lipnikov, D. Svyatskiy, and Y. Vassilevski. Interpolation-free monotone finite volume method for diffusion equations on polygonal meshes. *J. Comput. Phys.*, 228(3):703 – 716, 2009.

[162] I. Lunati and P. Jenny. Multiscale finite-volume method for compressible multiphase flow in porous media. *J. Comput. Phys.*, 216:616–636, 2006.

[163] I. Lunati and P. Jenny. Multiscale finite-volume method for density-driven flow in porous media. *Comput. Geosci.*, 12(3):337–350, 2008.

[164] I. Lunati and P. Jenny. Modeling complex wells with the multi-scale finite-volume method. *J. Comput. Phys.*, 228:687–702, 2009.

[165] B.T. Mallison. *Streamline-based simulation of two-phase multicomponent flow in porous media*. PhD thesis, Stanford University, 2004.

[166] B.T. Mallison, M.G. Gerritsen, K. Jessen, and F.M. Orr. High-order upwind schemes for two-phase, multicomponent flow. *SPE J*, 10(3):297–311, 2005. SPE 79691.

[167] B.T. Mallison, M.G. Gerritsen, and G. Kreiss. Asynchronous time integration of flux-conservative transport. *Proceedings of the 11th European Conf. on the Mathematics of Oil Recovery*, 2008.

[168] J. Marshall, C. Hill, L. Perelman, and A. Adcroft. Hydrostatic, quasi-hydrostatic, and nonhydrostatic ocean modeling. *J. Geophys. Res.*, 102(C3):5733–5752, 1997.

[169] M.J. Mlacnik and L.J. Durlofsky. Unstructured grid optimization for improved monotonicity of discrete solutions of elliptic equations with highly anisotropic coefficients. *J. Comput. Phys.*, 216(1):337–361, 2006.

[170] M.J. Mlacnik and Z.E. Heinemann. Using well windows in full-field reservoir simulation. *SPE Reserv. Eval. Eng.*, 6(4):275–285, 2003. SPE 85709.

[171] S. Mundal. *Conservative numerical methods for elliptic problems with applications to simulation of near-well flow*. PhD thesis, University of Bergen, 2009.

[172] J.R. Natvig and K.-A. Lie. Fast computation of multiphase flow in porous media by implicit discontinuous Galerkin schemes with optimal ordering of elements. *J. Comput. Phys.*, 227(24):10108 – 10124, 2008.

[173] J. C. Nedelec. Mixed finite elements in R^3. *Numer. Math.*, 35(3):315–341, September 1980.

[174] N. Nessyahu and E. Tadmor. Non-oscillatory central differencing for hyperbolic conservation laws. *J. Comput. Phys.*, 87(2):408 – 463, 1990.

[175] J. M. Nordbotten and I. Aavatsmark. Monotonicity conditions for control volume methods on uniform parallelogram grids in homogeneous media. *Comput. Geosci.*, 9(1):61–72, 2005.

[176] J. M. Nordbotten and P. E. Bjørstad. On the relationship between the multiscale finite-volume method and domain decomposition preconditioners. *Comput. Geosci.*, 12(3):367–376, 2008.

[177] J.M. Nordbotten, I. Aavatsmark, and G.T. Eigestad. Monotonicity of control volume methods. *Numer. Math.*, 106(2):255–288, 2007.

[178] J.M. Nordbotten and G.T. Eigestad. Discretization on quadrilateral grids with improved monotonicity properties. *J. Comput. Phys.*, 203(2):744–760, 2005.

[179] J.M. Nordbotten and H. Hægland. On reproducing uniform flow exactly on general hexahedral cells using one degree of freedom per surface. *Adv. Water Resour.*, 32(2):264 – 267, 2009.

[180] F.K. North. *Petroleum Geology*. Unwin Hyman Ltd., 1990. ISBN: 0-04-553004-1.

[181] S. Osher and F. Solomon. Upwind difference schemes for hyperbolic systems of conservation laws. *Math. Comput.*, 38(158):339–374, 1982.

[182] M. Pal, M.G. Edwards, and A.R. Lamb. Convergence study of a family of flux-continuous, finite-volume schemes for the general tensor pressure equation. *Int. J. Numer. Methods Fluids*, 51(9-10):1177–1203, 2006.

[183] C. Palagi. *Generation and Application of Voronoi grid to model flow in heterogeneous reservoirs*. PhD thesis, Stanford University, 1992.

[184] C.L. Palagi and K. Aziz. Use of Voronoi grid in reservoir simulation. *SPE Advanced Technology Series*, 2(2):69–77, 1994. SPE 22889.

[185] D.W. Peaceman. *Fundamentals of Numerical Reservoir Simulation*. North-Holland, 1977. ISBN: 0-444-41578-5.

[186] D.W. Peaceman. Interpretation of well-block pressures in numerical reservoir simulation. *SPE J*, 18(3):183–194, 1978. SPE 6893.

[187] D.W. Peaceman. Interpretation of well-block pressures in numerical reservoir simulation with nonsquare grid blocks and anisotropic permeability. *SPE J*, 23(3):531–543, 1983. SPE 10528.

[188] D.W. Peaceman. Further discussion of productivity of a horizontal well. *SPE Reserv. Eng.*, 5(3):437–438, 1990. SPE 20799.

[189] D.W. Peaceman. Interpretation of wellblock pressures in numerical reservoir simulation: Part 3–off-center and multiple wells within a wellblock. *SPE Reserv. Eng.*, 5(2):227–232, 1990. SPE 16976.

[190] D.W. Peaceman. Further discussion of productivity of a horizontal well. *SPE Reserv. Eng.*, 6(1):149–150, 1991. SPE 21611.

[191] D.Y. Peng and D.B. Robinson. A new two-constant equation of state. *Ind. Eng. Chem. Fund.*, 15(1):59–64, 1976.

[192] O.A. Perdrosa and K. Aziz. Use of a hybrid grid in reservoir simulation. *SPE Reserv. Eng.*, 1(1):611–621, 1986. SPE 13507.

[193] Ø. Pettersen and T.G. Kristiansen. Improved compaction modeling in reservoir simulation and coupled rock mechanics–flow simulation, with examples from the Valhall field. *SPE Reserv. Eval. Eng.*, 12(2):329–340, 2009. SPE 113003.

[194] A.M. Quarteroni and A. Valli. *Numerical approximation of partial differential equations*. Springer, 2008. ISBN: 3-540-85267-0.

[195] P.A. Raviart and J.M. Thomas. A mixed finite element method for 2nd order elliptic problems. *Mathematical Aspects of the Finite Element Method, Lecture Notes in Mathematics*, 606:292–315, 1977.

[196] P. L. Roe. Approximate Riemann solvers, parameter vectors, and difference schemes. *J. Comput. Phys.*, 43(2):357 – 372, 1981.

[197] P. L. Roe and D. Sidilkover. Optimum positive linear schemes for advection in two and three dimensions. *SIAM J. Numer. Anal.*, 29(6):1542–1568, 1992.

[198] B. Rubin and M.J. Blunt. Higher order implicit flux limiting schemes for black oil simulation. *Proc. of the SPE Symposium on Reservoir Simulation*, 1991. SPE 21222.

[199] T.F. Russel. Stability analysis and switching criteria for adaptive implicit methods based on the CFL criterion. *Proc. of the SPE Symposium on Reservoir Simulation*, 1989. SPE 18416.

[200] T.F. Russel and M.A. Celia. An overview of research on Eulerian-Lagrangian localized adjoint methods (ELLAM). *Adv. Water Resour.*, 25:1215–1231, 2002.

[201] T.F. Russel and M.F. Wheeler. *The Mathematics of Reservoir Simulation*, chapter Finite element and finite difference methods for continuous flows in porous media, pages 35–106. SIAM, 1983.

[202] T.F. Russell. Time stepping along characteristics with incomplete iteration for a Galerkin approximation of miscible displacement in porous media. *SIAM J. Numer. Anal.*, 22(5):970–1013, 1985.

[203] P.H. Sammon. An analysis of upstream differencing. *SPE Reserv. Eng.*, 3(3):1053–1056, 1988.

[204] Schlumberger. Eclipse: Technical description. 2007.

[205] Z. Sheng, J. Yue, and G. Yuan. Monotone finite volume schemes of nonequilibrium radiation diffusion equations on distorted meshes. *SIAM J. Sci. Comput.*, 31(4):2915–2934, 2009.

[206] C.-W. Shu. Essentially non-oscillatory and weighted essentially non-oscillatory schemes for hyperbolic conservation laws. *ICASE Report No. 97-65*, 1997.

[207] G.R. Shubin and J.B. Bell. An analysis of the grid orientation effect in numerical simulation of miscible displacement. *Comput. Methods Appl. Mech. Eng.*, 47:47–71, 1984.

[208] S.M. Skjæveland and J. Kleppe, editors. *Recent advances in improved oil recovery methods for North Sea sandstone reservoirs*. Norwegian Petroleum Directorate, 1992. ISBN: 82-7257-340-7.

[209] A.F. Stephansen. Convergence of the MPFA L-method on general grids. To be sumbitted.

[210] K. Stüben, T. Kees, H. Klie, and M.F. Wheeler. Algebraic multigrid methods (AMG) for the efficient solution of fully implicit formulations in reservoir simulation. *Proc. of the SPE Symposium on Reservoir Symulation*, 2007. SPE 105832.

[211] P. K. Sweby. High resolution schemes using flux limiters for hyperbolic conservation laws. *SIAM J. Numer. Anal.*, 21(5):995–1011, 1984.

[212] M.R Thiele and M.G. Edwards. Physically based higher order Godunov schemes for compositional simulation. *Proc. of the SPE Symposium on Reservoir Simulation*, 2001.

[213] G.W. Thomas and D.H Thurnau. Reservoir simulation using an adaptive implicit method. *SPE J*, 23(5):759–768, 1983. SPE 10120.

[214] D. Tiab and E.C. Donaldson. *Petrophysics: theory and practice of measuring reservoir rock and fluid transport properties*. Gulf Professional Publishing, 2004. ISBN: 0-7506-7711-2.

[215] M.R. Todd, P.M. O'Dell, and G.J. Hirasaki. Methods for increased accuracy in numerical reservoir simulators. *SPE J*, 12(6):515–530, 1972. SPE 3516.

[216] E.F. Toro. *Riemann solvers and numerical methods for fluid dynamics- A practical introduction*. 2nd edition, 1999. ISBN: 3-540-65966-8.

[217] J. A. Trangenstein and J. B. Bell. Mathematical structure of compositional reservoir simulation. *SIAM J. Sci. Stat. Comput.*, 10(5):817–845, 1989.

[218] J. A. Trangenstein and J. B. Bell. Mathematical structure of the black-oil model for petroleum reservoir simulation. *SIAM J. Appl. Math.*, 49(3):749–783, 1989.

[219] J.A. Trangenstein. Three-phase flow with gravity. *Contemp. Math.*, 100:147–159, 1989.

[220] L.N. Trefethen and D. Bau. *Numerical linear algebra*. SIAM, 1997. ISBN: 0-89871-361-7.

[221] U. Trottenberg, C.W. Oosterlee, and A. Schüller. *Multigrid*. Academic press, 2000. ISBN: 0-12-701070-X.

[222] P. van Ransbeeck and C. Hirsch. A general analysis of 2D/3D multidimensional upwind convection schemes. *Notes on numerical fluid dynamics*, 57:251–304, 1997.

[223] S.K. Verma. *Flexible grids for reservoir simulation*. PhD thesis, Stanford University, 1996.

[224] M. Vohralik. Equivalence between lowest-order mixed finite element and multi-point finite volume methods on simplicial meshes. *M2AN Math. Model. Numer. Anal.*, 40(2):367–391, 2006.

[225] J.R. Wallis, R.P. Kendall, and T.E. Little. Constrained residual acceleration of conjugate residual methods. *Proc. of the SPE Symposium on Reservoir Simulation*, 1985. SPE 13536.

[226] M.F. Wheeler and I. Yotov. A multipoint flux mixed finite element method. *SIAM J. Numer. Anal.*, 44(5):2082–2106, 2006.

[227] S. Whitaker. Flow in porous media i: A theoretical derivation of Darcy's law. *Transp. Porous Med.*, 1(1):3–25, March 1986.

[228] C. Wolfsteiner and L.J. Durlofsky. Near-well radial upscaling for the accurate modeling of nonconventional wells. *Presented at the SPE Western Regional/AAPG Pacific Section Joint Meeting*, 2002. SPE 76779.

[229] C. Wolfsteiner, L.J. Durlofsky, and K. Aziz. Calculation of well index for nonconventional wells on arbitrary grids. *Comput. Geosci.*, 7(1):61–82, 2003.

[230] C. Wolfsteiner, L.J. Durlofsky, and A. Khalid. Approximate model for productivity of nonconventional wells in heterogeneous reservoirs. *SPE J*, 5(2):218–226, 2000. SPE 62812.

[231] C. Wolfsteiner, S.H. Lee, and H.A. Tchelepi. Well modeling in the multiscale finite volume method for subsurface flow simulation. *Multiscale Model. Simul.*, 5(3):900–917, 2006.

[232] J.L. Yanosik and T.A. McCracken. 9-point, finite-difference reservoir simulator for realistic prediction of adverse mobility ratio displacements. *SPE J*, 19(4):253–262, 1979. SPE 5734.

[233] R.M. Younis, H. Tchelepi, and K. Aziz. Adaptively-localized-continuation-Newton: Reservoir simulation nonlinear solvers that converge all the time. *Proc. of the SPE Symposium on Reservoir Simulation*, 2009.

[234] G. Yuan and Z. Sheng. Monotone finite volume schemes for diffusion equations on polygonal meshes. *J. Comput. Phys.*, 227(12):6288–6312, 2008.

[235] A.B. Zolotukhin and J.-R. Ursin. *Introduction to Petroleum Reservoir Engineering*. Høyskoleforlaget, 2000. ISBN: 82-7634-065-2.

Part II

Included Papers